Multi-user MIMO-OFDM in practice:
Enabling spectrally efficient transmission over time-varying channels

vorgelegt von Diplom-Ingenieur
Jan Malte Schellmann
aus Lüneburg

von der Fakultät IV - Elektrotechnik und Informatik
der Technischen Universität Berlin
zur Erlangung des akademischen Grades

Doktor der Ingenieurwissenschaften
– Dr.-Ing. –

genehmigte Dissertation

Promotionsausschuss:

Vorsitzender: Prof. Dr. Wolfgang Heinrich
Berichter: Prof. Dr. Dr. Holger Boche
Berichter: Prof. Dr. Angel Lozano (Universitat Pompeu Fabra, Barcelona)

Tag der wissenschaftlichen Aussprache: 04. Juni 2009

Berlin 2009
D 83

To Mormor

Zusammenfassung

Die Kombination der MIMO Mehrantennentechnik mit der OFDM Mehrträgerübertragung verspricht das Erzielen hoher spektraler Effizienzen bei moderater Komplexität von Sender- und Empfängerstrukturen. Weiterhin erlaubt das MIMO-OFDM Systemkonzept die flexible Vergabe von Übertragungsressourcen in Zeit, Frequenz und Raum an unterschiedliche Nutzer. Diese Dissertation behandelt Verfahren zur Signalübertragung in Mehrnutzer MIMO-OFDM Systemen, die die Realisierung solcher Systeme in der Praxis ermöglichen sollen. Betrachtet wird hierbei eine isolierte Zelle, bestehend aus einer einzelnen Basisstation, die mehrere in der Zelle verteilte Nutzerterminals versorgt.

Im Allgemeinen sind praktische Mobilfunkkanäle geprägt durch zeitvariantes Verhalten, das von der Bewegung der Nutzerterminals oder aber von Unstimmigkeiten innerhalb der Übertragungskette herrührt. Jene Zeitvarianz kann zu massiven Störungen im Übertragungssystem führen, die die praktisch erzielbare spektrale Effizienz beschränken. Um dennoch möglichst nah an die von der theoretischen Analyse versprochenen spektralen Effizienzen heranzukommen, müssen geeignete Verfahren gefunden werden, mit denen die der Zeitvarianz geschuldeten Degradationseffekte wirksam überwunden werden können.

Die Dissertation gliedert sich in drei Hauptkapitel, in denen jeweils unterschiedliche Grade der Kanal-Zeitvarianz betrachtet werden. Die vorgestellten Ergebnisse zeigen, dass sich für alle betrachteten Fälle Lösungen mit moderaten Komplexitätsanforderungen für die Signalübertragung in MIMO-OFDM Systemen finden lassen, mit denen hohe spektrale Effizienzen auch in der Praxis erzielt werden können. Die spezifischen Inhalte und Ergebnisse der drei Kapitel werden im Folgenden kurz zusammengefasst:

1. Die einfachste Form der Zeitvarianz im Kanal wird verursacht durch einen Frequenzversatz der Signale an Sender und Empfänger. Kompensation der durch diesen Versatz hervorgerufenen Störeffekte ist Aufgabe der Synchronisation. Das erste Kapitel befasst sich daher mit der Entwicklung eines geschlossenen Konzeptes für die Synchronisation des Mehrnutzer MIMO-OFDM Gesamtsystems bestehend aus Vorwärtsstrecke (Downlink) und Rückwärtsstrecke (Uplink). Für die Präambelbasierte Downlink-Synchronisation wird mit Hilfe analytischer und simulativer Mittel der Einfluss von Frequenzdiversität, räumlicher Diversität sowie der Präambellänge auf die Synchronisationsperformanz untersucht. Verwenden die Terminals in der Uplink-Phase den im Downlink geschätzten Frequenzversatz zur Vorkompensation ihrer Sendesignale, können die durch Schätzfehler verbleibenden Störungen

direkt an der Basisstation kompensiert werden. Basierend auf einer Analyse der Signalbedingungen im Uplink wird ein einfaches Verfahren hierfür hergeleitet.

2. Nach erfolgreicher Synchronisation kann im Fall von nahezu statischen Verhältnissen in der Ausbreitungsumgebung ein adaptives Übertragungskonzept mit hoher spektraler Effizienz umgesetzt werden, das entsprechend der aktuellen Kanalbedingungen für jeden Nutzer die geeigneten Ressourcen sowie den bestmöglichen MIMO Übertragungsmodus auswählt. Ein solches Konzept wird für den Downlink eines Frequenz-Duplex Systems entwickelt, in dem die aktuelle Kanalzustandsinformation aller beteiligten Nutzer über einen begrenzten Feedback-Kanal bereitgestellt wird. Es wird gezeigt, dass mit diesem praktikablen Konzept unter idealen Bedingungen ein hoher Anteil der theoretisch erzielbaren Kapazität des MIMO Broadcast-Kanals realisiert werden kann.

   Mit zunehmender Mobilität der Nutzer und der damit einhergehenden schnellen Änderung der Kanalzustände erfährt dieses adaptive System jedoch eine Degradation der Systemleistung. Für moderate Fahrzeuggeschwindigkeiten und eine feste Antennenkonfiguration wird eine mögliche Erweiterung des Konzeptes aufgezeigt, die auf linearer Prädiktion der Nutzerkanäle beruht. Hiermit kann eine zuverlässige Funktion der adaptiven Übertragung auch bei Mobilität aufrechterhalten werden.

3. Bei sehr hohen Geschwindigkeiten der Nutzer verletzt die durch Doppler-Effekte hervorgerufene hohe Zeitvarianz des Kanals schließlich die Orthogonalität der OFDM Unterträgersignale; es kommt zur sogenannten Inter-Carrier Interferenz (ICI). Für allgemeine Doppler Kanäle wird für den Downlink ein einfaches Verfahren entwickelt, das die ICI mit Hilfe der am Empfänger verfügbaren Mehrantennen unterdrückt. Dieses Verfahren erhält die unterträgerweise Entzerrung im OFDM System aufrecht, wodurch es einfach zu realisieren ist. Die Schätzung der ICI kann anhand von gewöhnlichen Pilotsignalen durchgeführt werden und zeichnet sich durch einen geringen Realisierungsaufwand aus.

Summary

The combination of MIMO multiple antenna technique together with OFDM multi-carrier transmission promises to achieve high spectral efficiencies while setting moderate complexity demands on transmitter and receiver structures. Furthermore, the MIMO-OFDM system concept allows to flexibly allocate the resources in time, frequency and space to different users. This dissertation addresses methods for signal transmission in multi-user MIMO-OFDM systems, which are meant to be seen as enablers for the realization of such systems in practice. The focus thereby is on an isolated cell, where a single base station communicates with multiple user terminals distributed over the cell area.

In general, practical mobile radio channels are of time-variant nature, which is attributed to movement of the user terminals or to impairments in the transmission chain. The time variance may cause severe distortions in the transmission system, limiting the spectral efficiencies achievable in practice. To get close to spectral efficiencies promised from theoretical analysis though, suitable methods to effectively overcome the degradation induced by the channel's time variance need to be found.

The dissertation is structured into three main chapters that deal with different degrees of the channel's time variance. The presented results indicate that for all cases considered, solutions with moderate complexity demands can be found which allow to achieve high spectral efficiencies in MIMO-OFDM systems also in practice. The specific content and results of the three chapters are briefly summarized in the following:

1. The simplest form of time variance in the channel is caused by a frequency offset of the signals at transmitter and receiver. Compensation of the offset-induced distortions is the task of the synchronization process. Therefore, the first chapter addresses the development of a self-contained synchronization concept for the multi-user MIMO-OFDM system, consisting of downlink and uplink. For the preamble-based downlink synchronization, the impact of frequency diversity, spatial diversity as well as of the preamble length on the synchronization performance is investigated by analytical and simulative means. If the terminals use the offset estimated in the downlink for a pre-compensation of their transmit signals during the uplink phase, the residual distortions attributed to the estimation error can be compensated directly at the base station. Based on an analysis of the signal conditions in the uplink, a simple method for this purpose is derived.

2. In the case of quasi-static conditions in the propagation environment, the channel can be considered static itself after successful synchronization. Then an adaptive transmission concept with high spectral efficiency can be realized, which selects for each user the most suitable resources as well as the best-suited MIMO transmission mode according to its current channel conditions. Such a concept is developed for the downlink of a frequency division duplex system, where the current channel state information of each user is provided via a control channel with limited feedback. It is shown that under ideal conditions, this practical approach is capable of realizing a large proportion of the theoretically achievable capacity of the MIMO broadcast channel.

   However, with increasing mobility of the users, causing the user channels to vary rapidly over time, the performance of the adaptive system degrades. For moderate vehicular speeds and for a fixed antenna configuration, a possible extension of the concept is presented, which relies on linear prediction of the user channels. Herewith, a reliable operation of the adaptive transmission concept can be maintained even under user mobility.

3. At very high user speeds, the high time variance of the channel induced by Doppler effects violates the orthogonality of the OFDM subcarrier signals, giving rise to the so-called inter-carrier interference (ICI). For general Doppler channels, we develop a simple method for the downlink, which suppresses the ICI with the aid of the multiple antennas available at the receiver. This approach maintains the subcarrier-wise equalization in OFDM, facilitating its implementation. Estimation of the ICI can be carried out based on common pilot signals by a simple method with low demands on computational complexity.

Acknowledgements

During the past years I spent at the Fraunhofer Heinrich Hertz Institute, I met excellent conditions for scientific research in a stimulating atmosphere. I am deeply obliged to thank Prof. Holger Boche for allowing me to write my dissertation as a member of his scientific staff at this facility and for being my Ph.D. advisor. Prof. Angel Lozano from the Universitat Pompeu Fabra in Barcelona accepted the second referee. I am very thankful to both of them for the fruitful discussions we had and in particular for their critical comments, that have proven invaluable to this thesis.

My gratitude goes to Volker Jungnickel, who greatly supported me in gaining a foothold in the world of scientific research. I always found in him a critical reviewer of my work, whose inspiring discussions brought me up with new ideas and helped me to keep pace with research in the outside world. My thanks further go to my colleagues Lars Thiele, Thomas Wirth and Lei Jiang for sharing room and ideas with me, which resulted in several joint publications. These thanks are extended to all my colleagues at the Heinrich Hertz Institute, the German-Sino Lab for Mobile Communications (MCI) and the Technische Universität Berlin for valuable discussions during our seminars, trips and elsewhere.

Reasonable parts of the work of this thesis were performed in the framework of different cooperation projects. Therefore, I should not forget to express my gratitude to the colleagues from our long-standing industry partner Nokia Siemens Networks as well as to the colleagues from the European WINNER project for the stimulating discussions during our project meetings and for their continuous interest in the progress of my work. Last but not least, I want to thank Howard Huang for his helpful comments and for providing material on the capacity of the MIMO broadcast channel.

I end my acknowledgements with an ode to my whole family, who spent any effort of mental support anytime. The oldest member, my grandma Mormor, stands for all of them.

Table of Contents

1 Introduction

1.1 Motivation

In the past years, multiple-antenna systems (multiple-input multiple-output (MIMO)) have gained an extraordinary interest in radio communications, as they enable to substantially increase the capacity of the radio channel. These capacity gains result from the fact that in case of multi-path propagation, the channels between different transmit and receive antenna pairs can be assumed to fade independently. Hence, the radio channel is enhanced by a spatial dimension offering additional diversity. The additional degrees of freedom provided by the spatial diversity can be used either for simultaneous transmission of independent data streams, which actually increases the achievable data rate, or for a multiplicative transmission and reception of a single data stream, which improves the overall quality of the transmission.

In systems with multiple users, the spatial dimension of the channel also enables a novel multi-user access technology, which is referred to as space-division multiple access (SDMA). In SDMA, multiple users can be served on the same time/frequency resource by overlaying spatially precoded transmission signals dedicated to different users. The transmission resources in the spatial domain are correspondingly called *spatial layers*. As we can benefit from the multi-user diversity offered in these systems, the gains in the achievable system throughput significantly exceed the ones in point-to-point MIMO links. However, for proper application of SDMA, some information on the current channel state is required at the transmitter in general, which has to be provided by adequate means.

MIMO techniques come at the price of an increased cost in computational complexity. To benefit from the capacity gains from MIMO also in broadband wireless links at reasonable costs, it is necessary to apply techniques enabling a simplified signal processing at transmitter and receiver for precoding and equalization, respectively. A potential candidate therefore is seen in the orthogonal frequency division multiplexing (OFDM) technique, which achieves this goal while at the same time enabling high spectral efficiencies. In OFDM, signals are transmitted on orthogonal subcarriers, which experience flat-fading channel conditions and can be processed individually, explaining the reasonable computational demand. Combining MIMO with OFDM yields a MIMO-OFDM system, which correspondingly offers spatial as well as frequency diversity. Transmission resources now cover the subcarriers as well as the spatial layers per subcarrier. Thanks to the inde-

pendency of the subcarriers, a flexible handling of the resources is enabled for the resource management in these systems.

The achievable throughput in MIMO-OFDM based multi-user systems has been extensively studied in the literature. To realize the throughput gains enabled from MIMO techniques in practice, it is necessary to measure the current state of the communication channel first and then to adapt the transmission technique accordingly. The full gains, however, can be obtained only under quasi-static channel conditions. Time variances experienced in the communication channel will result in degradations, as the channel may have changed when the transmission technique, which has been selected based on an earlier channel measurement, is applied. Furthermore, time variances may also distort the orthogonality of the OFDM subcarrier signals. In practical systems, time variances are introduced not only by motion of user terminals as well as moving objects in the communication environment, but also by impairments in the transmission chain. A typical impairment of this kind is a difference in the frequencies of the oscillators at transmitter and receiver, resulting in a carrier frequency offset (CFO). The challenge for practical MIMO-OFDM systems thus is to overcome the various problems resulting from time-varying channel conditions to get close to the throughput gains promised by theoretical investigations.

1.2 Contribution

The objective of this thesis is the development of practical solutions for signal transmission in multi-user MIMO-OFDM systems over time-varying channels. These solutions are considered as enablers for the realization of spectrally efficient MIMO-OFDM transmission in practice. With the buzzword "practical", we also want to emphasize that our focus lies on the realizability of the solutions in terms of system complexity. In particular, system complexity can be understood in terms of requirements on control processes as well as on hardware capabilities. To enable an implementation on hardware platforms which are already available at present or in the near future, we keep an eye on reasonable complexity demands of the proposed algorithms. Within this work, different degrees of time variance will be considered, resulting in three main subjects, each being devoted a separate chapter:

We will first address time-variant distortions resulting from impairments in the wireless transmission chain. These need to be estimated and compensated in first place to establish the orthogonality of the OFDM subcarrier signals and to enable static channel conditions in static propagation environments. The regular process of calibration between transmitter and receiver units is referred to as *synchronization*. In this work, synchronization of the downlink as well as the uplink will be investigated, where users are granted simultaneous access to all resources over space and frequency through the SDMA

technique. With the results from these investigations, we end up with a self-contained synchronization concept for the entire system.

Once all communication units are properly synchronized, a channel-adaptive transmission concept can be realized, which allows to adapt the MIMO transmission to the instantaneous conditions of the wireless channel. By beneficial application of the SDMA technique, this concept paves the way to achieve a high overall system throughput. A practical concept is first developed for quasi-static channel conditions and extended thereafter to support time-varying channel conditions resulting from vehicular movement of terminals at moderate speeds.

At higher terminal velocities, adaptation to the instantaneous channel conditions can no longer be realized, since the channel varies too rapidly to provide useful feedback. For this case, it has been proposed previously that the transmission should be adapted according to long-term channel statistics, whereby a system throughput close to the ergodic capacity of the MIMO system can be achieved. At very high velocities finally, the channel's time variance distorts the orthogonality of the OFDM subcarriers and gives rise to inter-carrier interference (ICI). For that case, it is shown that the multiple antennas of the MIMO system can be used to suppress the ICI distortions. The technique can be realized with comparatively simple means.

1.3 Notation

Vectors are denoted in bold letters $\mathbf{s}$. Matrices are written in bold capital letters $\mathbf{H}$. A single matrix element found at row a and column b is denoted as $[\mathbf{H}]_{ab}$. The transpose operator is given as $[\cdot]^T$, while conjugate transpose is $[\cdot]^H$. The inverse of a matrix $\mathbf{A}$ is denoted by $\mathbf{A}^{-1}$. trace($\mathbf{A}$) denotes the trace of matrix $\mathbf{A}$, i.e. trace$(\mathbf{A}) = \sum_{k=1}^{n}[\mathbf{A}]_{kk}$, with n the total number of diagonal elements in $\mathbf{A}$. A diagonal matrix, whose diagonal is given by the vector $\mathbf{x}$, is characterized by diag($\mathbf{x}$). The identity matrix is represented by $\mathbf{I}$. $\|\mathbf{s}\|$ is the Euclidean norm of $\mathbf{s}$, i.e. $\|\mathbf{s}\|^2 = \mathbf{s}^H\mathbf{s}$.

The real part of the complex variable x is denoted as $\Re\{x\}$, while the imaginary part is $\Im\{x\}$. $\mathbb{C}$ and $\mathbb{N}$ denote the space of complex and integer numbers, respectively. For the discrete time index, we use n, whereas we use k for the discrete frequency index. A scalar time-domain function is characterized by a small letter, $s(n)$, its corresponding frequency-domain representation by the capital letter, i.e. $S(k)$. $[\cdot]^*$ denotes conjugate operator, and $|s|^2 = ss^*$ is the absolute square of s.

The expectation operator is $E\{\cdot\}$ and means expectation with respect to time. If an index is used additionally, i.e. $E_\lambda\{\cdot\}$, expectation is with respect to the random variable λ specified in the index. Statistical processes are modeled by adequate probability density functions (pdfs). The pdfs used in this thesis are (complex) Gaussian distributions, denoted as $\mathcal{N}(m, \sigma^2)$, or chi-square distributions with n degrees of freedom, denoted as $\chi_n^2(m, \sigma^2)$. m and σ^2 refer to the mean value and the variance of the corresponding random process. In particular, for the random variable λ, $m = E\{\lambda\}$ and

$$\sigma^2 = var(\lambda) = E\{|\lambda|^2\} - (E\{\lambda\})^2$$

We assume that real and imaginary part of the complex random variables are independent and have identical mean power. Note that based on these assumptions, the sum of N squares of absolute values stemming from an independent and identically distributed (i.i.d.) complex Gaussian process with zero mean and unit variance, i.e.

$$\sum_{i=1}^{N} |x_i|^2, \quad x_i \in \mathcal{N}(0, 1) \ \forall i,$$

yields a chi-square pdf with $2N$ degrees of freedom with $m = \sigma^2 = N$, i.e. $\chi_{2N}^2(N, N)$. Further, we use the notation $a \cdot \mathcal{N}(m, \sigma^2)$ to express that a random variable with distribution $\mathcal{N}(m, \sigma^2)$ is scaled with a constant factor a. By incorporating the constant factor into the distribution, we obtain $\mathcal{N}(am, a^2\sigma^2)$. Note that this basic scaling of expectation value and variance holds for arbitrary distributions.

2 Synchronization of multi-user MIMO-OFDM systems

The crucial requirement for the convenient application of the OFDM technique is a proper synchronization of the signals at transmitters and receivers in time and frequency. In particular, the receiving station needs to know the exact beginning of an OFDM symbol, denoted as *timing*, for the correct placement of the signal window that is used for the Fourier transformation. Further, if multiple signals from different stations are transmitted simultaneously, it has to be guaranteed that these signals arrive at the receiving station at the same time. The task of aligning the signals in time is referred to as time synchronization. Correspondingly, frequency synchronization refers to an accurate frequency alignment of the signals at transmitter and receiver. This is of crucial importance, as frequency shifts of the subcarrier signals destroy their mutual orthogonality, resulting in severe degradations of the system performance [46].

The local oscillators used at different transceivers do not run at exactly the same frequency, and hence a carrier frequency offset (CFO) may be present in a communication link between any two stations. To establish a reliable data communication, this CFO has to be estimated and compensated at first before any data transmission can be initiated. The initial estimation of CFO and timing, when no prior information on these two measures is available, is denoted as the *acquisition phase*. Evidently, as estimation is never perfect, a residual CFO will remain after acquisition that will result in phase drifts of the received signal over time. Hence, a continuous phase tracking is required during the data transmission phase to estimate and compensate the residual CFO. Further, as the sampling clock is derived from the local oscillator, a sampling frequency offset (SFO) is always incurred, and thus the estimated timing may also drift over time, resulting in a timing offset (TO). Thus, tracking of this measure becomes necessary as well.

For a single antenna link between a transmitting and a receiving station (single-input single-output (SISO) system), the optimum receiver design for time-varying channel environments has been presented in [97,98]. This design is based on an analysis of the effects from insufficient synchronization on the quality of signal transmission. The work presents a comprehensive solution comprising methods for all the synchronization tasks required for the acquisition as well as the tracking phase. The basic algorithms used therein for CFO and timing estimation in the acquisition phase have been proposed in [67,89,109].

These estimation approaches rely on the correlation of a periodically transmitted signal. Common OFDM transmission employs a cyclic prefix representing a periodically extension of the last N_g signal samples of any OFDM symbol. Hence, the inherent periodicity of these OFDM signals can be utilized for the correlation, as has been done in [97, 109]. Correspondingly, the length of the correlation window covering the samples to be correlated is restricted to the length of the cyclic prefix N_g, which actually limits the achievable detection and estimation performance. However, especially in noisy environments, it may happen that the correct timing cannot be reliably detected if the correlation window is chosen too short. Thus, application of a dedicated signal with periodic properties can be desired, whose length can be adapted according to desired performance targets, as proposed in [89]. This dedicated signal is called a *preamble*, which can be designed systematically to guarantee a desired synchronization performance under predefined signal conditions. The proper design of the preamble signal will be addressed in section 2.1.2 of this chapter.

There is a variety of contributions suggesting further improvements of the synchronization techniques used for the acquisition phase; for a good overview refer to [4, 50]. To track variations of the synchronization measures during the data transmission phase, two basically different approaches exist, namely the data aided (DA) and the non-data aided (NDA) methods. While the former require pilot signals embedded into the data signal stream, the NDA methods exploit inherent properties of the OFDM signals for the estimation of the desired measures. As NDA methods do not require any additional signals that have to be known a-priori at the receiver, they are also referred to as *blind* methods. Important solutions for blind frequency tracking have been proposed by Tureli et al. [57, 106] and Boelcskei [10]. The DA methods may utilize the pilot signals dedicated to channel estimation. In general, these methods have a smaller demand on computational complexity than the NDA methods, which is one of the reasons why they are favoured for practical applications. The solutions for time and frequency tracking that are mostly applied in practice have been presented in [97, 122]; further work can be found in the review paper [50].

For MIMO systems, the common synchronization approaches have been extended to benefit from the available spatial diversity, which results from independently fading channels between different transmit/receive antenna pairs. Solutions for OFDM-based synchronization over MIMO links which significantly improve the synchronization performance have been presented in [66, 87, 99, 110]; in [33] a short overview can be found. Finally, the optimal procedures for data-aided SFO and CFO tracking in MIMO-OFDM systems have been presented in [74], which represent solutions derived from the maximum likelihood (ML) estimation approach.

In MIMO-OFDM based multi-user radio systems, we distinguish between the downlink and the uplink phase. During downlink, signals are transmitted from a single base station

(BS) to multiple receiving user terminals (UTs). The transmission scenario thus can be considered as multiple parallel links between two stations, which can be individually synchronized by the techniques summarized above. In a cellular system, however, the UTs can be assumed to be distributed over a wide area, which results in a large dynamic spread of the signal conditions characterizing the quality of the individual user links. Hence, the synchronization techniques have to be designed to enable a satisfactory operation even for worst-case conditions, i.e. when the signal conditions are very poor. Thereby, special attention has to be paid to the initial acquisition process, as a failure during this process may hamper efficient data transmission. For that reason, we focus on this process in section 2.1, where we analyze the achievable synchronization performance under specific system conditions in the low SNR regime. Thereby, we show the value of utilizing the diversity available in the system to improve the performance of the initial synchronization. The findings enable new insights into the system parameters influencing the preamble-based synchronization and deliver a framework for the proper design of the preamble signal. Together with the optimal tracking procedures for SFO and CFO from [74], the results form a consistent concept for the synchronization of the MIMO downlink in cellular systems.

The synchronization demands for the multi-user uplink of MIMO-OFDM systems are slightly different and will be addressed in section 2.2. In that section, we will carry out an analysis of the distortions evoked by CFOs from multiple users, which simultaneously access the channel in the spatial domain. Based on this analysis, a practical concept for the proper synchronization of the MIMO-OFDM uplink is finally established.

2.1 Downlink synchronization – Acquisition

During the acquisition phase of the downlink, the UTs try to detect the preamble signal transmitted by the BS to obtain a coarse estimate on the timing information and the CFO. Assuming an OFDM system with N subcarriers, the discrete time-domain signal $r(n)$ received at any UT is given as

$$r(n) = \exp(j2\pi\omega n/N) \cdot \sum_{l=0}^{L-1} h(l)s(n-l) + z(n) \tag{2.1}$$

where $s(n)$ is the transmit signal propagating over a frequency-selective channel with impulse response $h(l), l \in \{0, \ldots, L-1\}$, and $\omega = \Delta f T_s N$ is the CFO Δf normalized to the subcarrier spacing $(T_s N)^{-1}$. $z(n)$ represents the system's noise, which is modeled as a circularly symmetric complex Gaussian variable with power σ_n^2 and independent and identically distributed (i.i.d.) elements for distinct values of n. In case of an additive

white Gaussian noise (AWGN) channel, the transmission equation reduces to

$$r(n) = \exp(j2\pi\omega n/N) \cdot s(n) + z(n) \tag{2.2}$$

In the following sections, we will briefly introduce the synchronization algorithm used for the acquisition phase and advise some modifications for the preamble design. The synchronization performance will then be analyzed for the AWGN channel based on the above model. Afterwards, diversity from the frequency-selective channel as well as from the spatial MIMO channel is taken into account, and it is shown how the synchronization performance is affected. The results suggest to utilize as much diversity as possible for the synchronization. Moreover, they provide practical guidelines for a suitable preamble design.

2.1.1 Synchronization algorithm

For initial frequency synchronization, Moose [67] proposed to transmit two identical OFDM symbols of N samples length, which effectively represent a periodic signal. He showed that the ML estimator for the CFO is obtained from a correlation of these two symbols at the receiver, whose output phase corresponds to the phase difference of the samples within the two symbols. In case of a noise-free transmission over a frequency-flat channel, the phase difference amounts to $\varphi = 2\pi\omega$. Measuring this quantity allows us to directly determine the normalized CFO ω. However, due to phase ambiguities of φ, the estimation range of the CFO is limited to $-0.5 \leq \omega \leq 0.5$. Once the CFO ω has been estimated, the received signal can be compensated for the CFO distortions by multiplying it with the inverse CFO distortion function, i.e.

$$\bar{r}(n) = \exp(-j2\pi\omega n/N) \cdot r(n) \tag{2.3}$$

Van de Beek et al. [109] as well as Schmidl and Cox [89] extended Moose's approach for initial timing estimation: Based on a periodic signal with period P, van de Beek et al. showed that the ML estimator for the correct timing detection incorporates the correlator proposed by Moose. Their metric derived from the ML approach yields

$$M_{ML}(n) = |C(n)| - \rho/2 \left(Q(n-P) + Q(n) \right) \tag{2.4}$$

with

$$C(n) \;=\; \frac{1}{W} \sum_{d=0}^{W-1} r(n+d)r^*(n+d+P) \tag{2.5}$$

$$Q(n) \;=\; \frac{1}{W} \sum_{d=0}^{W-1} |r(n+d+P)|^2 \tag{2.6}$$

where $C(n)$ is the correlator, which correlates the received signal $r(n)$ with its conjugate version shifted by P samples over an observation window of length W. $Q(n)$ represents the power of the signal samples received within the observation window of size W. Further, $\rho = SNR/(SNR+1)$ represents the correlation of the two signal periods of the preamble in the received signal.

The above metric is calculated continuously for each time sample n; the ML estimate of the correct timing n_0 is obtained at the location where the metric achieves its maximum:

$$\hat{n}_0 = \arg\max_n M_{ML}(n). \tag{2.7}$$

It is evident from (2.4) that the value of the metric is always negative; its maximum thus will be very close to zero.

The ML solution operates conveniently only in case of a continuous broadcast transmission. In case of bursty transmission, where frames are transmitted in a random fashion and thus periods of silence (i.e. no signal is transmitted) may frequently occur, the ML-based timing detector is likely to generate a false alarm. Further, the ML metric requires knowledge of the correct SNR to calculate ρ. However, in a practical system this knowledge is often not available when the UT is in the acquisition stage.

To avoid these effects, the ML metric can be modified: For a large observation window W and n being near n_0, we can assume that the received power in $Q(n)$ does not change significantly over n, i.e. $Q(n-P) \approx Q(n)$ holds. The ML metric can then be written as

$$M_{ML}(n) \approx |C(n)| - \rho Q(n) = \left(\frac{|C(n)|}{Q(n)} - \rho \right) Q(n)$$

With the assumption taken for $Q(n)$ and considering that ρ is a constant, we can reduce the metric to the fractional term in the above equation for the timing metric, which corresponds to the metric introduced by Schmidl and Cox [89] and was given as

$$M_{SC}(n) = \frac{|C(n)|^2}{(Q(n))^2} \quad \in [0,1] \tag{2.8}$$

To improve the reliability of the timing detection, a threshold value $p^2 \in [0,1]$ is usually introduced, which has to be exceeded before a maximum search according to (2.7) is

carried out. The choice of p^2 directly influences the detection performance; its proper choice is addressed in section 2.1.3.

Once the correct timing n_0 is detected, the CFO estimate $\hat{\omega}$ can easily be obtained from the phase of the corresponding correlator output $C(n_0)$, which corresponds to Moose's original approach [67] for ML-based CFO estimation:

$$\hat{\varphi} = \arg(C(n_0)) = \arctan\frac{\Im\{C(n_0)\}}{\Re\{C(n_0)\}} \tag{2.9}$$

Due to the shift P used within the correlation (2.5), the true phase difference resulting from the CFO ω now corresponds to $\varphi = 2\pi\omega P/N$. Hence, the estimate of the normalized CFO can be obtained from $\hat{\varphi}$ via this latter relation. Note that the estimation range of ω is correspondingly limited to $\pm N/(2P)$ now.

Schmidl-Cox algorithm in practice The SC-metric (2.8) for timing estimation still has an inconvenient property for practical applications, as the inherent division operation that has to be carried out continuously demands a considerable amount of computational complexity. However, this operation can easily be avoided: Recall that the search for the maximum of the SC-metric over n is activated if the threshold p^2 is exceeded, i.e. if

$$\frac{|C(n)|^2}{(Q(n))^2} > p^2 \quad \Leftrightarrow \quad |C(n)| > p \cdot Q(n) \tag{2.10}$$

Reformulating the threshold criterion as given on the right hand side yields a simple comparison of $|C(n)|$ with the scaled measure $p \cdot Q(n)$. Once the threshold is exceeded, we assume that we are near the timing instant n_0, where (for large W) $Q(n)$ is not expected to vary significantly over n. Hence, for the successive search of the maximum of the SC-metric, it is sufficient to consider the measure in the enumerator of (2.8) only, i.e.

$$\hat{n}_0 = \arg\max_n |C(n)|. \tag{2.11}$$

Note that this reduced metric for synchronization in the acquisition phase was also suggested in [50]. This simplified Schmidl-Cox algorithm for timing estimation can readily be implemented in practice.

2.1.1.1 Timing estimation

For accurate detection of the timing, the correlator should cover the entire length of the preamble, i.e. the preamble length should comprise $P + W$ samples. If the noise-free preamble signal is fed into the correlator (2.5), the output signal $|C(n)|$ is denoted as the *correlation profile*. For the timing estimation, this profile is of particular importance, as it has a direct influence on the expected estimation accuracy. Recall that the timing

is detected at the time instant $n = \hat{n}_0$, where the correlator output signal $|C(n)|$ is maximum. In the noise-free case, it is found at the index where the correlation profile exhibits its peak. As the noise will result in a distortion of the original profile, it is evident that the timing estimation will be less prone to errors if the magnitude of the peak substantially differs from the magnitude of the samples surrounding this peak in the profile. We thus conclude that for a convenient timing estimation, the preamble should be designed so that the correlation profile exhibits a clearly distinguishable maximum with a sharp peak. Shaping the correlation profile according to these desired requirements has been a topic of research; in [65], for example, a preamble consisting of multiple periods that are multiplied with a sign pattern has been proposed for that purpose. However, the improved timing estimation achievable with this preamble comes at the price of a degraded CFO estimation performance according to (2.9), as the applied sign pattern introduces some interference into the CFO estimation process. Hence, it should be decided for which of the two estimation measures – timing or CFO – the higher accuracy is desired. Further below, it will be shown that the timing estimate will be biased due to the delay spread in a frequency-selective channel. Due to that effect, it is suitable to carry out a fine-timing estimation after the initial estimate, which compensates for any timing inaccuracies. Thus, we can conclude here that if a fine timing estimation is applied, we should refrain from a preamble design that improves the correlation profile at the cost of the achievable CFO estimation quality.

If the preamble signal is transmitted via a frequency-selective channel as given in (2.1), the timing according to (2.11) is detected with a shift that corresponds to the delay Δ of the strongest path gain $|h(l)|$ of the actual channel impulse response (CIR) [50]:

$$\hat{n}_0 = n_0 + \Delta, \quad \Delta = \arg\max_l |h(l)|, \quad l \in \{0, \ldots, L-1\}$$

Thus, the timing estimate is biased. Usually the cyclic prefix provides a so called backoff-zone, which is designed to accommodate (small) shifts resulting from timing estimation errors as well as from timing jitter. Hence, as long as the delay Δ does not exceed the backoff, it will not necessarily cause any problem.

However, for large values of Δ, which may occur for long CIRs, the delay should be compensated. This can be done within a fine-timing synchronization process carried out after the channel estimation that usually follows the initial synchronization. A suitable fine-timing solution was proposed in [127], which relies on a time-domain estimate of the CIR and applies a ML estimation approach for the delay Δ. This ML estimator is based on a correlation of the estimated CIR with a measure derived from the channel's power delay profile (PDP) for different delays Δ. The value of Δ yielding the minimum output of the correlator is then selected as the ML estimate. To enable practical application, the authors propose a low-complexity version of the ML estimator, which performs close

to the optimum solution. This solution is shown to clearly outperform other fine-timing algorithms that try to identify the strongest peak of the time-domain CIR, like the one proposed in [122].

As mentioned above, the method requires a suitable estimate of the total CIR. If this is not yet available, one can alternatively use the solution from [72], where a cost function constituted from the received pilot tones is minimized in an iterative fashion. The method may be especially suited in case of long CIRs when only a sparse pilot grid is provided for channel estimation, where it has been shown to operate reliably.

2.1.2 Preamble design and configuration of the correlator

In this subsection, some considerations concerning the design of the preamble used for the synchronization process are presented. Firstly, its period and its length have to be determined, which can be deduced from the requirements on the parameters P and W of the correlator (2.5). Recall that due to the phase ambiguity of the estimation parameter φ, the maximum CFO ω that can be estimated with (2.9) is limited to $\pm N/(2P)$. Hence, the parameter P should be selected small enough, so that the maximum CFO that may occur in the system can be estimated conveniently. On the other hand, the noise suppression capabilities of the correlator (2.5) improve with increasing W, and hence we desire this value to be large to achieve a convenient performance under low SNR conditions. To fulfil both requirements, it is suitable to define a preamble that is composed of multiple periods of length s, as it has been proposed in [50, 70]. This preamble signal can be correlated in two different ways, which are depicted in Fig. 2.1: Let the two functions within the correlation (2.5) be denoted as $r_1(n) = r(n+d)$ and $r_2(n) = r(n+d+P)$ for $d \in \{0, \ldots, W-1\}$. Top Fig. 2.1 shows the correlator configuration where the two fractions of the preamble signals, $r_1(n_0)$ and $r_2(n_0)$, are non-overlapping. This requires to set $W \leq P$ and corresponds to the case which is commonly considered in the literature. In contrast to that, the bottom figure shows the case where both signals overlap, i.e. $W > P$ is allowed, and correspondingly the parameters W and P can be selected independently. However, it has to be considered that in the latter case the two signals $r_i(n_0)$ contain identical noise samples, which may have an impact on the performance of the synchronization process. This question will be addressed in the following subsection, where we analyze and compare the performance of the synchronization process for both cases considered.

As already mentioned in the preceding section, the correlator should be configured to cover the entire preamble signal at the correct timing instant $n = n_0$ to obtain the peak in the correlation profile, i.e. the preamble length should amount to $P + W$. Recall that in a frequency-selective channel, the timing estimation $\hat{n}_0$ is biased, which will result in the fact that at $n = \hat{n}_0$, the correlator will cover not only signals from the preamble, but also signals from the OFDM symbol succeeding the preamble. If we carry out the phase
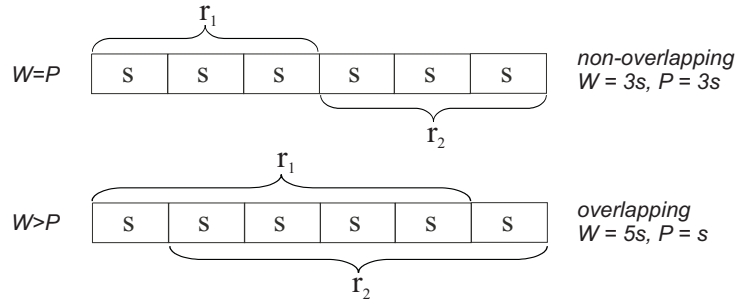
Fig. 2.1: The two modes of correlating a multi-periodic preamble.

estimation according to (2.9), these signal samples from the succeeding OFDM symbol will negatively affect the estimation of φ. To prevent this effect, it is suitable to use a second correlator for the phase estimation, which is identical to (2.5) except for the length of the correlation window W. This length should be shortened by the maximum delay Δ that may occur during timing estimation. A suitable choice in practice would be to shorten W by the length of the cyclic prefix, N_g, so that the CFO estimator yields

$$\hat{\varphi} = \arg(C'(n_0)) = \arctan \frac{\Im\{C'(n_0)\}}{\Re\{C'(n_0)\}} \quad \text{with } C'(n) = \sum_{d=0}^{W-N_g} r(n+d)r^*(n+d+P)$$

Preamble generation The preamble for the synchronization of an OFDM system with N subcarriers is usually defined in the frequency domain. To generate a periodic time-domain signal, the discrete frequency domain signal is required to have a comb structure, meaning that the subcarriers bearing the preamble signal will have a constant spacing of g subcarriers, and all others are set to zero. This will generate a time domain signal with g periods of length $s = N/g$. To take full benefit of the frequency diversity of a frequency-selective channel, a sequence with a constant amplitude is commonly used as preamble signal in frequency domain. Moreover, a constant amplitude would also be desirable in time domain to ensure a stable operation of the automatic gain control (AGC) unit. Both requirements can be satisfied by using so called CAZAC (Constant Amplitude Zero Auto-Correlation) sequences in the frequency-domain, like Frank-Zadoff-Chu sequences, as has been proposed in [20]. In case binary pseudo noise (PN) sequences shall be used for easier implementation, the above requirement can be alleviated in the sense that it will be sufficient for the preamble signal to have a low peak to average power ratio (PAPR) in time domain. Further, the preamble signal should be designed so that it generates a clearly distinguishable peak in the correlation profile. Unfortunately it is difficult to develop an analytical framework for the generation of binary PN sequence-based preamble signals that meet all the above requirements. Hence, a method chosen for practice is to limit the possible preamble signals to a confined set and carry out an exhaustive search process which is interrupted if a preamble signals exhibits the desired properties. In

particular, one can set a threshold for the desired PAPR and define a suitable criterion to discriminate the "sharpness" of the peak in the correlation profile. For all possible binary PN sequences, one can then calculate the PAPR, check the defined threshold and eventually check the properties of the correlation profile, until a suitable preamble signal has been found.

2.1.3 Analysis of the synchronization performance in AWGN channel

In this section we will analyze the performance of the synchronization algorithm for timing and CFO estimation in an AWGN channel based on the multi-periodic preamble signal introduced above for the general case $W \geq P$. Hence, the signals $r_i(n)$ may overlap, and the correlation window W spans an integer number of periods, $W = MP$ with $M \in \mathbb{N}$ (see bottom Fig. 2.1). The mean transmit power per time-domain signal sample is P_s, which holds for data transmission as well as for the preamble. According to (2.2), the signal at the receiver is distorted only by noise, which is modeled by an i.i.d. complex Gaussian process with noise power σ_n^2. The corresponding SNR thus yields SNR $= P_s/\sigma_n^2$. For our analysis, we will consider the two cases

- Transmission of preamble, i.e. $n = n_0$

- Transmission of pure data symbols

For both cases, we describe the statistical behaviour of $C(n)$ and $Q(n)$ by adequate probability density functions (pdfs). For the pdfs, we use (complex) Gaussian or chi-square distributions as introduced in section 1.3. The pdfs derived for $C(n)$ and $Q(n)$ are then used as a basis to analyze the synchronization performance. To evaluate the detection performance of the synchronization algorithm, we introduce two measures, namely the probability of a missed preamble, $p(miss)$, and the probability of a detection failure, $p(fail)$, which occurs if the detector reports a successful detection although no preamble was transmitted. Evaluation of both measures allows to determine adequate values for the threshold p as well as the observation window length W for practical employment. The quality of the CFO estimation is characterized by the variance of the estimate of phase φ.

Let the two signal parts correlated in (2.5) be denoted as

$$
\begin{aligned}
r_1(d) &= r(n+d) \\
r_2(d) &= r(n+d+P), \quad d \in \{0, \dots, W-1\}
\end{aligned}
$$

Let $R_i(k)$ be the frequency representations of $r_i(d)$, obtained from a W-point discrete Fourier transform (DFT). With Parseval's theorem, $C(n)$ and $Q(n)$ from (2.5) and (2.6)

can be rewritten as

$$C(n) = \frac{1}{W} \sum_{k=0}^{W-1} R_1(k) R_2^*(k) \tag{2.12}$$

$$Q(n) = \frac{1}{W} \sum_{k=0}^{W-1} |R_2(k)|^2 \tag{2.13}$$

2.1.3.1 Transmission of preamble

We will first assume that the correlation covers the received preamble, i.e. $n = n_0$. Without loss of generality, we assume that the CFO is zero and thus there is no phase difference between the received signals $R_1(k)$ and $R_2(k)$, i.e. $\varphi = 0$. Then

$$R_i(k) = S(k) + Z_i(k),$$

where $Z_i(k) \sim \mathcal{N}(0, \sigma_n^2)$ is the noise at frequency position k. As $W = MP$, the frequency-domain preamble signal $S(k)$ has a comb structure, where solely each Mth frequency position differs from zero. At these positions, $S(k)$ has a constant amplitude of $\sigma_s = \sqrt{MP_s}$ (constant amplitude preamble sequence). Due to the shift of one signal period P between $r_1(d)$ and $r_2(d)$, both signals contain the same fraction of the preamble signal, and hence $S(k)$ is identical in both signals $R_i(k)$. The two signals $R_i(k)$ thus only differ by the noise contained in $Z_i(k)$.

Statistical model for the correlator $C(n_0)$ According to its comb structure, the frequency domain preamble signal $S(k)$ consists of P non-zero signals at the frequency positions $k \in \{0, M, 2M, \ldots, (P-1)M\}$. With this finding, we may separate the correlation signal (2.12) into three components:

$$C_1 = \frac{1}{W} \sum_{k=0}^{P-1} |S(Mk)|^2 = \frac{P}{W} \sigma_s^2 = P_s \tag{2.14}$$

$$C_2 = \frac{1}{W} \sum_{k=0}^{P-1} S(Mk) \cdot Z_2^*(Mk) + Z_1(Mk) \cdot S^*(Mk) \tag{2.15}$$

$$C_3 = \frac{1}{W} \sum_{k=0}^{W-1} Z_1(k) \cdot Z_2^*(k) \tag{2.16}$$

For $W > P$, the noise samples contained in the signals $r_1(d)$ and $r_2(d)$ are partially identical, yielding a correlation of the noise $Z_1(k)$ and $Z_2(k)$. This correlation can be exposed by calculating the cross-correlation function of the two time-domain noise signals. Let $z_i(d)$, $d \in \{0, \ldots, W-1\}$, be the time-domain noise signals corresponding to $Z_i(k)$, which in fact represent the noise samples contained in the ith reception signal $r_i(d)$. The

periodic cross-correlation function $\theta_{z_1 z_2}(n)$ of the two signals $z_1(d)$ and $z_2(d)$ is calculated according to

$$\theta_{z_1 z_2}(n) = E\left\{\sum_{d=0}^{W-1} z_1^*(d) z_2([d+n] \bmod W)\right\} = (W-P)\sigma_n^2 \cdot \delta(n+P)$$

where mod denotes the modulo function. For a shift $n = -P$, the signals $z_1(d)$ and $z_2([d+n] \bmod W)$ are partially identical, and thus we yield expression based on the Dirac function on the right hand side. Transforming the cross-correlation function to the frequency domain yields the cross-power density function [75]

$$\Theta(k) = E\left\{Z_1^*(k)Z_2(k)\right\} = \underbrace{\frac{W-P}{W}}_{\rho} \sigma_n^2 \exp\left(j2\pi\frac{k}{M}\right)$$

As the $Z_i(k)$ are both assumed to be complex Gaussian with zero mean, $\Theta(k)$ also characterizes the covariance $cov(Z_1, Z_2)$ of the two random variables, and ρ thus represents the absolute value of the corresponding correlation coefficient. With this measure, we can model the distribution of the conditioned probability $p(Z_2|Z_1)$ by using theorem 10.1 in [49]: As Z_1 and Z_2 are complex Gaussian random variables, $p(Z_2|Z_1)$ is complex Gaussian as well with mean and variance given as:

$$
\begin{aligned}
E\{Z_2|Z_1\} &= E\{Z_2\} + \frac{cov(Z_1, Z_2)}{var(Z_1)}(Z_1 - E\{Z_1\}) = \rho \cdot \exp\left(j2\pi\frac{k}{M}\right)Z_1 \\
var(Z_2|Z_1) &= var(Z_2) - \frac{cov^2(Z_1, Z_2)}{var(Z_1)} = (1 - \rho^2)\sigma_n^2
\end{aligned}
$$

where $var(a)$ denotes the variance of the random process a and $E\{a\}$ corresponds to its mean value. Hence, if Z_1 is given, Z_2 can be modeled by

$$Z_2 = \rho \cdot \exp(j2\pi k/M)Z_1 + X \quad \text{with } X \sim \mathcal{N}(0, (1 - \rho^2)\sigma_n^2) \tag{2.17}$$

where Z_1 and X are random variables which are fully uncorrelated and thus independent now. We will use this model in the following, where we derive the pdfs for the signal components C_2 and C_3 from (2.15) and (2.16).

Note that C_1 is the useful signal that generates the peak value in $C(n)$ we intend to detect, which is strictly real-valued. Following the argument from [89], this useful signal will be affected mainly by the real dimension of the distorting terms C_2 and C_3 for sufficiently large W. Hence, we will derive separate pdfs for the real and imaginary parts of C_2 and C_3.

To account for the correlation of the noise in C_2, we substitute Z_2 in (2.15) by (2.17). At the frequency positions considered, the complex factor from (2.17) equals $\exp(j2\pi k) = 1$

and thus vanishes. For a fixed frequency position Mk, the signal components in (2.15) can be given by (for notational convenience, we omit the index Mk here):

$$
\begin{aligned}
SZ_2^* + Z_1 S^* &= S(\rho Z_1 + X)^* + Z_1 S^* \\
&= 2\rho \Re\{SZ_1^*\} + (1 - \rho)Z_1 S^* + SX^* \\
&= (1 + \rho)\Re\{SZ_1^*\} + (1 - \rho)\Im\{Z_1 S^*\} + SX^*
\end{aligned}
$$

Neglecting all imaginary parts, the real-valued signal fraction amounts to

$$
(1 + \rho)\Re\{SZ_1^*\} + \Re\{SX^*\}
$$

With the obtained results, the real-valued components of C_2 can now be given as

$$
\Re\{C_2\} = \frac{1}{W}\sum_{k=0}^{P-1}(1 + \rho)\Re\{S(Mk)Z_1^*(Mk)\} + \frac{1}{W}\sum_{k=0}^{P-1}\Re\{S(Mk)X^*(Mk)\} \tag{2.18}
$$

Both sum expressions represent sums of i.i.d. Gaussian variables, and hence each sum can be modeled by a Gaussian process itself, whose mean and variance is constituted from the sum of mean values and variances of the individual processes. Correspondingly, the first sum term, denoted as sum1, will yield zero mean and a variance of

$$
var(\text{sum1}) = 0.5\frac{(1 + \rho)^2}{W^2} \cdot P\sigma_s^2\sigma_n^2 = 0.5(1 + \rho)^2 P_s\sigma_n^2/W
$$

where we assumed that the total power of the random process will be contained to equal shares in the imaginary and the real component of the complex value $S(Mk)Z_1^*(Mk)$. The second sum term, sum2, yields zero mean as well and a variance of

$$
var(\text{sum2}) = 0.5\sigma_s^2\sigma_x^2 P/W^2 = 0.5(1 - \rho^2)P_s\sigma_n^2/W
$$

where $\sigma_x^2 = (1 - \rho^2)\sigma_n^2$ is the variance of the random variable X given in (2.17), which yields the expression on the right hand side. As the variables X and Z_1 are both independent, the two Gaussian distributions characterizing sum1 and sum2 can be merged to one, so that we yield

$$
\Re\{C_2\} \sim \mathcal{N}\left(0, (1 + \rho)P_s\sigma_n^2/W\right) \tag{2.19}
$$

We observe that a noise correlation $\rho > 0$ increases linearly the variance of $\Re\{C_2\}$. In a similar way, we can derive the pdf for the imaginary component of C_2, resulting in

$$
\Im\{C_2\} \sim \mathcal{N}\left(0, (1 - \rho)P_s\sigma_n^2/W\right)
$$

Interestingly, the variance of $\Im\{C_2\}$ differs from the one of $\Re\{C_2\}$ in the sign of the term depending on ρ, i.e. the variance decreases for $\rho \neq 0$ here.

Next, we turn to the signal component C_3. Plugging (2.17) into (2.16) yields

$$C_3 = \frac{1}{W} \sum_{k=0}^{W-1} \rho |Z_1(k)|^2 \exp\left(j2\pi\frac{k}{M}\right) + \frac{1}{W} \sum_{k=0}^{W-1} Z_1(k)X^*(k) \qquad (2.20)$$

In the following, the two sums will be modeled separately. The first sum term, denoted as sum3, consists of absolute squares of the Gaussian variable $Z_1(k)$, weighted by the complex factor $\exp(j2\pi k/M)$. This sum can be partitioned as follows:

$$\text{sum3} = \frac{\rho}{W} \sum_{k=0}^{M-1} \exp\left(j2\pi\frac{k}{M}\right) \sum_{l=0}^{P-1} |Z_1(kl)|^2$$

From this partitioning, we see that we can model the statistics of sum3 by M independent chi-square distributions with $2P$ degrees of freedom, $\sigma_n^2 \cdot \chi_{2P}^2(P, P)$, where each of these distributions is weighted with the factor $\rho/W \cdot \exp(j2\pi k/M)$, $k \in \{0, \ldots, M-1\}$. As we consider W (and thus also P) to be large, we can use the central limit theorem and model the chi-square distributions as Gaussians with identical mean and variance. As the M single distributions are i.i.d., we can merge them to one global Gaussian, whose mean and variance are constituted from the sum of the mean values and variances from the M single distributions. This yields

$$E\{\text{sum3}\} = \frac{\rho}{W} \sum_{k=1}^{M} \exp\left(j2\pi\frac{k}{M}\right) \sigma_n^2 \cdot P = 0$$

$$var(\text{sum3}) = \frac{\rho^2}{W^2} \sum_{k=1}^{M} \sigma_n^4 \cdot P = \rho^2 \sigma_n^4 / W$$

The second sum in (2.20), sum4, represents a sum of W products of two Gaussian variables. In general, this sum has no longer Gaussian properties itself; however, if W is sufficiently large, we can use the central limit theorem again to model it as a Gaussian with zero mean and variance

$$var(\text{sum4}) = \sigma_n^2 \sigma_x^2 / W = (1 - \rho^2)\sigma_n^4 / W$$

As the two sums constituting C_3 in (2.20) are based on the independent variables Z_1 and X, the corresponding Gaussian processes used to model sum3 and sum4 can be considered to be mutually independent. Therefore, we can merge these two Gaussian distributions into one. As we have to separate C_3 into its real and imaginary components again, note that sum3 is strictly real-valued for $M = 2$, whereas the power in the real and imaginary components is approximately balanced for $M > 2$ only. Hence, we yield

for the distributions of the real and imaginary component of C_3

$$\Re\{C_3\} \sim \Im\{C_3\} \sim \mathcal{N}(0,\, 0.5\sigma_n^4/W) \quad \text{for } M > 2 \tag{2.21}$$

We observe that the correlation does not show any influence on the distortion term C_3 if $M > 2$, as the characterizing pdf is independent of the correlation coefficient ρ.

Finally, the models for C_1 to C_3 can be merged to form a compound pdf for the correlation function $C(n)$: Note that the two Gaussians C_2 and C_3 are uncorrelated, which can easily be shown by computing their covariance yielding $cov(C_2, C_3) = 0$. Hence, the compound pdf for the correlation function can be given as a Gaussian, whose mean and variance are constituted from the sum of the corresponding measures of the Gaussians characterizing C_1 to C_3 given in (2.14), (2.19) and (2.21). The statistical properties of the correlation function $C(n)$ for $n = n_0$ and $M > 2$ can thus be characterized according to

$$\Re\{C(n_0)\} \sim \mathcal{N}\left(P_s,\, ((1+\rho)P_s + 0.5\sigma_n^2)\sigma_n^2/W\right) \tag{2.22}$$

$$\Im\{C(n_0)\} \sim \mathcal{N}\left(0,\, ((1-\rho)P_s + 0.5\sigma_n^2)\sigma_n^2/W\right) \tag{2.23}$$

Finally, we have found Gaussian pdfs to characterize the statistical behaviour of real and imaginary part of the correlator output at time instant $n = n_0$. To allow an analysis of the detection performance based on these results, we need a similar statistical model for the power term $Q(n_0)$, which is derived in the succeeding paragraph.

Statistical model for the power term $Q(n_0)$ In a similar way as done above, we can deduce a statistical model for the power term $Q(n_0)$ from (2.13). We first separate the signal into three components:

$$Q_1 = \frac{1}{W} \sum_{k=0}^{P-1} |S(Mk)|^2 = \frac{P}{W}\sigma_s^2 = P_s \tag{2.24}$$

$$Q_2 = \frac{1}{W} \sum_{k=0}^{P-1} 2\Re\{S(Mk) \cdot Z_2^*(Mk)\} \tag{2.25}$$

$$Q_3 = \frac{1}{W} \sum_{k=0}^{W-1} |Z_2(k)|^2 \tag{2.26}$$

By using the same arguments from the preceding paragraph, Q_2 can be modeled as a Gaussian with parameters

$$Q_2 \sim \mathcal{N}(0,\, 2P_s\sigma_n^2/W)$$

Q_3 should be modeled by a chi-square distribution with $2W$ degrees of freedom, yielding

$$Q_3 \sim \sigma_n^2/W \cdot \chi_{2W}^2(W,\, W)$$

For large W, the chi-square distribution approaches with the central limit theorem a Gaussian, which can be parameterized according to

$$Q_3 \sim \mathcal{N}(\sigma_n^2,\, \sigma_n^4/W)$$

All three components Q_1 to Q_3 are uncorrelated, as their covariance evidently yields zero; hence we can merge the pdfs of the three components to one Gaussian, which is given as

$$Q(n_0) \sim \mathcal{N}(P_s + \sigma_n^2,\, (2P_s + \sigma_n^2)\sigma_n^2/W) \tag{2.27}$$

With the expression found, the statistical behaviour of the power term $Q(n_0)$ can also be characterized by a simple Gaussian pdf. Together with the results found in the preceding paragraph, an analytical expression for the probability of a detection miss, $p(miss)$, can be derived. However, before doing so, we briefly examine the statistical behaviour for $C(n)$ and $Q(n)$ in case pure data symbols have been transmitted, providing the basis to derive the corresponding analytical expressions for the probability of a detection failure, $p(fail)$.

2.1.3.2 Transmission of pure data symbols

Now we consider the case that the synchronization algorithm is applied to an OFDM signal containing arbitrary data symbols. We assume that all subcarriers are occupied with i.i.d. complex data signals with mean power P_s, that follow a Gaussian-like distribution with zero mean. Hence, the signal $R_i(k)$ contained in (2.12) reads

$$R_i(k) = S_i(k) + Z_i(k)$$

where $S_i(k)$ represents the signal proportion devoted to the data symbols, and $Z_i(k)$ is the contribution from the noise. With the assumptions from above, $S_i(k)$ is non-zero for all k and has a Gaussian-like distribution with mean power P_s. As $Z_i(k)$ is a Gaussian as well with $Z_i(k) \sim \mathcal{N}(0,\, \sigma_n^2)$, which is independent of $S_i(k)$, we can model $R_i(k)$ as a single Gaussian according to

$$R_i(k) \sim \mathcal{N}(0,\, P_s + \sigma_n^2)$$

Thus, the signal $R_i(k)$ can be treated similarly like an AWGN source with power $P_s + \sigma_n^2$. With this model, it is easy now to derive the adequate pdfs for correlation (2.12) and

power term (2.13): With the Gaussian model for $R_i(k)$, the statistical behaviour of the correlation term (2.12) is equivalent to the one of component C_3 given in (2.16). Hence, the corresponding pdf can be derived equivalently and yields a similar result as for C_3 according to (2.21), where only the power σ_n^2 of the Gaussian $Z_i(k)$ needs to be substituted by the power $P_s + \sigma_n^2$ of the Gaussian $R_i(k)$:

$$C(n) \sim \mathcal{N}(0, (P_s + \sigma_n^2)^2/W) \tag{2.28}$$

In contrast to the former case $n = n_0$, there is no useful signal here allowing us to restrict our considerations on a single dimension of the complex signal space for the distortions. Hence, the entire signal power influences the statistical behaviour of $C(n)$ here.

Correspondingly, the statistical behaviour of the power term (2.13) is equivalent to the one of component Q_3 given in (2.26), and by adopting the way of deriving the adequate pdf we yield

$$Q(n) \sim \mathcal{N}(P_s + \sigma_n^2, (P_s + \sigma_n^2)^2/W) \tag{2.29}$$

Note that $C(n)$ in (2.28) is totally independent of the correlation ρ, which means that performing the correlation (2.5) with overlapping or non-overlapping signals does not affect the statistical behaviour of $C(n)$ in case pure data signals are correlated.

2.1.3.3 Performance analysis and comparison with simulations

Based on the pdfs found in the preceding sections, we formulate in this subsection the analytical expressions for the detection performance in terms of

1. the probability of a missed preamble, $p(miss)$

2. the probability of a detection failure, $p(fail)$

By a numerical evaluation of the expressions, we will show how adequate values for the parameters W and the threshold p can be found. The performance of the estimation of φ is determined by deriving an analytical expression for the estimation variance. All results are finally compared with simulations for verification.

Probability of a missed preamble   Let $C_a = |C|$ be the absolute value of the correlation (2.5). Further, let $f_{hit,c}(C_a)$ and $f_{hit,q}(Q)$ be the pdf of $C_a(n_0)$ and the pdf of the power term $Q(n_0)$, respectively. Evidently, $f_{hit,q}(Q)$ is given by (2.27). By comparing (2.22) and (2.23), it can be noted that for large W, the real component $\Re\{C(n_0)\}$ clearly dominates the imaginary component and thus $C_a = |C| \approx \Re\{C\}$ may be used. Hence, we have

$$f_{hit,c}(C_a) = \mathcal{N}\left(P_s, ((1+\rho)P_s + 0.5\sigma_n^2)\sigma_n^2/W\right) \tag{2.30}$$

$$f_{hit,q}(Q) = \mathcal{N}(P_s + \sigma_n^2, (2P_s + \sigma_n^2)\sigma_n^2/W) \tag{2.31}$$

According to the detection criterion (2.10), the preamble can be detected if the absolute value of the correlator $C_a(n_0)$ exceeds the threshold given by $p \cdot Q(n_0)$. Hence, given a power value of Q, the probability to miss the preamble can be calculated by the expression

$$p(C_a < pQ) = \int_{-\infty}^{pQ} f_{hit,c}(C_a|Q)dC_a$$

Note that C_a is in general correlated with Q, and hence we have to consider the conditional probability $f_{hit,c}(C_a|Q)$ within the integral. The proper pdf for this conditioned probability is derived further below. By averaging over all possible values for Q according to its pdf $f_{hit,q}(Q)$, we obtain the probability of a detection miss according to

$$p(miss) = \int_0^\infty f_{hit,q}(Q) \int_\infty^{pQ} f_{hit,c}(C_a|Q)dC_a \, dQ \qquad (2.32)$$

The conditional pdf $f_{hit,c}(C_a|Q)$ can be derived by using Theorem 10.1 from [49] again: As we modeled the two variables C_a and Q as Gaussians, the conditional pdf $f_{hit,c}(C_a|Q)$ can be modeled as a Gaussian as well with mean and variance given as

$$E\{C_a|Q\} = E\{C_a\} + \frac{cov(C_a, Q)}{var(Q)}(Q - E\{Q\})$$
$$var(C_a|Q) = var(C_a) - \frac{cov^2(C_a, Q)}{var(Q)} \qquad (2.33)$$

To proceed further, we need the covariance of the two measures, $cov(C_a, Q)$, which is defined as [49]

$$cov(C_a, Q) = E\{C_a \cdot Q^*\} - E\{C_a\} \cdot E\{Q\}$$

Recalling the separation of the two measures into three components according to (2.14)-(2.16) and (2.24)-(2.26), respectively, we may write

$$cov(C_a, Q) = E\{\Re\{C_1 + C_2 + C_3\} \cdot (Q_1^* + Q_2^* + Q_3^*)\} - P_s \cdot (P_s + \sigma_n^2) \qquad (2.34)$$

The product within the brackets of the expectation operator yields a sum of 9 single terms representing all possible pairings of the components $\Re\{C_i\}$ and Q_i. For each of these terms, expectation can be determined separately. Analysis of the single terms can be carried out in a way similar as done in the preceding subsection; hence, we will skip the details of this analysis and proceed directly with the results: It turns out that there are only three pairings that yield a non-zero expectation value; in particular these are $E\{\Re\{C_1\}Q_1^*\}$, $E\{\Re\{C_2\}Q_2^*\}$ and $E\{\Re\{C_1\}Q_3^*\}$. Further,

$$E\{\Re\{C_1\}Q_1^*\} + E\{\Re\{C_1\}Q_3^*\} = P_s^2 + P_s \cdot \sigma_n^2$$

As this expression is equivalent to the constant term given at the end of equation (2.34), the covariance finally yields

$$cov(C_a, Q) = E\{\Re\{C_2\}Q_2^*\} = (1 + \rho)P_s\sigma_n^2/W$$

Inserting this expression into (2.33) and using the mean values and variances for C_a and Q from (2.30) and (2.31), we obtain for the mean and the variance of the conditional pdf $f_{hit,c}(C_a|Q)$

$$E\{C_a|Q\} = -\rho P_s + \frac{(1 + \rho)P_s}{2P_s + \sigma_n^2}(Q + P_s)$$

$$var(C_a|Q) = \frac{\sigma_n^2}{(2P_s + \sigma_n^2)W}\left((1 - \rho^2)P_s^2 + (2 + \rho)P_s\sigma_n^2 + 0.5\sigma_n^4\right)$$

With this result, we can now evaluate (2.32) and determine the probability of a missed preamble depending on W, ρ and the SNR P_s/σ_n^2.

Probability of a detection failure Now we consider the case where pure OFDM data signals have been transmitted. Recall the distributions for this case given in (2.28) and (2.29):

$$C(n) \sim (P_s + \sigma_n^2) \cdot \mathcal{N}(0, 1/W)$$
$$Q(n) \sim (P_s + \sigma_n^2) \cdot \mathcal{N}(1, 1/W)$$

The representation used here reveals that the power term $(P_s + \sigma_n^2)$ takes the role of a simple scaling of the random variable $C(n)$ and $Q(n)$, respectively. This means that the power level does actually not change the statistical properties of both variables, and hence we can conclude here that the probability of a detection failure will be independent of the power level and thus the SNR conditions.

For the analytical expression of the probability of a detection failure, we will thus omit the scaling factors in the above pdfs. Let $f_{dat,q}(Q)$ denote the (unscaled) pdf of the power term $Q(n)$, which is now

$$f_{dat,q}(Q) = \mathcal{N}(1, (1/W)$$

The measure $C_a = |C|$ requires the absolute value of the complex Gaussian $C(n)$. Instead of determining the appropriate distribution for C_a, we choose to use $C_{a2} = |C|^2$, which can be modeled by a chi-square distribution with 2 degrees of freedom. Based on the Gaussian model from above without the scaling factor, $C(n) \sim \mathcal{N}(0, 1/W) = \sqrt{1/W} \cdot \mathcal{N}(0, 1)$, we obtain

$$C_{a2} \sim 1/W \cdot \chi_2^2(1, 1) = f_{dat,c}(C_{a2})$$

As we use $C_{a2} = |C|^2$ now, the threshold from (2.10) has to be adapted to p^2Q^2. Given a

power value Q, the probability of a detection failure can be characterized by the expression

$$p(C_{a2} > p^2 Q^2) = \int_{p^2 Q^2}^{\infty} f_{dat,c}(C_{a2}) dC_{a2}$$

Averaging over all possible Q finally yields the overall probability of a detection failure

$$p(fail) = \int_{0}^{\infty} f_{dat,q}(Q) \int_{p^2 Q^2}^{\infty} f_{dat,c}(C_{a2}) dC_{a2} dQ \qquad (2.35)$$

In contrast to (2.32), $f_{dat,c}(C_{a2})$ is not conditioned on Q here, as both variables C_{a2} and Q are claimed to be statistically independent. We substantiate this claim by noting that the variables $C(n)$ and $Q(n)$ are uncorrelated in case of pure data transmission, as their covariance yields zero. To confirm this, recall that it was shown in the subsection "Transmission of pure data symbols" that C and Q could be modeled like the terms C_3 and Q_3 from (2.16) and (2.26), respectively. It is easy to show that the expectation of $E\{C_3 \cdot Q_3^*\}$ yields zero, which thus also holds for the covariance $cov(C, Q)$ in case of pure data transmission. Although this note is not sufficient to prove statistical independence of C_{a2} and Q here (as C_a is non-Gaussian), we will see in the evaluation section that the analyzed performance is quite close to the simulated one, and hence (2.35) can be used as a suitable analytical characterization of the probability of a detection failure.

Detection performance Fig. 2.2 illustrates the numerical evaluation of (2.32) and (2.35) versus the threshold p for a fixed SNR of 0 dB and different values for W and ρ, respectively. The selected SNR may serve as a reference for cell-edge users in a cellular system, which usually experience worst SNR conditions. As it has to be ensured that the synchronization process works reliably also for these users, we focus on this SNR within our investigations here.

For $p(miss)$, we observe that for a fixed correlation window length W, $\rho \neq 0$ degrades the detection performance only slightly. This degradation seems to become less significant for increasing correlation window length W. Considering that the choice of overlapping correlation signals allows to choose a larger correlation window W independent of the correlation shift P, this is a clear argument in favour of overlapping correlation signals and thus of using a multi-periodic preamble.

To determine a suitable threshold value p, we can use the intersection point of the two probability curves related to a given parameter set W and ρ, where simultaneously the smallest values for both probability measures $p(miss)$ and $p(fail)$ are yield. For the parameter sets considered here, all intersection points are located in close vicinity near $p = 0.3$, hinting for the fact the threshold value may not strongly depend on the selected system parameters. It is clearly seen that both probabilities drop with increasing correlation window length W, emphasizing the capabilities for efficient noise suppression
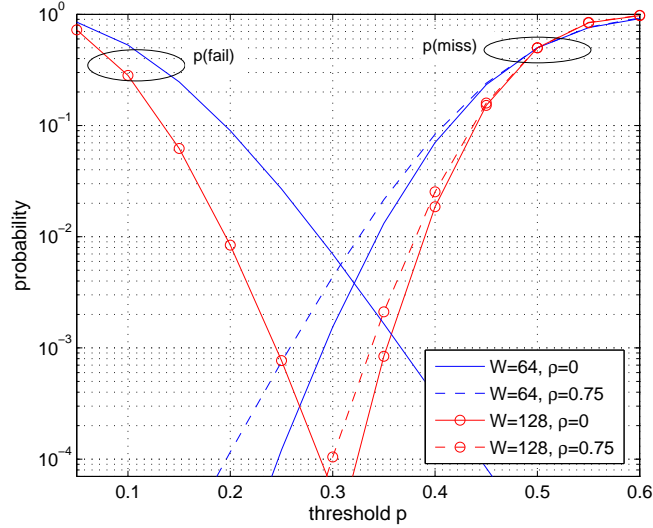
Fig. 2.2: Probability of detection failure $p(fail)$ and of missed preamble $p(miss)$ versus threshold p at SNR $=0$ dB. Analytical results in AWGN channel.

of the correlator. Hence, the adequate choice of W can be taken according to a desired detection performance that should be achieved at a given SNR operating point.

In Fig. 2.3 we compare the results from analysis with simulations for a correlation window length of $W = 64$. For $\rho = 0.75$, we use a multi-periodic preamble that has been designed according to the requirements stated in section 2.1.2. It is composed of 5 periods of length $s = 16$ samples. Correspondingly, the correlator is configured to $P = s$ and $W = 4s$, as shown in bottom Fig. 2.1. For $\rho = 0$, the preamble spans 128 samples, and the correlator is configured to $W = P = 64$. We observe that the analytical curves for $p(miss)$ are quite close to the simulated ones, however, analytical results are slightly worse. This can be attributed to the approximation we have used within the analysis; in particular using $|C(n_0)| \approx \Re\{C(n_0)\}$ and approximating the distribution of C_3 in (2.16) and Q_3 in (2.26) by a Gaussian.

Similar relations can be observed for $p(fail)$, however, the difference between simulated and analytical curves is slightly larger than in the former case. Unlike the analytical case, where ρ was shown to have no impact on the probability $p(fail)$, we further observe a slight difference of the simulated curves for $\rho = 0$ and $\rho = 0.75$: The latter shows a slightly improved performance compared to $\rho = 0$. As above, we may conclude that these deviations from the analytical case can be attributed to the approximation we used within the analysis. In particular, note that Q according to (2.29) is originally composed of pure chi-square distributions, but has been modeled by a global Gaussian. In this modeling, we can also find a reason why the deviation from the analytical curve is larger than in case of $p(miss)$: For this measure, we also used a Gaussian distribution to model Q according to (2.27), while it originally is composed of a mixture of Gaussians from Q_2 and chi-square distributions from Q_3. However, due to this mixture, the overall distribution
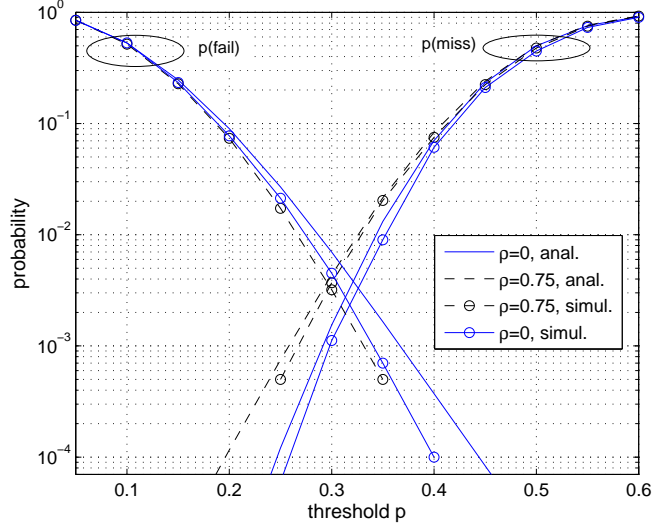
Fig. 2.3: Comparison of the analytical detection performance with simulation results at SNR = 0 dB, $W = 64$. AWGN channel.

can be expected to be closer to a Gaussian than the original distribution of Q affecting $p(fail)$. Thus, deviations between analyzed and simulated results for $p(miss)$ are smaller finally.

Fig. 2.4 depicts the analytical and simulated detection performance in terms of $p(miss)$ versus the SNR for a constant threshold $p = 0.3$. We observe that the curves exhibit a steep slope over the SNR, which lies at about one decade per dB near SNR = 0 dB – which is the operating SNR that has been used to determine the adequate values for p and W in the preceding figure. This clearly suggests that the detection performance degrades significantly if the synchronization process is operated in an SNR range below the one it has been configured for. We further observe similar differences between the curves for different ρ as in the preceding figure. Simulation again confirm close correspondence with analytical results.

Performance of the phase estimation   As the estimation error of φ is independent of its actual value, we will derive the variance of the estimate of φ based on the analytical results from above, where we assumed no CFO to be present, i.e. $\varphi = 0$. Note that for this case, the estimation error $\Delta\varphi$ corresponds to the estimated phase according to (2.9).

We assume the error to be small, and hence we can use the approximation $\arctan(x) \approx x$, which means neglecting the arctan operator. From (2.9), we now have

$$\Delta\varphi = \frac{\Im\{C(n_0)\}}{\Re\{C(n_0)\}} \tag{2.36}$$

The statistics of denominator and enumerator can be modeled by the Gaussian distributions given in (2.22) and (2.23). Note that the mean of the denominator is much
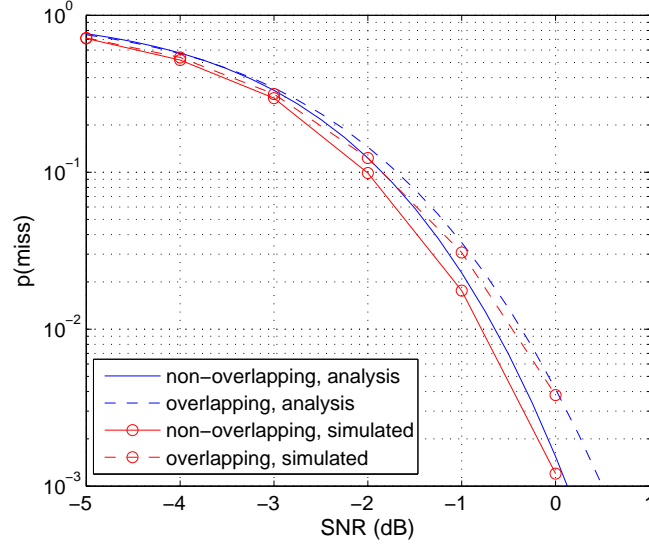
Fig. 2.4: Probability of missed preamble versus SNR for constant threshold $p = 0.3$ in AWGN channel. $W = 64$

larger than its variance for large W, and hence we can expect that this variance will not significantly impact the variance of $\Delta\varphi$. Correspondingly, it will suffice to reduce the denominator solely to its constant mean value P_s and thus limiting the variance of the CFO estimate to the one of the enumerator. We thus obtain

$$\Delta\varphi \sim P_s^{-1} \cdot \mathcal{N}\left(0, \left((1-\rho)P_s + 0.5\sigma_n^2\right)\sigma_n^2/W\right)$$

Incorporating the constant factor P_s^{-1} into the variance of $\Delta\varphi$ yields

$$var(\Delta\varphi) = \frac{\left((1-\rho)P_s + 0.5\sigma_n^2\right)\sigma_n^2}{P_s^2 \cdot W} = \frac{P \cdot P_s\sigma_n^2 + 0.5W\sigma_n^4}{W^2 \cdot P_s^2} \tag{2.37}$$

For high SNR, the influence of the term depending on σ_n^4 can be neglected. In this case, the above analytical expression for $\rho = 0$ is identical to the variance derived in [67]. From our result, a very interesting conclusion can be drawn: We observe that with increasing correlation ρ, the variance of the estimation error decreases. Hence, using overlapping correlation signals clearly enhances the quality of the CFO estimate. On the right hand side of equation (2.37), we substituted $\rho = (W - P)/W$. This relation further reveals that if we increase the length of the correlation window W while keeping the correlation period P fixed, the variance of the estimation error improves proportional to the square of W at high SNR.

In Fig. 2.5 we compare the analytical results for the CFO estimation performance with simulated ones for different lengths W versus the SNR. We observe that the variance derived in (2.37) exactly matches the simulated one for an SNR ≥ 0 dB. Below this SNR, the simulated result diverges from the analyzed one, which is due to the fact that
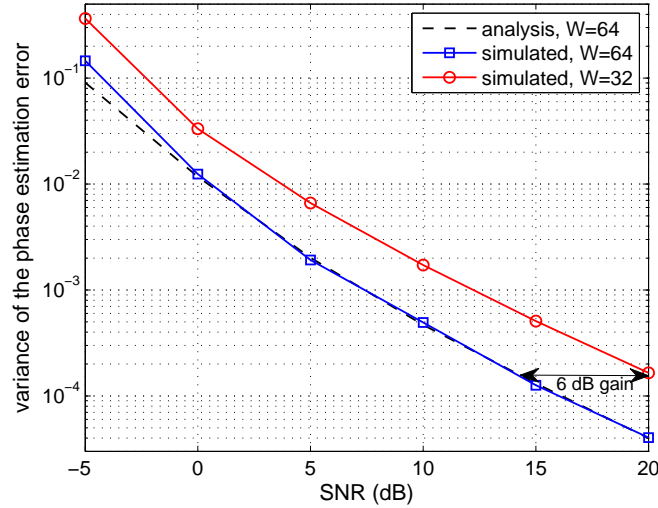
Fig. 2.5: Variance of the phase estimation error versus SNR for overlapping correlation
signals in AWGN channel. Constant correlation period $P = 16$.

the variance of the denominator in (2.36) may no longer be neglected. We also observe
clearly a performance gain of 6 dB at high SNR if we compare the estimation performance
for $W = 32$ and $W = 64$, i.e. doubling the length W indeed delivers a performance gain
of factor 4.

Based on all the results found in this subsection, we conclude that it is beneficial to
use a multi-periodic preamble for the initial synchronization of OFDM systems with a
total length of $P + W \geq 4P$ samples.[1] This does not only enable a significantly improved
CFO estimation performance, but it also allows to select the parameters W and P of the
correlator (2.5) independently, enabling an efficient utilization of the preamble for the
synchronization purpose.

2.1.4 Signal conditions in the frequency-selective channel

While we analyzed the signal conditions for the synchronization process in an AWGN
channel in the preceding section, we will now turn our focus on the frequency-selective
fading channel. If the frequency-domain preamble sequence $S(k)$ spans multiple coherence
bandwidth intervals of the channel, the synchronization process benefits directly from the
frequency diversity of the channel. With increasing degree of frequency diversity pro-
vided by the channel, we show that the signal conditions for the synchronization process
approach the ones experienced in an AWGN channel. Hence, we can achieve a similar
synchronization performance as in an AWGN channel if the degree of frequency diversity
utilized within the synchronization process is large enough. This claim is substantiated
by simulation results.

---

[1]The minimum length of the preamble of at least 4 periods of length P stems from $M = W/P > 2$,
which is the requirement for (2.21) to hold.

2.1.4.1 Analysis

Transmission of a signal $s(n)$ via a frequency-selective channel is described according to equation (2.1). A CIR with a length of L taps results in a frequency-domain OFDM channel with L coherence bandwidth intervals, where each of them spans $N_c = N/L$ subcarriers. As an approximation, we can assume that the OFDM channel does not change significantly over the subcarriers lying within the channel's coherence bandwidth, while channel coefficients for subcarriers with a spacing larger than the coherence bandwidth can be considered to be independent.

For the analysis, we adapt our signal model introduced in section 2.1.3 to the frequency selective case and derive a corresponding pdf for the output of the correlator $|C(n_0)|$. For the AWGN channel, the corresponding pdf was given in (2.22). As the AWGN channel is frequency-flat, we would achieve the same result if we concentrated the entire power of the preamble signal on a single subcarrier. With this idea in mind, we update our signal model to form the basis for a simple analysis of the signal conditions in the frequency-selective channel: We use only a single subcarrier within each coherence interval for the preamble signal, which is allocated the power

$$\sigma_s^2 = N_c \cdot P_s = N/L \cdot P_s$$

Thus, we can capture the total frequency diversity of the channel with a minimum number of occupied subcarrier symbols, and we can assume that the channels seen at the subcarrier positions occupied by the preamble signal are are all independent.

We consider the case of non-overlapping correlation signals ($\rho = 0$) and a preamble signal of length $N + P$ samples. Correspondingly, the correlation window length is set to $W = N$. This special setting does not imply a loss of generality, but it simplifies the analysis significantly. The received preamble signal $R_i(k)$ in (2.12) now reads

$$R_i(k) = H(k)S(k) + Z_i(k)$$

where $H(k)$ is the channel coefficient and $Z_i(k)$ the noise with mean power σ_n^2 at frequency position k. As the correlation signals are non-overlapping, the $Z_i(k), i \in \{1, 2\}$, are independent. The preamble sequence $S(k)$ is non-zero for $k \in \{0, N_c, \dots, (L-1)N_c\}$ only. The channel coefficients at the corresponding positions $H(k)$ are modeled as i.i.d. according to the Rayleigh-fading assumption, i.e. they are drawn from a complex Gaussian distribution $\mathcal{N}(0, \sigma_h^2 = 1)$. Separating (2.12) into three components as done in (2.14)-

(2.16) yields

$$C_1 = \frac{1}{W} \sum_{k=0}^{L-1} |H(N_c k)|^2 \cdot \sigma_s^2 \tag{2.38}$$

$$C_2 = \frac{1}{W} \sum_{k=0}^{L-1} H(N_c k) S(N_c k) \cdot Z_2^*(N_c k) + Z_1(N_c k) \cdot H^*(N_c k) S^*(N_c k) \tag{2.39}$$

$$C_3 = \frac{1}{W} \sum_{k=0}^{W-1} Z_1(k) \cdot Z_2^*(k) \tag{2.40}$$

We first focus on (2.38), which represents a sum of L absolute squares of the complex Gaussian variable $H(k)$. Hence, C_1 can be modeled by a chi-square distribution with $n = 2L$ degrees of freedom, which is scaled by $\sigma_s^2/W = P_s/L$. The pdf for C_1 thus yields

$$C_1 \sim P_s/L \cdot \chi_{2L}^2(L, L) \xrightarrow{L \gg 1} \mathcal{N}(P_s, P_s^2/L) \tag{2.41}$$

For large L, the chi-square distribution approaches a Gaussian, which is given on the right hand side.

As the two terms $Z_1(k)$ and $Z_2(k)$ are assumed i.i.d., the two sums in (2.39), denoted as sum1 and sum2, have identical statistics and are mutually independent. Focussing on sum1, we observe that it consists of L products of the independent complex Gaussian variables $H(k)$ and $Z_2^*(k)$ and the deterministic preamble signal $S(k)$ with power $\sigma_h^2 = 1$ and σ_n^2 and σ_s^2, respectively. Let the pdf of the product $H(k)S(k)Z_2^*(k)$ be given as $\mathcal{P}(0, \sigma^2)$, with zero mean and variance of $\sigma^2 = \sigma_h^2 \cdot \sigma_n^2 \sigma_s^2$. As the L elements in sum1 are all assumed to be statistically independent, the overall distribution can for sufficiently large L be approximated by a Gaussian (central limit theorem), whose mean and variance amount to L-times the corresponding measure of pdf $\mathcal{P}(0, \sigma^2)$. Thus, we obtain

$$\text{sum1} \sim \mathcal{N}(0, L\sigma_h^2 \cdot \sigma_n^2 \sigma_s^2,) = \mathcal{N}(0, P_s\sigma_n^2/W,)$$

As sum1 and sum2 are mutually independent, we yield for the distribution of C_2

$$C_2 \sim \mathcal{N}(0, 2P_s\sigma_n^2/W,)$$

Finally, the term C_3 in (2.40) is identical to the one from (2.16), and hence the pdf is the same as the one found for the AWGN case in (2.21), i.e.

$$C_3 \sim \mathcal{N}(0, \sigma_n^4/W)$$

With all these partial results, we can now model the pdf for the correlation function $|C(n_0)|$. As in the AWGN case, the useful signal portion C_1 is strictly real valued. Hence,

we use the approximation $|C(n_0)| \approx \Re\{C(n_0)\}$ again and focus on the real valued distortions of components C_2 and C_3 only. By assuming that the power of both measures is distributed uniformly over the real and imaginary component, we yield for large L

$$\Re\{C_2\} \sim \mathcal{N}(0, P_s\sigma_n^2/W,)$$
$$\Re\{C_3\} \sim \mathcal{N}(0, 0.5\sigma_n^4/W) \tag{2.42}$$

As the three components C_1 to C_3 are all uncorrelated (the covariance of any pair yields zero), we can merge their Gaussian pdfs in (2.41) and (2.42) to one compound Gaussian. For large L, we thus yield

$$|C(n_0)| = \Re\{C(n_0)\} \sim \mathcal{N}\left(P_s, \ P_s^2/L + (P_s + 0.5\sigma_n^2)\sigma_n^2/W\right) \tag{2.43}$$

According to this result, the degree of diversity L has an impact on the variance of $|C(n_0)|$ in terms of an additive term, which tends to zero for increasing L. In other words, the variance is steadily decreasing for increasing diversity L of the channel. For $P_s^2/L = 0$, we observe that the pdf is identical to the one obtained for the AWGN channel in (2.22) for $\rho = 0$. Hence, by increasing the degree of diversity utilized for the synchronization process, we can conclude that the synchronization performance improves steadily and finally approaches the one which is achievable in the AWGN channel. Note that this result corresponds to a fundamental finding from Kennedy [51] saying that the capacity of a Rayleigh-fading channel approaches the one of an AWGN channel if the channel bandwidth goes to infinity, while the average received power is kept constant.

2.1.4.2 Numerical results

With simulative means we will illustrate how the degree of frequency diversity used for the synchronization affects its performance. We apply the transmission model from (2.1) here. A uniform PDP is assumed for the CIR $h(l)$, $l \in \{0, \ldots, L-1\}$, the single channel weights $h(l)$ are modeled independently following a Rayleigh-fading distribution. Simulations are carried out for a large number of channel realizations, the performance results are then averaged.

To capture the channel's full frequency diversity for the synchronization process, we have to use a preamble whose frequency-domain structure is constituted of at least L equispaced subcarriers signals that cover the entire signal bandwidth; i.e. we do not consider any guard bands here. This yields a preamble period of $s \geq L$. Further, to exclude signal transition effects which are attributed to OFDM symbols that pre- and succeed the preamble, we assume a periodic transmission of the preamble and determine the detection performance at the true timing instant n_0. This approach enables us to gain an isolated view on how the diversity impacts the synchronization performance.

Fig. 2.6 shows the simulated detection performance in terms of $p(miss)$ and $p(fail)$ for different channel lengths L and a correlation window length $W = 64$. Firstly, we observe that the degree of diversity L utilized for the synchronization process significantly impacts the performance of $p(miss)$; a low value of L causes a large deviation from the AWGN performance. To explain this, note that the variation of the channel gain $H(k)$ results in a fluctuation of the instantaneous SNR conditions at the receiver. By recalling the result from Fig. 2.4, where we have shown that the performance of $p(miss)$ in AWGN degrades substantially if the SNR drops down, we can conclude here that the degradations observed here are due to the SNR fluctuations caused by the fading channel. By increasing the degree of diversity L, we clearly observe that the performance approaches the AWGN curve. However, the convergence seems to be rather slow, as with $L = 32$ there is still a considerable gap for probabilities $p(miss) < 0.1$.

For $p(fail)$, the degree of diversity does not seem to have a significant impact on the performance, which is not surprising as $p(fail)$ was shown to be independent of the SNR conditions. Nevertheless, a slight performance degradation can be observed if the degree of diversity L is increased, which, however, is very limited. For an explanation, notice that the received signal

$$R_i(k) = H(k)S_i(k) + Z_i(k) \, ,$$

which is constituted of pure data signals $S_i(k)$, does no longer have pure Gaussian properties, but rather depends on the product of the two random variables $H(k)$ and $S_i(k)$ now. Consequently, the correlation (2.12) can no longer be characterized by a Gaussian, which results in the observed deviations of the corresponding performance curves from the AWGN case. Obviously, the statistical properties of the correlator are more Gaussian-like for a small degree of diversity, as seen for $L = 2$ in the figure.

Fig. 2.7 depicts the simulated detection performance for different correlation window lengths W. The performance of $p(fail)$ improves by increasing W similarly as in the AWGN case depicted in Fig. 2.3. As pointed out in the observations made for the previous figure, the degree of diversity L impacts the slope of the performance curves only slightly. However, relations are different for $p(miss)$: Here we observe that it depends on the degree of diversity L whether we can achieve a performance gain by increasing W. An explanation for this can be found by examining the analyzed distribution of $|C(n_0)|$ in (2.43): Both values W and L influence the variance of the distribution in terms of a summand. Evidently, if the term depending on W is small compared to the term depending on L, then the impact of increasing W vanishes. For SNR = 0 dB, this condition is met if $W/L \gg 1.5$. Hence, we can observe hardly any gain if we increase W for the case of $L = 2$ in the figure, and a rather small gain for the case of $L = 8$.

These results clearly suggest that it is crucial to utilize as much diversity of the channel as possible within the synchronization process to achieve a convenient performance. In
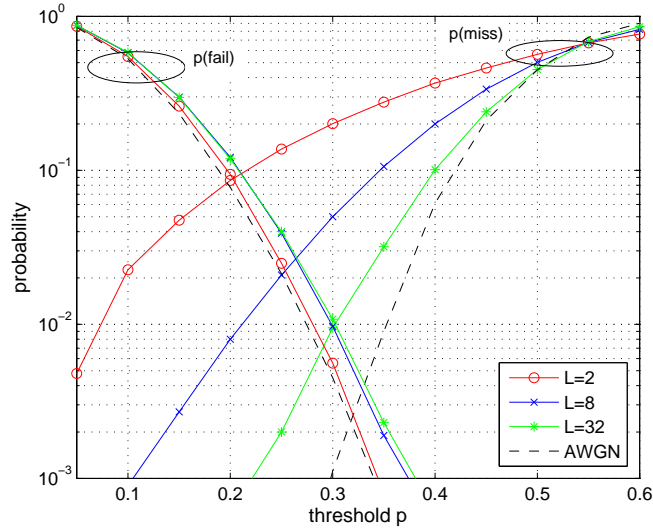
Fig. 2.6: Simulated detection performance in the frequency-selective channel with vari-
ous degrees of frequency diversity L. SNR = 0 dB, $W = 64$, non-overlapping
correlation signals ($\rho = 0$).

particular, this means that the bandwidth occupied by the preamble signal should be
maximized. Furthermore, we note that choosing a larger correlation window length W
cannot compensate for a performance loss that is caused by a decrease of the utilized
degree of diversity.

Fig. 2.8 finally shows the phase estimation performance of φ versus SNR for $W = 64$
and for an estimation based on overlapping correlation signals (system setting similar as
in Fig. 2.5). Here we observe that the performance converges quite rapidly to the AWGN
performance for increasing L. Increasing L from 1 to 2 yields a significant gain, and with
$L = 8$, we are already quite close to the AWGN performance, especially a high SNR.
The results confirm the value of utilizing the diversity for the synchronization, although
it should be noted that a much smaller degree of diversity is required for the phase
estimation to achieve an estimation performance close to AWGN than it was observed for
the performance of the preamble detection itself.

2.1.5 Utilizing spatial diversity in MIMO systems

Similarly as the frequency diversity addressed in the previous subsection, the spatial di-
versity offered in a MIMO system can be utilized within the synchronization process
to improve its performance. A first proposal how to exploit receive diversity for the
synchronization was given in [22]. Mody and Stueber [66] then proposed a concept to
benefit from transmit diversity, which was based on using sequences with good auto- and
cross-correlation properties as preambles for simultaneous transmission from the trans-
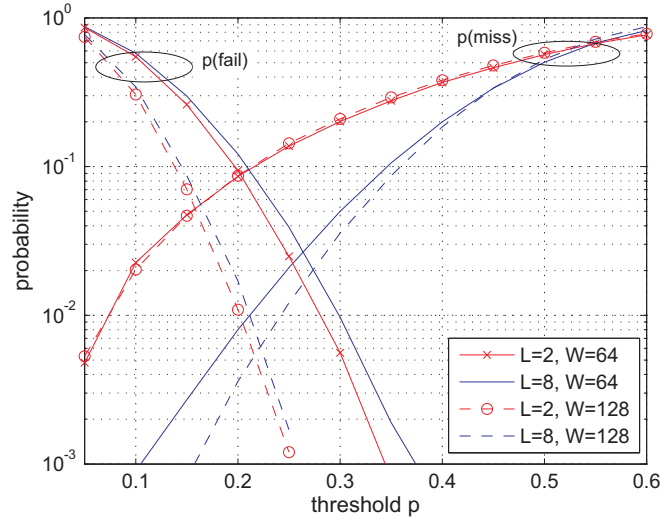mit antennas. Finally, Schenk and van Zelst presented an approach that combines both

Fig. 2.7: Simulated detection performance in the frequency-selective channel for different degrees of diversity L and correlation window widths W. SNR $= 0$ dB.
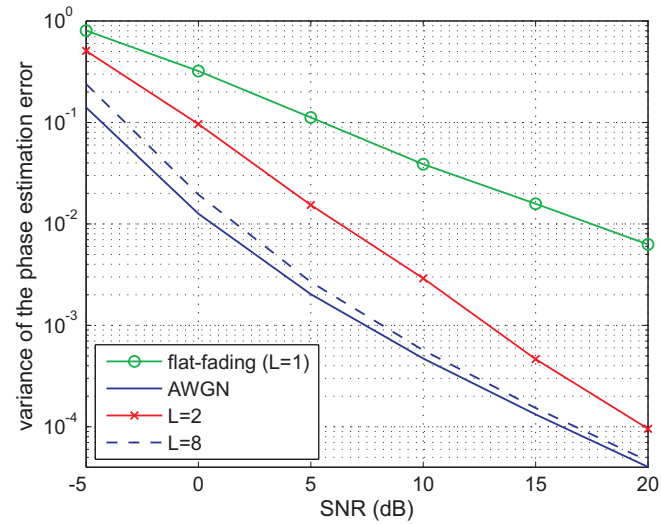

Fig. 2.8: Performance of the phase estimation φ in the frequency-selective channel versus SNR. $W = 64$, $P = 16$

concepts and thus captures the full spatial diversity of the MIMO system for the synchronization [87]. Therein, the achievable performance gains of the phase estimation φ has been systematically examined.

In addition to the results presented in [87], we will show in this subsection that similar to frequency diversity, utilization of spatial diversity enables us to approach the detection performance in the AWGN channel. We briefly sketch the methods how to capture spatial diversity for the synchronization and thereby show why preamble signals with good cross-correlation properties for the transmit antennas are a suitable choice.

2.1.5.1 Transmit diversity

To utilize the transmit diversity of a MIMO system, a preamble signal should be transmitted simultaneously from all antennas with the total transmit power P_s being uniformly distributed among them. At the receiver, a coherent addition of signals which propagated via the different paths from those antennas must then be enabled within the correlation (2.5). To reveal the essential requirement for the preamble design, we consider a preamble consisting of two periods of length P. Let the P elements of one preamble period transmitted from antenna j be stacked into the signal vector $\mathbf{s}_j$. For simple illustration, we assume a system with 2 transmit and one receive antenna and model the channels between any transmit and receive antenna pair as flat fading, yielding the channel coefficient h_j. The received signal vector containing the first period of the preamble then is given as

$$\mathbf{r}_1 = e^{j\varphi_0}(h_1\mathbf{s}_1 + h_2\mathbf{s}_2) + \mathbf{z}_1$$

where φ_0 is the phase stemming from the CFO at time instant n_0 and $\mathbf{z}_1$ comprises the noise samples distorting the reception signal. Note that the total transmit power P_s has to be distributed uniformly now over the transmit antennas, i.e. the mean power of a sample in $\mathbf{s}_j$ amounts to $P_s/2$. The reception vector containing the second period of the preamble reads correspondingly

$$\mathbf{r}_2 = e^{j(\varphi_0+\varphi)}(h_1\mathbf{s}_1 + h_2\mathbf{s}_2) + \mathbf{z}_2$$

With the vector notation, the correlation (2.5) can be written as a scalar product of the two reception vectors, i.e.

$$
\begin{aligned}
C(n_0) &= \mathbf{r}_2^H\mathbf{r}_1 \\
&= e^{j\varphi}(|h_1|^2\mathbf{s}_1^H\mathbf{s}_1 + 2\Re\{h_1^*h_2\mathbf{s}_1^H\mathbf{s}_2\} + |h_2|^2\mathbf{s}_2^H\mathbf{s}_2) + \xi
\end{aligned}
\tag{2.44}
$$

ξ comprises all contributions from the noise vectors $\mathbf{z}_1$ and $\mathbf{z}_2$ that distort the useful signal component of the correlator output. Regarding the useful signal components reveals that the powers of signals $\mathbf{s}_j$ add up with weights corresponding to the power of the channels

h_j. This already matches our desired target to capture the transmit diversity for quality improvement of the correlator output. However, the intermediate term $2\Re\{h_1^* h_2 \mathbf{s}_1^H \mathbf{s}_2\}$ may reduce the magnitude of the overall sum, as it may become negative. This possible magnitude reduction that would degrade the achievable signal quality can be avoided if the product $\mathbf{s}_1^H \mathbf{s}_2$ yields a value near zero. This can easily be achieved by using sequences $\mathbf{s}_j$ with a low cross-correlation value. The simplest solution to this end is to cyclically shift the preamble period P used for the second transmit antenna by $P/2$ samples, as has been proposed in [87]. For the general case of a system with N_t transmit antennas, the period should be shifted by P/N_t samples to enable the utilization of spatial diversity from all transmit antennas within the synchronization process. Note that in a frequency-selective channel, the shift P/N_t should be larger than the maximum channel excess delay L to avoid the magnitude reduction for any possible combination of multi-path signals within the output of the correlator $C(n_0)$.

2.1.5.2 Receive diversity

To have an isolated view on the receive diversity, we consider the preamble signal $s(n)$ to be transmitted from a single antenna here. In a system with N_r receive antennas, the reception signal based on flat-fading channel conditions is given as

$$\mathbf{r}(n) = \exp(j2\pi\omega n/N) \cdot \mathbf{h}s(n) + \mathbf{z}(n)$$

where all vectors comprise the signals for the N_r receive antennas. To capture the receive diversity in the synchronization process, the authors in [87] proposed to use the scalar product $\mathbf{r}^H(n+d+P)\mathbf{r}(n+d))$ of the reception vectors for the correlation in (2.5). This operation is equivalent to performing a correlation of the signal at each receive antenna separately and summing their outputs afterwards, which was also one of the suggestions in [22]. We recall the vector notation from the preceding subsection and focus on a system with 2 receive antennas, which receives the preamble consisting of two periods $\mathbf{s}$ transmitted from a single antenna via frequency-flat channels. At receive antenna m, the reception signals containing the first and second period of the preamble are given as

$$\begin{aligned}
\mathbf{r}_{1,m} &= e^{j\varphi_0} h_m \mathbf{s} + \mathbf{z}_{1,m} \\
\mathbf{r}_{2,m} &= e^{j(\varphi_0+\varphi)} h_m \mathbf{s} + \mathbf{z}_{2,m}
\end{aligned}$$

with h_m being the flat-fading coefficient of antenna m. The correlation of the reception signals at each receive antenna m yields according to (2.44)

$$C_m(n_0) = \mathbf{r}_{2,m}^H \mathbf{r}_{1,m} = e^{j\varphi}|h_m|^2 \mathbf{s}^H \mathbf{s} + \xi_m$$

where ξ_m comprises all contributions from the noise vectors $\mathbf{z}_{1,m}$ and $\mathbf{z}_{2,m}$ that distort the useful signal component of the correlator output. The output of the modified correlator as described above is constituted from the sum of the two correlator outputs $C_m(n_0)$, i.e.

$$C(n_0) = C_1(n_0) + C_2(n_0) = e^{j\varphi}(|h_1|^2 + |h_2|^2)\mathbf{s}^H\mathbf{s} + \xi_1 + \xi_2$$

Clearly, we observe that the proposed receiver processing yields an addition of the powers from the preamble signals received at the different antennas, which means the receive diversity is fully captured. By assuming that the noise at the different receive antennas is i.i.d., we can further conclude that the contributions from the noise in ξ_1 and ξ_2 add up incoherently. Thus we can conclude here that for the proposed receiver processing, the system is capable of achieving a combining gain similar to maximum ratio combining (MRC) – a result which has already been noted in [87]. In accordance with a further result from [87], we can modify the analytical expression for the variance of $\Delta\varphi$ given in (2.37) by adding the MRC gain factor N_r to its denominator according to

$$var(\Delta\varphi) = \frac{P \cdot P_s\sigma_n^2 + 0.5W\sigma_n^4}{L^2 \cdot P_s^2 N_r} \qquad (2.45)$$

This yields the AWGN phase estimation performance for multiple receive antenna systems. To fully benefit from the receive diversity also for the detection of the preamble, the power function $Q(n)$ from (2.6) should be modified according to the above idea as well, i.e. the product of scalars $r(n+d)r^*(n+d+P)$ in (2.6) should be replaced by the scalar product $\mathbf{r}^H(n+d+P)\mathbf{r}(n+d)$). The Schmidl-Cox algorithm according to (2.10) and (2.11) can then be applied on the modified measures $C(n)$ and $Q(n)$, respectively.

2.1.5.3 Simulation results

We now evaluate the performance of the synchronization process utilizing the spatial diversity of a MIMO system with simulative means. We use the same preamble and system setting as in the preceding section where we examined the frequency-selective channel, but we assume a system with $N_t = N_r = 2$ transmit (Tx) and receive (Rx) antennas now. By utilizing transmit, receive and then both diversities simultaneously, we show the performance improvement that can be yield.

Fig. 2.9 shows the detection performance in terms of $p(fail)$ and $p(miss)$ at an SNR of 0 dB, where we assume all channels between Tx/Rx antenna pairs to have a degree of frequency diversity of $L = 4$. In case of 2 transmit antennas, the total degree of available diversity in the system is $N_tL = 8$. Correspondingly, the detection performance $p(miss)$ is similar to the one achieved in the frequency-selective channel for $L = 8$ from Fig. 2.6. By using 2 receive antennas, we achieve a slightly improved performance $p(miss)$ compared to the 2 transmit antenna case, which is due to the additional MRC gain. By
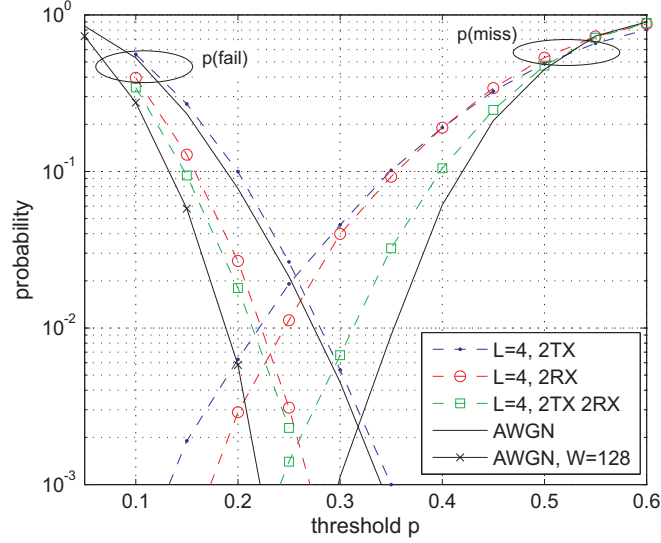
Fig. 2.9: Simulated detection performance in the frequency-selective channel with utiliza-
tion of spatial diversity. SNR = 0 dB, $W = 64$, non-overlapping correlation
signals ($\rho = 0$).

utilizing the diversity from the transmit and receive antennas simultaneously, the overall
degree of diversity yields $N_t N_r L = 16$, and $p(miss)$ approaches quite close to the AWGN
performance. Note that the performance of this configuration utilizing the full spatial
diversity of the 2×2 MIMO system is close to the one achievable in a frequency-selective
channel with diversity $L = 32$, which was given in Fig. 2.6. This improved performance
can again be attributed to the additional MRC gain the multi-antenna receiver is able to
realize, suggesting already that the utilization of receive diversity is of highest value in
improving the detection performance.

For $p(fail)$ we note that in case of 2 transmit antennas, the performance is quite close to
the the one in an AWGN channel – which is even a bit better than the performance in the
frequency-selective channel with similar degree of diversity, $L = 8$. Most interestingly, we
observe that utilization of receive diversity improves the $p(fail)$ performance significantly;
the MRC gain of factor 2 lets the performance approach the one in the AWGN channel
for a system with a correlation window length W increased by factor 2 (i.e. 128 samples).
Hence, we can conclude that it is most valuable to use the receive diversity, as it improves
the $p(fail)$ performance similarly as increasing W by factor 2 – without any additional
cost in overhead. Utilizing both transmit and receive diversity simultaneously provides
an additional, however small, performance gain. These results suggest that the available
spatial diversity of the system should be fully utilized, as transmit as well as receive
diversity help to get close to the AWGN performance. Thanks to the additional MRC
gain yielding the largest performance improvements, utilization of receive diversity may
be attributed the highest relevance.

Finally we show simulation results for the CFO estimation in Fig. 2.10. The system
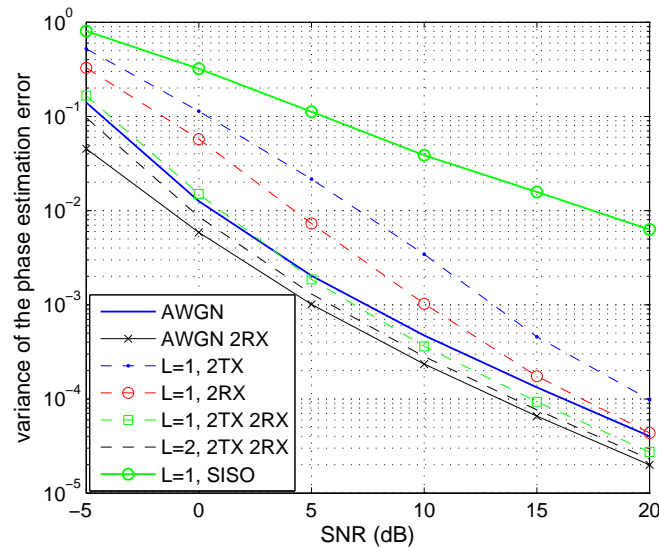
Fig. 2.10: Performance of the phase estimation φ in the fading channel with utilization of spatial diversity versus SNR. $W = 64$, $P = 16$

setting is similar as the one used for Fig. 2.8, and again we assume a 2×2 MIMO system. We observe that by utilizing the spatial diversity in a flat-fading channel, we rapidly approach the AWGN performance. By utilizing transmit and receive diversity simultaneously, we achieve an estimation performance that exceeds the one for a single-antenna AWGN channel above an SNR of 5 dB. By adding a degree of frequency diversity ($L = 2$), we approach the performance of the AWGN with 2 receive antennas. The lowermost curve represents the simulated estimation performance in that latter channel, which is identical to the analytical performance from (2.45) for the depicted SNR range. Similar as in Fig. 2.8, the results show that a degree of diversity $N_t N_r L = 8$ is sufficient to get close to the performance in the corresponding AWGN channel.

2.1.6 Synchronization specifications for current OFDM-based systems

It is worth peeping into specifications for current OFDM-based radio systems to see how these systems utilize the diversity available in the wireless system for the synchronization process. In particular, we will take a look a the preamble definitions used for initial acquisition for the specifications of Worldwide Interoperability for Microwave Access (WiMAX), 3G Long Term Evolution (3G-LTE) and Ultra Mobile Broadband (UMB) system. All three systems support a scalable signal bandwidth from 1.25 up to 20 MHz. Over 20 MHz, 2048 OFDM subcarriers are accommodated. The bandwidth scaling is done simply by accessing a subset of the available subcarriers only. In WiMAX [39] OFDMA mode, the preamble covers the full signal bandwidth, occupying each third subcarrier with a PN sequence with constant amplitude. Thus, the synchronization process can take advantage

of the full frequency diversity available in the system. A similar preamble signal is defined for the UMB [2] system, consisting of a sequence of complex number with constant amplitude occupying every fourth subcarrier. The covered system bandwidth is limited to the inner 512 subcarriers, which corresponds to 5 MHz. However, for the CIR lengths that can be expected during operation, this bandwidth should in general capture a large degree of frequency diversity. Finally, the 3G-LTE system [1] in its current version provides a preamble signal consisting of a constant amplitude sequence, which covers the subcarriers limited to the minimum supported signal bandwidth, i.e. 1.25 MHz. Moreover, here the signal is no longer periodic in time domain, but mirror-symmetric. Therefore, an alternative algorithm for preamble detection has to be applied, which has been suggested in [125]. As the captured frequency diversity is rather small if the system operates in one of the broadband modes (i.e. bandwidth > 1.25 MHz), the achievable detection performance is limited, as has been shown in [82]. Alternatively, one can also rely on correlation of the cyclic prefix in the broadband modes to obtain the OFDM symbol timing. For data transmission, in general all signal bearing subcarriers are occupied with data or pilot signals with similar mean power. Thus, correlating the cyclic prefix allows to capture the full frequency diversity. Note that the length of the cyclic prefix in time-domain samples increases when going to a higher bandwidth mode. Hence, the size of the correlation window increases correspondingly, so that for the higher bandwidth modes an improved performance can be achieved.

Interestingly, none of the current systems supports the use of transmit diversity, although all systems support the employment of multiple transmit antennas. A reason for that could be found in the fact that the code sequences used for the preamble signals also contain information for cell identification. This information has to be recovered without any channel information by correlation operations in frequency domain. If cyclically shifted preamble signals would be used to capture the transmit diversity, the frequency selectivity of the channel would effectively be increased, which hampers proper recovery of the cell information contained in the preamble. On the other hand, the use of additional orthogonal codes at the transmit antennas would not only increase the demand on available codes significantly, but would also increase the complexity of the cell information recovery process.

2.1.7 Conclusion chapter 2.1

In this section, we focussed on initial synchronization of the MIMO-OFDM downlink based on a dedicated preamble signal. We analyzed the achievable synchronization performance under AWGN channel conditions in terms of three measures, namely the probability of a detection failure and of a missed preamble as well as the estimation accuracy of the phase shift φ resulting from a CFO. It was shown that using a preamble with multiple signal periods enables more flexibility in the configuration of the correlator used at the receiver, as the correlation shift P and the correlation window width W can be selected independently. However, selecting $W > P$ results in overlapping correlation signals, and correspondingly the noise in the correlation process becomes correlated. It was shown that this noise correlation has a negligible influence on the detection performance, but supports the performance of the CFO estimation, as the variance of the phase estimate decreases with W^2 for high SNR. Further, we addressed a suitable choice of the detection threshold p for fixed SNR conditions. For varying SNR conditions with a constant threshold, a high sensitivity of the detection performance has been observed. This result suggests to design system parameters like W and p according to a performance target for the worst-case SNR conditions.

We then drew our focus on the fading channel and examined by analytical and simulative means how utilizing diversity in frequency and space affects the synchronization performance. It was shown that the fading channel degrades the achievable synchronization performance in general. However, by utilizing diversity from frequency and space, the performance can be improved, and it gradually approaches the AWGN performance. As shown already in [87], utilization of receive diversity delivers an additional gain equivalent to MRC, which lets the performance improvements grow faster than in case of transmit or frequency diversity. Furthermore, due to the additional power received at additional receive antennas, the AWGN performance of a single antenna system can even be excelled in this case. The results suggest that as much diversity as possible should be utilized within the synchronization process to get close to the AWGN performance. Evidently, the highest value is attributed to the receive diversity due to the additional MRC-like performance gain. All the results presented in this section enable to derive a framework for the design of parameters for the initial synchronization process to achieve a desired synchronization performance under predefined signal conditions.

Note that after the initial synchronization phase, a continuous tracking of residual SFO and CFO errors is typically performed to improve the timing and frequency estimates during signal transmission [97]. The optimal tracking procedures for MIMO-OFDM links have been proposed in [74], which – thanks to their moderate complexity demands – are ready to be applied in practice.

2.2 Synchronization in the multi-user uplink

In the multi-user MIMO-OFDM uplink, multiple UTs access the channel simultaneously to communicate with a single BS. The spatial MIMO channel allows different users to share even the same frequency resources at the same time, which is referred to as space-division multiple access (SDMA). MIMO-OFDM systems enabling SDMA in the uplink are also denoted as OFDM-SDMA systems. In [111] such a systems has firstly been evaluated in a practical context, i.e. based on equalization techniques with moderate complexity demands that are ready to be used in practice, and it has been illustrated that a convenient system performance can be achieved. However, a prerequisite for SDMA to work properly and to deliver the expected gains in system performance is a convenient synchronization between all participating UTs. In contrast to the downlink, which can be considered as a number of parallel single-user links that can be synchronized individually (see section 2.1), synchronization of the uplink is much more challenging: Concerning the timing, it has to be ensured here that the simultaneously transmitted signals from the UTs arrive at the BS at the same time, which requires an estimation and compensation of the propagation delays of the transmission signals from the UTs. However, this issue can be considered to be conveniently solved for practice. A technique to compensate for the propagation delays after proper estimation has already been applied in the context of Global System for Mobile Communications (GSM) networks, where the corresponding process is referred to as *timing advance*. According to proposals for next generation communication standards like WiMAX [39], the following *ranging process* has been proposed to synchronize the timing for all participating UTs: Firstly, the UTs obtain the timing information from the BS by performing the timing estimation described in section 2.1.1. Afterwards, the UTs transmit a so called "ranging signal", which is a specially designed preamble signal used to carry out an estimation of a user's timing at the BS. The difference between the timing at BS and the estimated timing of the UT corresponds to the roundtrip time for signal transmission to that UT. From the roundtrip time, the propagation delay of a user's transmit signal is derived and reported back to the UT via a control channel. The UT then compensates for the propagation delay by adapting its timing information for transmission, i.e. the timing is advanced by the propagation delay. For further details of the ranging process and suitable algorithms, refer to [30, 128]. The ranging process has proven to be very robust; it has been shown to operate conveniently even in high mobility environments [83].

A much more challenging issue is the frequency synchronization of the simultaneously transmitted OFDM signals from the UTs. Unfortunately, a frequency compensation at the receiver side similar to the one for single-user links according to equation (2.3) is not possible, since CFOs from different users are independent, and thus compensating for a single user's CFO will misalign the signal of all other users. As the frequency shifts of

the user signals destroy the orthogonality of the OFDM subcarrier signals, inter-carrier interference (ICI) arises, making the compensation a complex task.

The influence of CFOs from multiple users in an OFDM-based uplink has been studied extensively in the context of OFDMA systems, where simultaneous access is granted to multiple users by individually assigning distinct sets of subcarriers to them [25, 55, 104]. An overview of existing synchronization techniques together with a sound summary of the general requirements for uplink synchronization can be found in [69]. Estimation of multiple users' CFOs can be performed based on blind techniques exploiting specific properties of the utilized OFDM signals and their statistics [6, 9, 14, 107, 123] or based on pilot-based techniques [68, 78]. For CFO compensation, the simplest approach is to feed back the estimated CFO to the corresponding UT, so that it may adapt its oscillator accordingly or apply a pre-compensation to its transmit signal [107]. However, the drawback of this feedback approach is that large delays may occur before the CFOs are properly compensated. There also exist some proposals for CFO compensation to be carried out directly at the receiver by adequate signal processing. These approaches are either based on the inversion of a high dimensional matrix representing the ICI-affected channel for a complete OFDMA symbol [15, 38], or they make use of successive interference cancelation techniques [26], which may be performed in an iterative fashion [37]. Unfortunately, all these approaches result in a significant increase of computational complexity compared to common OFDM processing, whose favourable property is to enable an independent subcarrier-wise processing. Although the complexity of the above approaches based on matrix inversion can be further reduced if specific properties of the signal model are exploited [14, 36, 43], it still remains considerable. A suboptimum solution maintaining the subcarrier-wise signal processing at the receiver is presented in [18]: The user signals are separated first, whereafter they are individually compensated for their user-specific CFO. Although not all ICI can be removed, a satisfactory performance is achieved if the CFOs do not become too large.

2.2.1 CFOs in multi-user SDMA uplink and their compensation

The major difference in OFDM-SDMA systems compared to OFDMA systems is that the channel is enhanced by a spatial dimension. To separate the users' signals, knowledge of the SDMA channel per subcarrier is required. With CFO distortions present, solutions to estimate the SDMA channel have been proposed in [3, 84]; joint estimation of SDMA channels and the users' CFOs can be found in [32, 95, 121]. Contributions [3, 121] also provide approaches to compensate for the CFO distortions at the receiver, which, however, have complexity demands that are similar to the OFDMA techniques mentioned above.

The work presented in this section was motivated by seeking for a simple receiver-based CFO compensation method for the uplink of an OFDM-SDMA system. Hereby,

the subcarrier-wise channel equalization is supposed to be maintained to facilitate implementation in a real-time system. Therefore, we resort to the basic idea from [18] and develop a system concept where the user signals are first separated by common OFDM-SDMA equalization and are compensated for their individual CFO distortions afterwards. As this approach is clearly suboptimum, the major focus of our work lies in the proper analysis of the achievable signal conditions with respect to the amount of interference that remains in the system after such compensation. In particular, we derive closed-form expressions characterizing the bounds for the signal to interference ratio (SIR) before and after CFO compensation, which are verified by numerical bit error rate analysis. This way, we obtain insights into the suitability of the approach and reveal the limits of its application range.

Based on our results, it turns out that the proposed CFO compensation concept operates conveniently only if the size of the CFOs present in the system can be kept below a few percent of the subcarrier spacing. Therefore, the approach has to be seen as a technique for fine-synchronization. Correspondingly, a coarse frequency synchronization of all users' signals has to be ensured. This coarse synchronization can be achieved by a so-called frequency-advance, where terminals pre-compensate their signals with the CFO estimated in the preceding downlink phase. The concept of frequency-advance was recently realized in a practical system, as reported in [48].

2.2.2 Signal model

2.2.2.1 Vector notation of OFDM

Consider an OFDM system with a total of N subcarriers. The transmission equation for a CFO distorted SISO link is given by

$$\mathbf{y} = \mathbf{F}\mathbf{P}_2\mathbf{C}(\varphi)\mathbf{H}\mathbf{P}_1\mathbf{F}^H \cdot \mathbf{x} \tag{2.46}$$

$\mathbf{x}$ is the data vector comprising the N data symbols constituting the OFDM symbol, $\mathbf{F}$ is the $N \times N$ DFT matrix, and $\mathbf{P}_1$ and $\mathbf{P}_2$ are permutation matrices used to append and cut the cyclic prefix (CP) of length N_g samples. Further, $\mathbf{H}$ is the $(N + N_g) \times (N + N_g)$ Toeplitz channel matrix constituted from the CIR h_l, $l \in \{0, \ldots, L_e\}$, where $L_e \leq N_g$. Finally,

$$\mathbf{C}(\varphi) = \mathrm{diag}([\exp(-j\varphi N_g) \cdots \exp(j\varphi(N - 1))])$$

is the CFO distortion matrix, where the phase rotation factor φ is defined as $\varphi = 2\pi\omega/N$, with $\omega \in [-0.5, 0.5]$ being the CFO normalized to the subcarrier spacing. For $\varphi = 0$ (no CFO), the effective channel

$$\mathbf{F}\mathbf{P}_2\mathbf{H}\mathbf{P}_1\mathbf{F}^H = \boldsymbol{\Lambda} \tag{2.47}$$

yields a diagonal matrix, whose elements on the diagonal λ_k, $k \in \{1, \ldots, N\}$, represent the N-point DFT of the CIR h_l. By a few simple transformations, the diagonal matrix $\mathbf{\Lambda}$ can be restored in (2.46), yielding

$$\mathbf{y} = \mathbf{F}\bar{\mathbf{C}}(\varphi)\mathbf{F}^H\mathbf{F}\mathbf{P}_2\mathbf{H}\mathbf{P}_1\mathbf{F}^H \cdot \mathbf{x} = \mathbf{U}\mathbf{\Lambda} \cdot \mathbf{x} \tag{2.48}$$

where we introduced

$$\bar{\mathbf{C}}(\varphi) = \mathrm{diag}([1 \ \exp(j\varphi) \ \cdots \ \exp(j\varphi(N-1))]) \tag{2.49}$$

and $\mathbf{U} = \mathbf{F}\bar{\mathbf{C}}(\varphi)\mathbf{F}^H$. Note that $\mathbf{F}$ is unitary and thus $\mathbf{F}^H\mathbf{F}$ equals the identity matrix $\mathbf{I}$.

2.2.2.2 OFDM-SDMA signal model

Next the focus is turned to an OFDM-SDMA system, where Q single-antenna terminals transmit their signals simultaneously to an M-antenna base station on the same frequency resource. The users' transmission signals propagate via different paths and will be marked with different spatial signatures, which enable the multi-antenna receiver to separate and recover the users' transmission signals.

For the system model, the OFDM signal vectors $\mathbf{x}_q$, $q \in \{1, \ldots, Q\}$ from the Q users are stacked into one large vector $\bar{\mathbf{x}}$ of dimension QN. Correspondingly, the M OFDM reception vectors $\mathbf{y}_m$ are stacked into one large vector $\bar{\mathbf{y}}$. Each user may have an individual CFO, resulting in Q different CFO distortion matrices $\mathbf{U}_q$, which are generated from individual phase factors $\varphi_q = 2\pi\omega_q/N$. For simplicity, let us assume the number of users to be $Q = 2$. Based on the signal model in (2.48), the transmission equation in the OFDM-SDMA system reads

$$\underbrace{\begin{pmatrix} \mathbf{y}_1 \\ \vdots \\ \mathbf{y}_M \end{pmatrix}}_{\bar{\mathbf{y}}} = \underbrace{\begin{pmatrix} \mathbf{U}_1\mathbf{\Lambda}_{11} & \mathbf{U}_2\mathbf{\Lambda}_{12} \\ \vdots & \vdots \\ \mathbf{U}_1\mathbf{\Lambda}_{M1} & \mathbf{U}_2\mathbf{\Lambda}_{M2} \end{pmatrix}}_{\mathbf{H}_C} \cdot \underbrace{\begin{pmatrix} \mathbf{x}_1 \\ \mathbf{x}_2 \end{pmatrix}}_{\bar{\mathbf{x}}} \tag{2.50}$$

where each of the single user/receive antenna links is characterized by its own diagonal channel matrix $\mathbf{\Lambda}_{mq}$.

2.2.2.3 Statistical channel model

We will assume Rayleigh-fading conditions for the discrete multipath channel, meaning that the channel coefficients h_l are drawn independently from complex Gaussian distributions with mean power σ_l^2. For $l \in \{0, \ldots, L_e\}$, $\sigma_l^2 = E\{|h_l|^2\}$ represents the PDP of the channel, which is assumed to be monotonically decreasing for increasing l. Furthermore,

we assume the channel to be passive, i.e. the sum of the mean powers of all channel coefficients is equal to unity, $\sum_{l=0}^{L_e} \sigma_l^2 = 1$. To specify suitable bounds within our analysis, we will frequently use a uniform PDP with constant power for all channel taps, which is defined as $\sigma_l^2 = 1/(L_e + 1)\, \forall l$. From these assumptions, it follows for the subcarrier channels λ_k that they behave like random variables which are drawn from complex Gaussian distributions with unit power. The correlation between the channels at adjacent subcarrier positions is characterized by the frequency-domain auto-correlation function $r(\kappa)$, $\kappa \in \{0, \ldots, N-1\}$, where κ refers to the distance between subcarriers. $r(\kappa)$ is obtained from the N-point DFT of the PDP, i.e.

$$r(\kappa) = \sum_{l=0}^{L_e} \sigma_l^2 \, \exp(-j2\pi l\kappa/N)\,, \quad \kappa \in \{0, \ldots, N-1\}$$

In the OFDM-SDMA system, the channels of the QM single antenna links are characterized by the same statistical properties, but are assumed to be statistically uncorrelated. In particular, we assume all channels to have identical channel length L_e and identical PDP, which may be reasonable for UTs experiencing non line of sight (NLOS) multipath fading.

2.2.3 Analysis of single-antenna OFDM link

To prepare analysis of the SIR conditions in the OFDM-SDMA system, we focus in this section on a separate single-antenna OFDM link. In the following, we analyze the impact of CFO distortions and derive a bound for the SIR (section 2.2.3.1). To enable a simplified equalization process in the OFDM-SDMA system, where the user signals are first spatially separated and thereafter individually compensated for their CFO distortions, we modify this signal model accordingly (section 2.2.3.2). This model introduces an additional error term, which cannot be compensated by simple means. Hence, its power and the resulting SIR conditions are analyzed in section 2.2.3.3. The proper process for partial compensation of the CFO distortions after channel equalization is then presented in section 2.2.3.4.

2.2.3.1 Impact of CFO distortions

In (2.48), matrix $\mathbf{U} = \mathbf{F}\bar{\mathbf{C}}(\varphi)\mathbf{F}^H$ is a circular matrix, whose rows are circularly shifted versions of $u(\kappa)$ being the DFT of the diagonal in $\bar{\mathbf{C}}(\varphi)$, i.e.

$$u(\kappa) = \frac{1}{N} \sum_{n=0}^{N-1} \exp\left(j2\pi\omega\frac{n}{N}\right) \exp\left(j2\pi\frac{\kappa n}{N}\right)$$

with $\kappa \in \{0, \ldots, N-1\}$. The expression above represents a geometric series, and hence it can be simplified to [67]

$$u(\kappa) = \frac{1}{N} \exp\left(j\pi(\omega + \kappa)\frac{N-1}{N}\right) \frac{\sin(\pi(\omega + \kappa))}{\sin(\pi(\omega + \kappa)/N)}$$

As the DFT is periodic, the definition range may be changed to $\kappa \in \{-N/2, \ldots, N/2-1\}$. By doing so, we can use an approximation for large N based on the si-function $\mathrm{si}(x) = \sin(x)/x$, so that $u(\kappa)$ can be given as

$$u(\kappa) = (-1)^{\kappa} \exp(j\pi\omega) \cdot \mathrm{si}(\pi(\omega + \kappa)) \tag{2.51}$$

Multiplying the circular matrix $\mathbf{U}$ with a frequency-domain signal vector represents a cyclic convolution of that signal vector with function $u(\kappa)$, which introduces the ICI. For $\kappa \neq 0$, $u(\kappa)$ specifies the amount of ICI that is induced on any subcarrier from a subcarrier signal which is spaced κ subcarriers apart. $u(0)$ itself represents the attenuation of the power of each subcarrier signal. From (2.51), we observe that multiplication with function $u(\kappa)$ imposes a constant phase rotation $\exp(j\pi\omega)$ on all subcarrier signals. This constant phase factor corresponds to the mean CFO-induced phase rotation observed over the total duration of the time-domain OFDM symbol of N samples length. It is also referred to as the common phase error (CPE) induced by the CFO distortions.

Next, we will examine the mean power of the ICI and the resulting SIR. From (2.48), the received signal y_k at subcarrier position $k \in \{1, \ldots, N\}$ can with the above results be written as

$$y_k = u(0)\lambda_k x_k + \sum_{j=1, j \neq k}^{N} u(j-k)\lambda_j x_j$$

where x_k denotes the transmit symbol at subcarrier k. The first term in the above equation denotes the useful signal received at subcarrier k, while the second term represents the ICI from all other subcarriers. Let the transmit symbols x_k be i.i.d. with constant mean power P_s. Then, as $E\{|\lambda_k|^2\} = 1$, the mean power of the useful signal P_u at subcarrier k amounts to $P_u = P_s|u(0)|^2$. Furthermore, the mean power of the ICI from all other subcarriers distorting the useful signal yields $P_{ICI} = P_s \sum_{j=1}^{N-1} |u(j)|^2$, which can be upper bounded by $P_s(1 - |u(0)|^2)$. This bound is tight in case all N available subcarriers are occupied with data symbols. Using (2.51), we can lower bound the SIR resulting from the ICI as follows [46]

$$\mathrm{SIR}_{ICI} = \frac{P_u}{P_{ICI}} \geq \frac{\mathrm{si}^2(\pi\omega)}{1 - \mathrm{si}^2(\pi\omega)} \tag{2.52}$$

2.2.3.2 Modified model for simplified equalization in SDMA

The common method to compensate distortions from a single CFO is to rotate the phase φ in the received time-domain signal back to zero prior to any DFT operation [89]. Afterwards, the diagonal channel $\boldsymbol{\Lambda}$ can be equalized subcarrier-wise, as common in OFDM. As already mentioned, this proceeding is not applicable in OFDM-SDMA systems, as compensating for the CFO of a single user would misalign the signal of any other user. However, to maintain the simplified subcarrier-wise equalization OFDM systems are favoured for, it would be desirable to interchange the order of compensation and equalization operation, so that the user signals can first be separated and compensated for their individual CFOs afterwards. This approach requires a modification of the signal model (2.46), where the CFO distortion matrix $\mathbf{U}$ should be moved to the right hand side of channel matrix $\mathbf{H}$. To achieve that, we insert the matrix product $\mathbf{C}(-\varphi)\mathbf{C}(\varphi) = \mathbf{I}$ into (2.46) to the right next to $\mathbf{H}$ and obtain

$$\mathbf{y} = \mathbf{F}\mathbf{P}_2\bar{\mathbf{H}}\mathbf{C}(\varphi)\mathbf{P}_1\mathbf{F}^H \cdot \mathbf{x} \tag{2.53}$$

with the modified channel matrix $\bar{\mathbf{H}} = \mathbf{C}(\varphi)\mathbf{H}\mathbf{C}(-\varphi)$. This matrix has the same structure as the original $\mathbf{H}$, but the channel coefficients are now modified according to $\bar{h}_l = h_l \cdot \exp(j\varphi l)$. The corresponding diagonal matrix $\bar{\boldsymbol{\Lambda}}$ in frequency domain results from (2.47) based on $\bar{\mathbf{H}}$, i.e.

$$\bar{\boldsymbol{\Lambda}} = \mathbf{F}\mathbf{P}_2\bar{\mathbf{H}}\mathbf{P}_1\mathbf{F}^H \tag{2.54}$$

Correspondingly, the diagonal of $\bar{\boldsymbol{\Lambda}}$ represents the DFT of $\bar{h}_l$.

To restore the diagonal matrix $\bar{\boldsymbol{\Lambda}}$ in (2.53), the term $\mathbf{P}_1\bar{\mathbf{C}}(\varphi)$ has to be used instead of $\mathbf{C}(\varphi)\mathbf{P}_1$, with $\bar{\mathbf{C}}(\varphi)$ as defined in (2.49). The difference between these two terms amounts to

$$\boldsymbol{\Gamma} = \mathbf{C}(\varphi)\mathbf{P}_1 - \mathbf{P}_1\bar{\mathbf{C}}(\varphi)$$

Matrix $\boldsymbol{\Gamma}$ will in the following be denoted as the error matrix, as it represents the error that will be introduced if the two matrix products are replaced directly. Its structure will be characterized succeedingly: Recall that the $(N + N_g) \times N$ dimensional matrix $\mathbf{P}_1$ appends a cyclic prefix of N_g samples to the N-dimensional input vector $\mathbf{x}$; hence its structure can be described by a $N_g \times N_g$ identity matrix which is located in the upper right corner on top of a $N \times N$ identity matrix, and all other elements being zero. The structure of the error matrix $\boldsymbol{\Gamma}$ thus contains mainly zeros except in its upper right $N_g \times N_g$ submatrix, which itself is a diagonal matrix whose diagonal is composed of the elements γ_n, $n \in \{-N_g, \ldots, -1\}$, with

$$\gamma_n = \exp(jn\varphi)\left(1 - \exp(jN\varphi)\right). \tag{2.55}$$

Plugging $\mathbf{C}(\varphi)\mathbf{P}_1 = \mathbf{P}_1\bar{\mathbf{C}}(\varphi) + \boldsymbol{\Gamma}$ into (2.53) now yields

$$\mathbf{y} = \bar{\boldsymbol{\Lambda}} \cdot \underbrace{\mathbf{F}\bar{\mathbf{C}}(\varphi)\mathbf{F}^H}_{\mathbf{U}} \cdot \mathbf{x} + \underbrace{\mathbf{F}\mathbf{P}_2\bar{\mathbf{H}}\boldsymbol{\Gamma}\mathbf{F}^H}_{\mathbf{V}} \cdot \mathbf{x} \qquad (2.56)$$

The first part of the equation exhibits the desired signal structure, where the location of the CFO distortion and channel transmission operations have been interchanged compared to (2.48). Thus, the suggested receiver processing can be enabled. However, we have an additive error term $\mathbf{V}\mathbf{x}$ generated from the error matrix $\boldsymbol{\Gamma}$. The inner product $\mathbf{P}_2\bar{\mathbf{H}}\boldsymbol{\Gamma}$ of this term is a matrix with mainly zero elements except in its upper right $L_e \times L_e$ submatrix $\mathbf{V}_u$. This submatrix is an upper triangular matrix with the following structure:

$$\mathbf{V}_u = \begin{pmatrix} \gamma_{-L_e} \cdot \bar{h}_{L_e} & \gamma_{-L_e+1} \cdot \bar{h}_{L_e-1} & \cdots & \gamma_{-1} \cdot \bar{h}_1 \\ 0 & \gamma_{-L_e+1} \cdot \bar{h}_{L_e} & & \gamma_{-1} \cdot \bar{h}_2 \\ \vdots & & \ddots & \vdots \\ 0 & 0 & & \gamma_{-1} \cdot \bar{h}_{L_e} \end{pmatrix}$$

We observe that the elements in this submatrix reflect the (complex) difference of the effective channel echoes seen by the samples in the CP and their cyclic repetition at the end of the OFDM symbol. If these two signal fractions are no longer identical owing to the CFO, the periodic property of the OFDM signals is violated, resulting in interference to all subcarrier signals. With this finding, the total CFO-induced interference contained in model (2.56) can be segregated into two different types: The first type is given as ICI of the original subcarrier signal in $\mathbf{x}$, generated by the cyclic convolution in $\mathbf{U}$, and the second type is given as interference caused by the violation of the periodicity of the OFDM signals, represented in the term $\mathbf{V}\mathbf{x}$.

If equalization and CFO compensation are carried out as described above, the power from $\mathbf{V}\mathbf{x}$ will remain in the system and distort the signal as interference. In the following, we will therefore analyze its power as well as the resulting SIR conditions.

2.2.3.3 Interference remaining after CFO compensation

Obviously, $\mathbf{V}$ is the all-zero matrix if $\varphi = 0$ (i.e. no CFO is present) or if the channel is frequency flat ($L_e = 0$). Otherwise, the total power contained in $\mathbf{V}\mathbf{x}$ depends on the actual number of the channel echoes L_e. The mean power P_V contained in this term can be calculated by

$$P_V = \mathrm{tr}\left(E\left\{\mathbf{V}\mathbf{x}\mathbf{x}^H\mathbf{V}^H\right\}\right)$$

The expression given in the argument of the trace operator represents the correlation matrix $\mathbf{R}_e$ of the error term $\mathbf{V}\mathbf{x}$. As the elements constituting $\mathbf{V}$ and $\mathbf{x}$, respectively, can

be considered to stem from independent stochastic processes, we may write

$$\mathbf{R}_e = E\left\{\mathbf{V}\mathbf{x}\mathbf{x}^H\mathbf{V}^H\right\} = E\{\mathbf{V}E\left\{\mathbf{x}\mathbf{x}^H\right\}\mathbf{V}^H\} \tag{2.57}$$

With the i.i.d. assumption for the symbols contained in $\mathbf{x}$ with mean power P_s, $E\left\{\mathbf{x}\mathbf{x}^H\right\}$ is a diagonal matrix scaled with P_s. In case all subcarriers are occupied with data symbols, it equals $P_s \cdot \mathbf{I}$, and we obtain $\mathbf{R}_e = P_s \cdot E\{\mathbf{V}\mathbf{V}^H\}$. Inserting the matrix product constituting $\mathbf{V}$ from (2.56) and considering the structure of the inner product $\mathbf{P}_2\bar{\mathbf{H}}\boldsymbol{\Gamma}$ with its submatrix $\mathbf{V}_u$, the power P_V yields

$$P_V = \mathrm{tr}(\mathbf{R}_e) = P_s \cdot E\left\{\mathrm{tr}\left(\mathbf{V}_u\mathbf{V}_u^H\right)\right\}$$

With $\mathbf{V}_u$ from above, we obtain

$$\mathrm{tr}\left(\mathbf{V}_u\mathbf{V}_u^H\right) = 4\sin^2(\pi\omega)\sum_{m=1}^{L_e}\sum_{l=m}^{L_e}|h_l|^2$$

where the expression $4\sin^2(\pi\omega)$ results from $|\gamma_n|^2$. Taking the expected value of this expression relates P_V to fractions of the channel's PDP. Resorting to the characteristics of the considered channel model given in section 2.2.2.3, we can upper bound P_V according to

$$P_V \leq P_s L_e \cdot 2\sin^2(\pi\omega) \tag{2.58}$$

where the relation holds with equality for a uniform PDP.

Once we know the total power of the interference generated by the error matrix $\boldsymbol{\Gamma}$, we examine next how this interference power affects the single subcarrier signals. For this purpose, we first focus on the correlation of this additive interference in the frequency domain. The structure of matrix $\mathbf{V}_u$ reveals that the interference affects only the first L_e samples of the time-domain OFDM symbol, hence the interference in frequency domain will be highly correlated. To obtain more insight, we focus on the $N \times N$-dimensional time-domain correlation matrix, which we obtain from (2.57) as $\mathbf{R}_{e,t} = \mathbf{F}^H\mathbf{R}_e\mathbf{F} = E\{\mathbf{P}_2\bar{\mathbf{H}}\boldsymbol{\Gamma}\boldsymbol{\Gamma}^H\bar{\mathbf{H}}^H\mathbf{P}_2^H\}P_s$. As the channel taps $\bar{h}_l$ in $\bar{\mathbf{H}}$ are uncorrelated, $\mathbf{R}_{e,t}$ is a diagonal matrix with its diagonal representing the time-domain interference power profile $r_{e,t}(n)$. Only the first L_e elements of $r_{e,t}(n)$ differ from zero and are proportional to partial sums of the PDP

$$r_{e,t}(n) \sim \sum_{l=n}^{L_e}\sigma_l^2 \leq 1 - \frac{n}{L_e+1}, \quad n \in \{1,\ldots,L_e\} \tag{2.59}$$

The values of $r_{e,t}(n)$ can be bounded according to the expression on the right hand side, holding with equality for a uniform PDP. The frequency correlation matrix $\mathbf{R}_e = \mathbf{F}\mathbf{R}_{e,t}\mathbf{F}^H$ now is circular, which means the correlation between the subcarriers is independent of

the actual subcarrier position k. We thus conclude that the mean interference power P_i that distorts each subcarrier signal amounts to

$$P_i(\omega) = P_V/N \leq P_s L_e \cdot 2\sin^2(\pi\omega)/N \,, \tag{2.60}$$

indicating that the mean interference power P_V is uniformly spread over all the subcarrier signals.

To find out the correlation of the interference over frequency, we can determine the frequency correlation function $r_e(\kappa)$, which is calculated from the N-point DFT of the time-domain interference power profile $r_{e,t}(n)$. According to (2.59), $r_{e,t}(n)$ can be represented by a linear function with slope $\beta = (L_e + 1)^{-1} \leq 0.5$ which is multiplied by a rectangular window of width L_e to confine it to the specified range. The corresponding frequency correlation function $r_e(\kappa)$ thus can be generated by a convolution of the DFT of that linear function with the DFT of the rectangular window. It is quite evident that for the constrained slope β, the rectangular function will dominantly influence the spread of the correlation function, and hence we restrict our inspection on this component only. The DFT of the rectangular function of width L_e is

$$r_e(\kappa) \sim \frac{1}{N} \sum_{n=1}^{L_e} \exp\left(j2\pi\frac{\kappa n}{N}\right) \sim \frac{L_e}{N} \cdot \mathrm{si}\left(\pi\kappa\frac{L_e}{N}\right)$$

The subcarrier distance $|\kappa|$ where the normalized correlation drops down to a value below 0.5 can be estimated by

$$K_c = |\mathrm{si}^{-1}(0.5)| \cdot \frac{N}{\pi L_e} \approx 0.2\frac{N}{L_e} \tag{2.61}$$

K_c can be interpreted as a delimiter of the region around any subcarrier at position k where the power of the interference is highly correlated; we thus denote it as *interference correlation range*. The distance grows inversely proportional with the channel length L_e; a short channel length thus results in a high correlation of the interference. We will see later that the correlation of the interference supports a simplified CFO compensation process, which yields an improved error performance.

Further, it has to be considered that the interference contained in the term $\mathbf{Vx}$ from (2.56) is constituted of two different types, which affect the signal conditions at subcarrier position k differently. In particular, we encounter self-interference stemming from the signal at subcarrier k itself, which is represented by the diagonal elements in $\mathbf{V}$, and ICI-like distortion stemming from all other subcarrier signals, which is represented by the off-diagonal elements of $\mathbf{V}$. As the transmit symbols in $\mathbf{x}$ are assumed i.i.d., the ICI can be assumed to be uncorrelated with the signal at subcarrier k, and hence the distortion effect due to the ICI can be considered similar to the one of AWGN. The self-interference, however, may be strongly correlated with the signal at subcarrier k and thus may directly
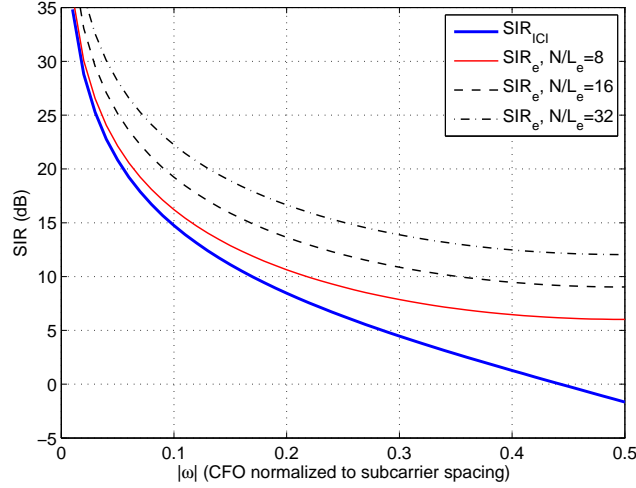
Fig. 2.11: SIR conditions for uncompensated CFO (2.52) and compensated CFO (2.62) based on the signal model in (2.56).

influence its signal level in a deterministic fashion. However, in the paragraph at the end of this subsection it is shown that the influence of the deterministic distortion evoked by the self-interference is negligible if $L_e \ll N$ holds, and consequently we may consider the total interference from $\mathbf{Vx}$ as pure ICI-like distortion here.

The power of the useful signal per subcarrier amounts to P_s. Thus, a closed form expression for a lower bound of the SIR resulting from the error matrix $\mathbf{\Gamma}$ can finally be given as

$$\text{SIR}_e = \frac{P_s}{P_i(\omega)} \geq \frac{N}{2L_e \cdot \sin^2(\pi\omega)} \tag{2.62}$$

We observe that an increasing channel length L_e decreases the SIR proportionally. As the proposed CFO compensation process ignores the error $\mathbf{\Gamma}$, we will not be able to overcome this SIR bound, even if the distortion measures $\bar{\mathbf{\Lambda}}$ and $\mathbf{U}$ needed for the compensation process are estimated perfectly.

To illustrate the obtained results, Fig. 2.11 compares the SIR bound for an uncompensated CFO from (2.52) with the SIR bound (2.62) achievable after applying the simplified CFO compensation process. The amount of interference power that can be removed by the suggested process corresponds to $\Delta P_i = \text{SIR}_{ICI}^{-1} - \text{SIR}_e^{-1}$. If $L_e = 0$, the interference can be removed completely by the CFO compensation process. For increasing L_e, however, an increasing share of the interference power is contained in the term $\mathbf{Vx}$ in (2.56), remaining in the system after compensation. If we set $\Delta P_i = 0$ and solve for L_e, we obtain the channel length where the compensation process is not capable of providing any gain. The minimum value for this length L_e is obtained for $|\omega| \rightarrow 0$, yielding $N/6$. This means that if $L_e > N/6$, the gains delivered by the CFO compensation process become vanishingly small, so that its application will no longer be suitable. In Fig. 2.11, this can be observed as the SIR_e curves approach the SIR_{ICI} curve for decreasing values of N/L_e.

For $N/L_e = 8$, the SIR gains achieved after compensation for small CFOs $|\omega| < 0.2$ have become already very small.

Correlation between self-interference and useful signal   To determine the correlation between the self-interference and the useful signal at any subcarrier k, we determine the covariance between the self-interference coefficient (i.e. the kth diagonal element of matrix $\mathbf{V}$) and the channel coefficient λ_k. As indicated above, the interference conditions evoked by matrix $\mathbf{V}$ are independent of the actual subcarrier position k, and hence it suffices to determine the covariance at a single subcarrier position; specifically we choose $k = 1$. The channel coefficient is given as $\lambda_1 = \sum_{l=0}^{L_e} \bar{h}_l$. Denote the first diagonal element of $\mathbf{V}$ as v_{11}. Considering the structure of matrix $\mathbf{V}$ based on the submatrix $\mathbf{V}_u$ (see section 2.2.3.2), v_{11} can be calculated as

$$v_{11} = \frac{1}{N} \sum_{m=0}^{L_e-1} \sum_{l=m+1}^{L_e} \gamma_{-l+m} \bar{h}_l$$

As both coefficients λ_1 and u_{11} have an expectation value of zero, the covariance is defined as $\mathrm{cov} = E\{\lambda_1^* v_{11}\}$. With the uniform PDP, we yield for the covariance of the two coefficients

$$\mathrm{cov} = \frac{\gamma_{-1}}{N(L_e+1)} \sum_{m=1}^{L_e} \sum_{l=0}^{L_e-m} \exp(-j\varphi l)$$

The second sum term on the right hand side represents a geometric series, so that similarly to (2.51) the si-function can be used to obtain an approximation, which is given as

$$\sum_{l=0}^{L_e-m} \exp(-j\varphi l) = \underbrace{\exp\left(-j\pi\omega \frac{L_e-m}{N}\right)}_{\approx 1} \underbrace{\mathrm{si}\left(\pi\omega \frac{L_e-m+1}{N}\right)}_{\approx 1} \cdot (L_e - m)$$

As usually $L_e \ll N$ holds, the exponential function as well as the si-function generate values that are very close to one for any $m \in \{1, \dots L_e\}$. Hence, both terms can be upper bounded with constant value one. Herewith the covariance can be upper bounded by

$$\mathrm{cov} < \gamma_{-1} L_e/(2N)$$

Assuming the signals λ_1, v_{11} to be Gaussian, the amount of power P_c devoted to the self-interference can with Theorem 10.1 from [49] be determined by

$$P_c = |\mathrm{cov}|^2 \cdot P_s < \frac{L_e^2}{N^2} \sin^2(\pi\omega) \cdot P_s$$

With this result, we can assess the ratio of the self-interference power to the total inter-

ference power $P_i(\omega)$ given in (2.60), yielding

$$\frac{P_c}{P_i(\omega)} \approx \frac{L_e}{2N}$$

For $L_e \ll N$, we conclude that the amount of self-interference is vanishingly small; hence there is no need to consider the self-interference separately to account for its special properties.

2.2.3.4 CFO compensation after channel equalization

We focus now in more detail on the CFO compensation process based on the signal model (2.56), which is carried out after channel equalization by multiplying the equalized signal vector $\hat{\mathbf{y}} = \bar{\mathbf{\Lambda}}^{-1}\mathbf{y}$ with the Hermitian matrix $\mathbf{U}^H$ (note that matrix $\mathbf{U}$ has unitary property). This latter operation represents a convolution of the subcarrier signals in $\hat{\mathbf{y}}$ with $u^*(-\kappa)$, which is given in (2.51). As the amplitude $u(\kappa)$ drops with $1/\kappa$, it may be sufficient to consider only the subcarriers in closest vicinity to the subcarrier k within the convolution process, which would simplify the entire process significantly. Let the vicinity range of subcarriers therefore be limited to K_l, i.e. $|\kappa| \leq K_l$. The convolution operation can then be specified by

$$\hat{x}_j = \sum_{\kappa=-K_l}^{K_l} u^*(\kappa) \cdot \hat{y}_{j+\kappa} \tag{2.63}$$

where $\hat{y}_k$ is the k-th symbol of vector $\hat{\mathbf{y}}$, and $\hat{x}_j$ is the j-th subcarrier signal obtained after equalization and CFO compensation.

To specify a suitable value for the delimiter K_l, note that $\hat{\mathbf{y}}$ is distorted by interference from $\mathbf{V}\mathbf{x}$, which is strongly correlated over the interference correlation range $|\kappa| \leq K_c$ specified in (2.61). Furthermore, note that $u(\kappa)$ given in (2.51) is near to being point-symmetric, i.e. $u(-\kappa) \approx -u(\kappa)$ holds. This near point-symmetric property of $u(\kappa)$ results in the fact that the correlated interference affecting the subcarrier signals in close vicinity of subcarrier j is canceled out almost completely in (2.63). For that reason, it seems to be reasonable to set the delimiter $K_l = [K_c]$, where $[x]$ denotes the integer nearest to x. Interestingly, simulation results presented in section 2.2.5 show that we are able to achieve a slight performance improvement with this selection compared to the full CFO compensation, where the interference from the total N subcarrier signals is taken into account.

Note that CFO compensation according to (2.63) can be realized with comparatively small demands on system complexity: Firstly, for practical system setups, K_l can be limited to small values. Furthermore, $u(\kappa)$ in (2.51) exhibits a single complex factor independent of κ, which represents the CPE. Compensation of the CPE can be incorporated into the channel equalization process. Therefore, (2.63) reduces to a convolution with a

simple, strictly real-valued function.

2.2.4 SIR analysis in OFDM-SDMA system

Recall the OFDM-SDMA transmission equation from (2.50). If we want to equalize the effective channel $\mathbf{H}_C$ completely, the only viable approach based on linear techniques is to invert the entire channel matrix $\mathbf{H}_C$ – which relates to the approach for OFDMA systems conducted in [15, 38]. However, this matrix is of dimension $MN \times QN$, and hence the complexity of this approach will quickly become infeasible for practical realizations. Although complexity can be reduced by exploiting the block-diagonal band structure of this matrix, it still remains considerably high. Moreover, as CFOs induce phase rotations of the effective subcarrier channels over time, the matrix $\mathbf{H}_C$ changes every OFDM symbol and thus has to be recomputed frequently, which increases the complexity for the inversion-based compensation even further.

An equalization approach that maintains the subcarrier-wise signal processing for the equalization and thus requires low complexity demands can be enabled if we alternatively adopt the signal model (2.56) derived in section 2.2.3.2. Herewith, the compound channel $\mathbf{H}_C$ can be written in the structured form

$$\mathbf{H}_C = \begin{pmatrix} \bar{\mathbf{\Lambda}}_{11} & \bar{\mathbf{\Lambda}}_{12} \\ \vdots & \vdots \\ \bar{\mathbf{\Lambda}}_{M1} & \bar{\mathbf{\Lambda}}_{M2} \end{pmatrix} \cdot \begin{pmatrix} \mathbf{U}_1 & \mathbf{0} \\ \mathbf{0} & \mathbf{U}_2 \end{pmatrix} + \begin{pmatrix} \mathbf{V}_{11} & \mathbf{V}_{12} \\ \vdots & \vdots \\ \mathbf{V}_{M1} & \mathbf{V}_{M2} \end{pmatrix}$$

The OFDM-SDMA transmission equation then yields

$$\bar{\mathbf{y}} = (\, \mathbf{\Lambda}_C \cdot \mathbf{U}_C \, + \, \mathbf{V}_C \,)\, \bar{\mathbf{x}} \tag{2.64}$$

where $\mathbf{\Lambda_C}, \mathbf{U}_C$ and $\mathbf{V}_C$ are the matrices constituting the compound channel matrix $\mathbf{H}_C$ above. Evidently, this notation enables the two-step equalization process introduced in the previous section: We first equalize the channel contained in matrix $\mathbf{\Lambda}_C$ by a subcarrier-wise equalization of the flat-fading SDMA channel and thereby spatially separate the single user signals. The separated user signals may then be compensated individually for their CFO distortions $\mathbf{U}_q$ as described in section 2.2.3.4. The entire receiver processing for the simplified CFO compensation in the SDMA system is illustrated in Fig. 2.12.

In what follows, we will analyze how the CFO-induced interference will affect spatial diversity gains that can be achieved with a linear multi-antenna receiver. As there is some correlation between signal and interference channels, distortion effects from the interference can no longer be expected to be similar to the one of AWGN. In particular, we will analyze the degree of correlation between the channel of the useful signal and the interference channels and derive SIR bounds describing the equivalent situation for AWGN.
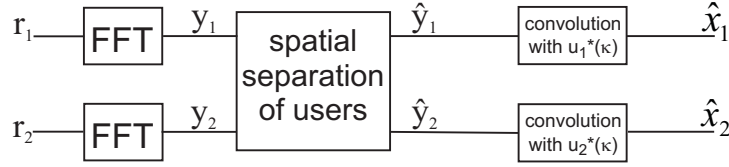
Fig. 2.12: Receiver processing for simplified signal reconstruction with CFO compensation in the SDMA uplink.

Analysis will be carried out for the case of no CFO compensation and compensation according to the proposed scheme separately.

2.2.4.1 Spatial diversity gain

In a brief intermezzo, we derive the basic relations concerning spatial diversity gains that are achievable with linear receivers in case of correlated signals. These relations form the basis for the analysis of the signal conditions in CFO-distorted OFDM-SDMA systems, which will be performed in the succeeding subsections. In particular, we examine here how interference that propagates via a correlated channel will affect the signal conditions at a multi-antenna receiver providing spatial diversity gain μ. Following the notion from [119], the spatial diversity gain can be illustrated by assuming a MRC receiver that combines the signals from μ independent receive antennas: Assume a signal x_1 with mean power P_s, which is transmitted via μ independent Rayleigh-fading channels h_{m1}, $m \in \{1, \ldots, \mu\}$, with unit mean power. At each receiving antenna m, the signal is distorted by AWGN with power N_0. MRC operation then yields a post-MRC signal to noise ratio (SNR) of $\mu P_s / N_0$. The SNR thus is increased by factor μ compared to the SNR of the signal at a single receive antenna.

Instead of AWGN, we consider an interfering signal x_2 with mean power N_0 now. The signal at m-th receive antenna reads

$$y_m = h_{m1} x_1 + h_{m2} x_2 \tag{2.65}$$

Let the two signal x_q be uncorrelated, while some correlation between the two channels h_{mq} is assumed. Both variables h_{mq} are assumed to be zero-mean Gaussian variables with variance $\text{var}(h_{mq}) = E\{h_{mq}^* h_{mq}\}$. The correlation between both variables can be characterized by the correlation coefficient defined as [49]

$$\rho = \frac{\text{cov}(h_{m1}, h_{m2})}{\sqrt{\text{var}(h_{m1})\text{var}(h_{m2})}} \ , \quad \rho \in [0, 1] \tag{2.66}$$

where $\text{cov}(h_{m1}, h_{m2})$ stands for the covariance of the two variables given in the parentheses. According to Theorem 10.1 in [49], the distribution of h_{m2} conditioned on h_{m1} can be

characterized by the two measures

$$
\begin{aligned}
E\{h_{m2}|h_{m1}\} &= \rho\sqrt{\frac{\mathrm{var}(h_{m2})}{\mathrm{var}(h_{m1})}}h_{m1} \\
\mathrm{var}(h_{m2}|h_{m1}) &= (1-\rho^2)\mathrm{var}(h_{m2})
\end{aligned}
$$

Accordingly, h_{m2} can be rewritten as

$$
h_{m2} = \rho\sqrt{\frac{\mathrm{var}(h_{m2})}{\mathrm{var}(h_{m1})}}\,h_{m1} + \sqrt{(1-\rho^2)\mathrm{var}(h_{m2})}\,z_m
$$

where we introduced a new Gaussian variable z_m with zero mean and unit power, which is independent of h_{m1}. Substituting this equation in (2.65) yields

$$
y_m = \underbrace{h_{m1}x_1}_{s}+\underbrace{\rho\sqrt{\frac{\mathrm{var}(h_{m2})}{\mathrm{var}(h_{m1})}}\,h_{m1}x_2}_{f_1}+\underbrace{\sqrt{(1-\rho^2)\mathrm{var}(h_{m2})}\,z_m\cdot x_2}_{f_2} \qquad (2.67)
$$

MRC operation delivering the spatial diversity gain is carried out by multiplying each received signal y_m with the conjugate channel seen by the useful signal x_1 and summing up the signals over all μ receive antennas: $y^{MRC} = \sum_{m=1}^{\mu} h_{m1}^* y_m$. Within this summation, the signal portions from the first two components in (2.67), s and f_1, which both depend on h_{m1}, add up constructively, yielding a mean power of

$$
\begin{aligned}
\mu^2 E\{ss^*\} &= \mu^2\mathrm{var}(h_{m1})P_s \\
\mu^2 E\{f_1 f_1^*\} &= \mu^2\rho^2\mathrm{var}(h_{m2})N_0
\end{aligned}
$$

after MRC operation. In contrast to that, the signal portions from the third component in (2.67), f_2, add up with arbitrary phase, so that the mean power for these signal portions yields after MRC

$$
\mu E\{f_2 f_2^*\} = \mu(1-\rho^2)\mathrm{var}(h_{m2})N_0
$$

Now let, for simplicity, $\mathrm{var}(h_{m1}) = \mathrm{var}(h_{m2}) = 1$. With the above results, we obtain for the post-MRC SIR

$$
\mathrm{SIR}^{MRC} = \frac{\mu P_s}{[(\mu-1)\rho^2+1]\,N_0} = \nu\cdot\mu\frac{P_s}{N_0} \qquad (2.68)
$$

clearly revealing that the spatial diversity gain factor μ is diminished by

$$
\nu = [(\mu-1)\rho^2+1]^{-1} < 1
$$

Thus, ν represents the effective SNR loss factor owing to the channel correlation $\rho > 0$.

2.2.4.2 No compensation of CFO distortions

Now we turn our focus back on the signal conditions in the OFDM-SDMA system in case the ICI distortions are not compensated. Consider the signal received at antenna m, which, according to (2.50), is given as

$$\mathbf{y}_m = \mathbf{U}_1\boldsymbol{\Lambda}_{m1}\mathbf{x}_1 + \mathbf{U}_2\boldsymbol{\Lambda}_{m2}\mathbf{x}_2$$

In case all subcarriers carry signals with identical transmit power, the statistical properties of the ICI are identical for all the elements contained in $\mathbf{y}_m$. Therefore, we carry out the analysis exemplarily for the first element of vector $\mathbf{y}_m$, denoted as y_m. To separate the ICI from the useful signal, we define $\bar{\mathbf{u}}_q$ as the first row vector of matrix $\mathbf{U}_q$, where the first element has been replaced by zero. The transmission equation then yields

$$y_m = u(0)(\lambda_{m1}x_1 + \lambda_{m2}x_2) + \underbrace{\bar{\mathbf{u}}_1\boldsymbol{\Lambda}_{m1}\mathbf{x}_1 + \bar{\mathbf{u}}_2\boldsymbol{\Lambda}_{m2}\mathbf{x}_2}_{ICI} \tag{2.69}$$

where λ_{mq} is the channel coefficient for the first subcarrier extracted from matrix $\boldsymbol{\Lambda}_{mq}$, and x_q is the transmit signal of user q at the first subcarrier. We set x_1 as the useful signal. An appropriate equalizer is able to remove the signal portion $\lambda_{m2}x_2$, if estimates of the channels λ_{mq} can be obtained with sufficient quality. The two scalar products within equation (2.69), however, will remain in the system as ICI. The signal structure in the above equation is now similar to (2.65), and hence we can use the results from the preceding subsection to determine achievable spatial diversity gains here. Clearly, the two scalar products representing the ICI in (2.69) are constituted of multiple interfering signals. However, as all elements within vector $\mathbf{x}_q$ are assumed i.i.d., each scalar product can be modeled by a single random variable, whose power is constituted from the sum of powers from the single elements in $\bar{\mathbf{u}}_q\boldsymbol{\Lambda}_{mq} =: \mathbf{f}_q$. In particular, we yield for the power of the interfering channel

$$E\{\mathbf{f}_q\mathbf{f}_q^H\} = E\{\bar{\mathbf{u}}_q\boldsymbol{\Lambda}_{mq}\boldsymbol{\Lambda}_{mq}^H\bar{\mathbf{u}}_q^H\} = \sum_{j=1}^{N-1}|u(j)|^2 \leq 1 - \text{si}^2(\pi\omega_q)$$

where we used the upper bound for P_{ICI} presented in section 2.2.3.1. The covariance between the useful channel λ_{m1} and the interference channels $\bar{\mathbf{u}}_q\boldsymbol{\Lambda}_{mq}$ is determined by

$$\mathbf{z}_q = E\{\lambda_{m1}^*\bar{\mathbf{u}}_q\boldsymbol{\Lambda}_{mq}\}$$

As channels from different users are assumed uncorrelated, $\mathbf{z}_q$ yields a vector with non-zero entries for $q = 1$ only. The N elements of the covariance vector $\mathbf{z}_1$ can be characterized

by the function

$$z(\kappa) = \begin{cases} 0 & \kappa = 0 \\ u(\kappa) \cdot r(\kappa) & \kappa \in \{1, \ldots, N-1\} \end{cases}$$

with $r(\kappa)$ being the subcarrier correlation function defined in section 2.2.2.3. The total power of the covariance vector $\mathbf{z}_1$ is determined as

$$\mathbf{z}_1^H \mathbf{z}_1 = \sum_{\kappa=1}^{N-1} |u(\kappa)|^2 |r(\kappa)|^2$$

which can be read as the power of the covariance $|\text{cov}|^2$ of an equivalent random process based on a single random variable. With these results, we can determine a measure representing the correlation between the useful channel and the sum of interference channels, which is calculated equivalently to the correlation coefficient in (2.66):

$$\rho^2 = \frac{\mathbf{z}_1^H \mathbf{z}_1}{E\{\lambda_{m1}^* \lambda_{m1}\} E\{\mathbf{f}_1 \mathbf{f}_1^H\}} \geq \frac{\sum_{\kappa=1}^{N-1} |u(\kappa)|^2 |r(\kappa)|^2}{1 - \text{si}^2(\pi \omega_1)} \tag{2.70}$$

Evaluating this measure for varying L_e reveals that $\rho^2 \approx 1$ for $L_e \ll N$, suggesting that the useful channel and the interference channels for the ICI generated from $\mathbf{x}_1$ are nearly fully correlated. Evidently, this results mainly from the high frequency correlation of subcarrier channels that is valid for $L_e \ll N$.

Consequently, we can conclude here that if an MRC-like signal combination is performed at the multi-antenna receiver, not only the signal portions of the useful signal x_1, but also the ones of the interference from $\mathbf{x}_1$ will add up fully coherently. In contrast to that, there is no correlation between the useful channel λ_{m1} and the interference channels $\bar{\mathbf{u}}_q \mathbf{\Lambda}_{mq}$, $q \neq 1$, as the covariance of the corresponding channels yields zero. Consequently, this distortion will behave similarly to AWGN. Resorting to the derivation of the SIR in (2.68) in the preceding section, we yield for the achievable SIR in an OFDM-SDMA system with spatial diversity gain μ

$$\text{SIR}_{ICI}^{MRC} \geq \frac{\mu \, \text{si}^2(\pi \omega_1)}{\mu(1 - \text{si}^2(\pi \omega_1)) + (1 - \text{si}^2(\pi \omega_2))}$$

where we have used the bounds for P_u and P_{ICI} from section 2.2.3.1 for the total power of useful signal and ICI, respectively. This result shows that in the OFDM-SDMA system with diversity gain μ, the ICI power generated by any user $q \neq 1$ is effectively attenuated by factor μ (i.e. the diversity gain can be realized completely), while the ICI generated from the CFO of user $q = 1$ himself is fully preserved (i.e. no diversity gain is achievable). If all users Q have a CFO of the same size, $\omega_q = \omega \; \forall q$, then the effective reception SIR[2]

---

[2] referring to the mean power of each user's signal measured at any receive antenna m

for the equivalent AWGN case can be given as

$$\text{SIR}_{ICI} \geq [\mu + Q - 1]^{-1} \frac{\text{si}^2(\pi\omega)}{1 - \text{si}^2(\pi\omega)} \tag{2.71}$$

This result is equivalent to the SIR bound for the single-antenna case (2.52), reduced by the effective SIR-loss factor $\eta = [\mu + Q - 1]^{-1}$.

2.2.4.3 Compensation of CFO distortions

Next we consider the case where the CFO distortions are compensated according to the proposed concept. Then interference results from the signal components contained in matrix $\mathbf{V}_C$ in (2.64) only, and the signal received at antenna m reads

$$\mathbf{y}_m = \bar{\boldsymbol{\Lambda}}_{m1}\mathbf{U}_1\mathbf{x}_1 + \bar{\boldsymbol{\Lambda}}_{m2}\mathbf{U}_2\mathbf{x}_2 + \mathbf{V}_{m1}\mathbf{x}_1 + \mathbf{V}_{m2}\mathbf{x}_2$$

Again, we define $\mathbf{x}_1$ as the useful signal. The proposed equalization and ICI compensation concept removes the interference from $\bar{\boldsymbol{\Lambda}}_{m2}\mathbf{U}_2\mathbf{x}_2$ as well as the the ICI induced by $\mathbf{U}_1$, and correspondingly solely the interference from $\mathbf{V}_{mq}\mathbf{x}_q$ remains in the system. Equivalently to the analysis carried out in the preceding subsection, we will now determine the correlation between useful channels and the channels of the residual interference to specify achievable spatial diversity gains. However, to ease analysis here, we initially focus on the entire channel matrices $\bar{\boldsymbol{\Lambda}}_{m1}$ and $\mathbf{V}_{mq}$ to specify the overall statistical properties. Afterwards, we determine the signal conditions per subcarrier signal by averaging over the total N subcarriers of the system.

The mean power of the interfering channel $\mathbf{V}_{mq}$ per subcarrier amounts to

$$\frac{1}{N}\text{tr}\left(E\{\mathbf{V}_{mq}^H\mathbf{V}_{mq}\}\right) \leq \frac{L_e}{N} \cdot 2\sin^2(\pi\omega_q)$$

For the bound, we used the result from (2.58). Correspondingly, the mean power of the useful channel $\bar{\boldsymbol{\Lambda}}_{m1}$ yields

$$\frac{1}{N}\text{tr}\left(E\{\bar{\boldsymbol{\Lambda}}_{m1}^H\bar{\boldsymbol{\Lambda}}_{m1}\}\right) = \frac{1}{N}\text{tr}\left(\mathbf{I}\right) = 1$$

The covariance between useful channel and interfering channel can be characterized by the covariance matrix

$$\mathbf{Z}_q = E\{\bar{\boldsymbol{\Lambda}}_{m1}^H\mathbf{V}_{mq}\}$$

As $\mathbf{V}_{mq}$ is constituted of the channel coefficients related to channel $\bar{\boldsymbol{\Lambda}}_{mq}$, the covariance matrix $\mathbf{Z}_q$ will have non-zero entries for $q = 1$ only. The corresponding matrix $\mathbf{Z}_1$ can be determined as follows: Using the definitions of $\bar{\boldsymbol{\Lambda}}$ from (2.54) and $\mathbf{V}$ from (2.56), $\bar{\boldsymbol{\Lambda}}_{m1}^H\mathbf{V}_{m1}$ can be written as $(\mathbf{F}\mathbf{P}_1^H\bar{\mathbf{H}}_{m1}^H\mathbf{P}_2^H)(\mathbf{P}_2\bar{\mathbf{H}}_{m1}\boldsymbol{\Gamma}_1\mathbf{F})$. For the moment we will exclude

the outer DFT matrices $\mathbf{F}$ and determine the expectation value of the inner matrix product. $\mathbf{P}_1^H \bar{\mathbf{H}}_{m1}^H \mathbf{P}_2^H$ is a circular Toeplitz matrix based on the channel impulse response $\bar{h}_l$, and $\mathbf{P}_2 \bar{\mathbf{H}}_{m1} \mathbf{\Gamma}_1$ was shown in section 2.2.3.2 to be a matrix with zero entries except for the submatrix $\mathbf{V}_u$ found in its upper right corner. The expectation value of the product of these two components thus yields a matrix with zero entries except for the $L_e \times L_e$ anti-diagonal submatrix in its upper-right corner, whose L_e anti-diagonal elements ξ_i represent partial sums of the channel power weighted by γ_{-i}:

$$\xi_i = \gamma_{-i} \sum_{l=i}^{L_e} \sigma_l^2, \quad i \in \{1, \ldots, L_e\}$$

with γ_n defined in (2.55). From the covariance matrix, we can determine the mean power of the covariance between useful and interfering channels per subcarrier signal according to

$$\frac{1}{N} \text{tr}(\mathbf{Z_1 Z_1}^H) = \sum_{i=1}^{L_e} |\xi_i|^2 \leq |\gamma_n|^2 \frac{1}{(L_e + 1)^2} \sum_{i=1}^{L_e} i^2 = |\gamma_n|^2 \frac{L_e(2L_e + 1)}{6(L_e + 1)}$$

where the upper bound is obtained for a uniform PDP. Note that $|\gamma_n|^2 = 4 \sin^2(\pi \omega_1)$. Similar to (2.70), we can now determine a measure equivalent to the squared correlation coefficient:

$$\rho^2 = \frac{N^{-1} \text{tr}(\mathbf{Z_1 Z_1}^H)}{N^{-1} \text{tr}\left(E\{\bar{\mathbf{\Lambda}}_{m1}^H \bar{\mathbf{\Lambda}}_{m1}\}\right) N^{-1} \text{tr}\left(E\{\mathbf{V}_{m1}^H \mathbf{V}_{m1}\}\right)} \approx \frac{2L_e + 1}{3(L_e + 1)} < \frac{2}{3} \tag{2.72}$$

Assuming again a receiver with spatial diversity gain μ, we may now determine the SIR for the useful signal after an MRC-like signal combination over μ independent observations. Resorting to the derivation of the SIR in in (2.68), we yield for the interference from $\mathbf{V}_{m1} \mathbf{x}_1$ a mean power of $\mu \nu^{-1} P_i(\omega_1)$, with the interference power $P_i(\omega)$ according to (2.60) and the SIR loss factor ν from (2.68). As all other interference channels $\mathbf{V}_{mq}$, $q \neq 1$, are uncorrelated with the useful channel $\bar{\mathbf{\Lambda}}_{m1}$, the corresponding interference $\mathbf{V}_{mq} \mathbf{x}_q$ adds up incoherently, yielding a mean power of $\mu P_i(\omega_2)$. Hence, we obtain the post-MRC SIR

$$\text{SIR}_e^{MRC} = \frac{\mu P_s}{\nu^{-1} P_i(\omega_1) + P_i(\omega_2)}$$

If we have multiple users Q who all have a constant CFO, i.e. $\omega_q = \omega \, \forall q$, the effective reception SIR at any antenna m for the equivalent AWGN case can be bounded by

$$\text{SIR}_e \geq [(\mu - 1)\rho^2 + Q]^{-1} \frac{N}{2L_e \sin^2(\pi \omega)} \tag{2.73}$$

where we used the bound for $P_i(\omega)$ from (2.60), and ρ^2 should be used as specified in (2.72). This expression is equivalent to the SIR bound found for the single-antenna case

in (2.62) reduced by the effective SIR-loss factor $\eta_e = [(\mu-1)\rho^2+Q]^{-1}$. Note here that the CFO-induced interference scales with the number of parallel SDMA users Q. In case of full correlation ($\rho = 1$), the SIR-loss factor η_e is identical to η, the factor found in case of no CFO compensation in (2.71). As a major result, we conclude here that the correlated interference from the CFO distortion results in an increase of the effective SIR-loss if a receiver with spatial diversity gain $\mu > 1$ is employed.

2.2.5 Simulation results

In this section we will provide numerical simulations to verify our analytical results found in the previous sections. For the simulations, we assume OFDM signal transmission via a noisy channel, i.e. the transmission equation (2.50) is now given by

$$\bar{\mathbf{y}} = \mathbf{H}_C \cdot \bar{\mathbf{x}} + \mathbf{n}$$

where $\mathbf{n}$ is a vector consisting of MN AWGN samples with power N_0. Thus, the mean reception SNR amounts to P_s/N_0 for the signal of any user at any receive antenna. As we have indicated that the CFO-induced interference can be expected to behave like AWGN, it can be assumed that this interference degrades the interference-free AWGN performance (i.e. no CFO is present) according to the amount of interference power. In particular, if the SNR P_s/N_0 is equal to the CFO-induced SIR, we can expect that the transmission experiences a performance degradation of 3 dB compared to the interference-free case.[3] This basic principle will be used to verify the SIR bounds derived in the preceding sections.

We consider an OFDM-SDMA system with $N = 64$ subcarriers, where $Q = 2$ single-antenna user terminals are granted simultaneous access. For the bounds to be tight, all N subcarriers are occupied with transmission symbols from both users. The channel between each antenna link is modeled as Rayleigh-fading with $L_e+1 = 5$ channel taps and a uniform PDP. The normalized CFO is fixed to $\omega = 0.1$. As a performance measure, we use the bit error rate (BER) that is achieved for an uncoded transmission of uncorrelated 16QAM symbols, averaged over both users. We use a zero forcing (ZF) equalizer to equalize the channel distortions and spatially separate the user signals per subcarrier. The diagonal channel $\mathbf{\Lambda}_C$ from (2.64) as well as the CFOs ω_q are assumed to be known perfectly at the receiver.

Based on the signal model (2.56), we first examine the achievable performance for a single-antenna link (SISO). Results are given in Fig. 2.13. The solid bold line shows the achievable BER performance in case no CFO is present. The suggested compensation approach shows a significantly degraded performance. At an SNR P_s/N_0 equal to the SIR bound (2.62), which amounts to 19 dB for the given parameter setting, it clearly exhibits

---

[3]As interference and AWGN are assumed to be independent, their joint distortion can be considered as Gaussian-like with power equal to the sum of powers from the two independent processes.
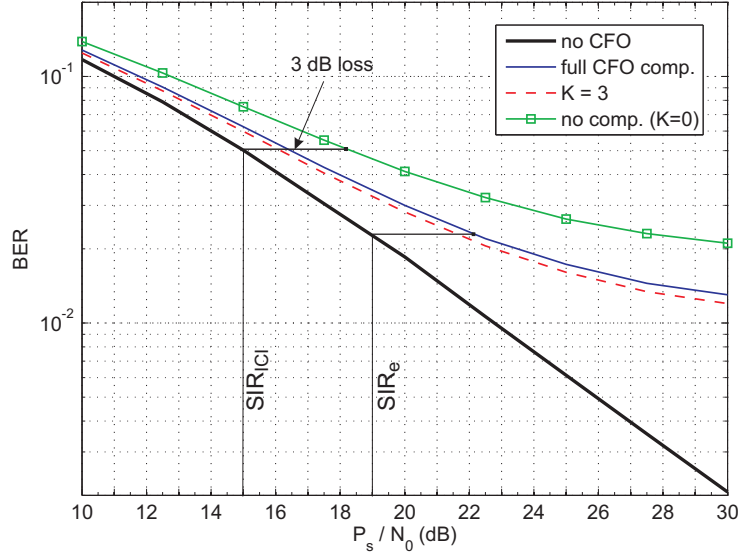
Fig. 2.13: BER performance of SISO system distorted by normalized CFO $\omega = 0.1$ based on the signal model in (2.56).

a performance loss of 3 dB. This observation thus verifies the bound derived in (2.62).

The performance curve of the CFO compensated system runs into an error floor for high SNR that corresponds to the BER performance achievable with the CFO-free performance at about 22 dB – which is about 3 dB higher than the SIR bound. The reason for that can be found in the distribution of the interference generated from the distortion terms in $\mathbf{Vx}$ in (2.56): Note that the values in $\mathbf{Vx}$ are generated from products of the independent random variables $\bar{h}_l$ in $\mathbf{V}$ and the data symbols in $\mathbf{x}$, which are all assumed to be Gaussian. The resulting distribution function for the values in $\mathbf{Vx}$ is thus in general no longer Gaussian. Instead, we observe that the majority of the values from this distribution is much more concentrated around their mean than in the Gaussian case. Due to this fact, the achieved error floor is significantly lower than it would be if the interference behaved like Gaussian noise with identical power. However, it is worth noting that with increasing L_e and thus with an increasing number of independent variables $\bar{h}_l$ in $\mathbf{V}$, the distribution of the values in $\mathbf{Vx}$ approaches the Gaussian case – thanks to the central limit theorem.

If we apply the CFO compensation technique that removes the ICI from the subcarriers in close vicinity $\kappa \leq K_l$ only (see section 2.2.3.4), we obtain the performance given by the dashed line for $K_l = [K_c] = 3$. Interestingly, for the choice of K_l according to K_c given in (2.61), the CFO compensation accounting only for some of the ICI distortion achieves a slight performance improvement compared to the full CFO compensation. Obviously, this is a benefit related to the correlated interference from $\mathbf{Vx}$ in (2.56), as detailed in section 2.2.3.4.

If we do not compensate for the ICI caused by the CFO but compensate for the CPE only, which corresponds to the case of applying the compensator (2.63) with $K_l = 0$, we obtain the performance represented by the uppermost curve. For an SNR equal to
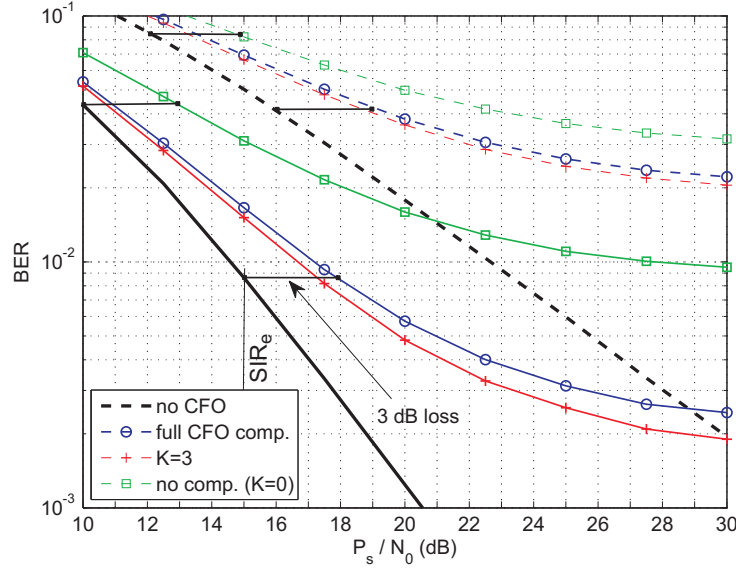
Fig. 2.14: BER performance of 2-user SDMA system distorted by normalized CFO $\omega = 0.1$ with ZF receiver. Dashed: diversity gain $\mu = 1$. Solid: $\mu = 2$.

the bound in (2.52), which amounts to 15 dB for the given parameter setting, we clearly observe a performance loss of 3 dB compared to the performance where no CFO is present.

For the 2-user SDMA case, we consider ZF equalization to separate the signals of the different users. In [119] the diversity gain delivered by the ZF receiver has been shown to yield $\mu = M - Q + 1$. For our examinations, we consider two cases; a receiver with $M = 2$ and $M = 3$ antennas, providing a diversity gain of $\mu = 1$ and $\mu = 2$, respectively. Performance results are shown in Fig. 2.14. The dashed curves refer to $\mu = 1$, while the solid curves refer to $\mu = 2$. The curves representing full CFO compensation according to the proposed scheme exhibit a 3 dB performance loss at an SNR equal to the SIR from (2.73) compared to the curve of CFO-free transmission, which amounts to 16 dB for $\mu = 1$ and 15 dB for $\mu = 2$, respectively, for the given parameter setting. These losses are highlighted in Fig. 2.14 by the horizontal black lines, clearly verifying the bound derived in (2.73). As in the SISO case, we observe that we can achieve a slight performance improvement if we use the simplified CFO compensation process based on (2.63) with $K_l = 3$. In case we do not compensate the ICI caused by the CFO, we achieve a severely degraded performance, which clearly exhibits a 3 dB performance loss at an SNR of 12 dB for $\mu = 1$ and 10 dB for $\mu = 2$, respectively, corresponding to the analytical bound (2.71).

In Fig. 2.15 we examine the behaviour of the BER when the CFO compensation process based on (2.63) is applied for different values of the delimiter K_l. We focus on a constant SNR $P_s/N_0 = 20$ dB, which reflects the BER of the error floor for $\mu = 1$. For the selected values of N/L_e, the subcarrier correlation range K_c from (2.61) amounts to 3.2 and 1.6, respectively. Interestingly, the corresponding curves exhibit their minimum at $K_l = 3$ and $K_l = 2$, respectively, which is the integer nearest to K_c. Hence, selecting $K_l = \lceil K_c \rceil$ indeed seems to be a good choice. This result leads us to the conclusion that it suffices
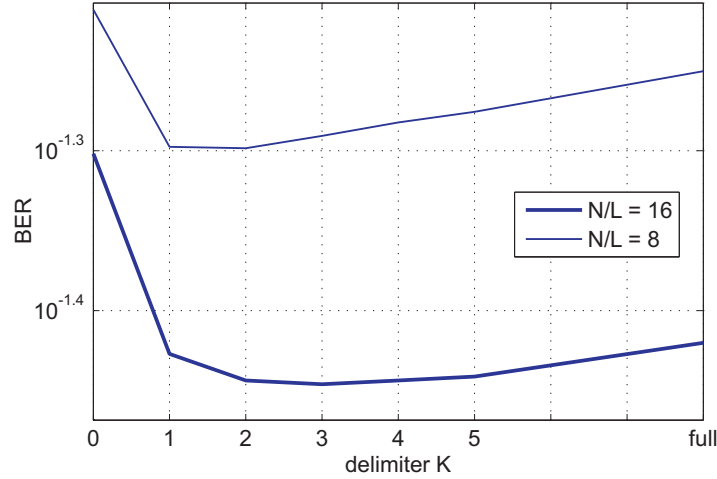
Fig. 2.15: BER performance at SNR $= 20$ dB vs. delimiter K_l. $\mu = 1$, $Q = 2$, $\omega = 0.1$

to consider only the subcarrier signals in closest vicinity within the CFO compensation via (2.63).

To illustrate the performance degradation caused by the incomplete compensation of the CFO effects in the OFDM-SDMA system, we specify the effective SNR loss ΔSNR based on the ratio of the interference power bound from (2.73) and the noise power N_0 as done in [25], which yields (in dB)

$$\Delta\text{SNR} = 10\log_{10}\left(1 + \frac{\eta_e N P_s}{2L_e \sin^2(\pi\omega)N_0}\right)$$

The numerical evaluation of the effective SNR loss for various CFO sizes ω is depicted versus the SNR P_s/N_0 in Fig. 2.16; the corresponding parameter setting is specified in its caption. In accordance with the observations drawn from Fig. 2.14, where evaluations where based on a CFO of size $\omega = 0.1$, the corresponding curve indicates here a 3 dB SNR loss at an SNR $P_s/N_0 = 16$ dB. For comparison, we also added the SNR loss for the case of no ICI compensation (dashed curves), where we used the interference power bound from (2.71). Although we observe that the proposed CFO compensation is able to reduce the SIR loss significantly, it still increases steeply for increasing CFO size ω. If the CFO amounts to 20% of the subcarrier spacing, the performance of the system is degraded by 3 dB already at an SNR level of about 10 dB.

These results show that the system's sensitivity towards CFO errors is still very high, and hence we conclude that with the suggested approach, we can conveniently compensate CFOs of small size only. Thus, the method is suitable for a fine frequency synchronization only, and hence it has to rely on a coarse synchronization, which has to be established in advance. In a practical system, such a coarse synchronization can be achieved if the terminals use their frequency estimates obtained during the preceding downlink phase for a
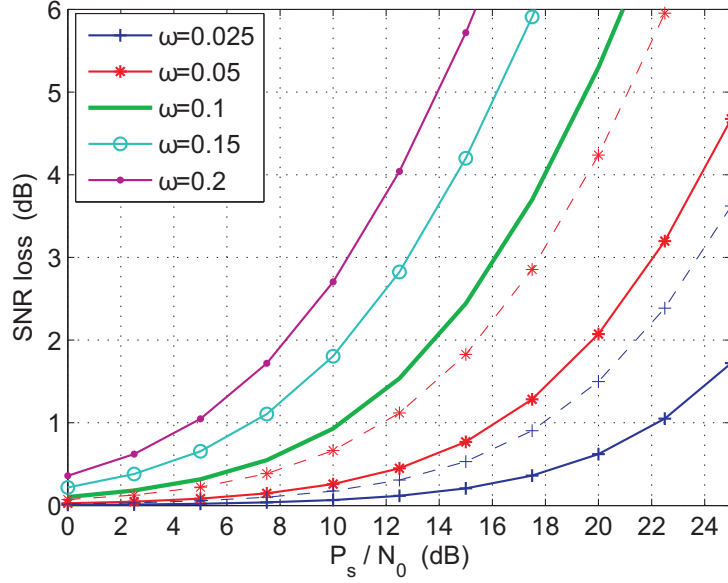
Fig. 2.16: SNR loss after CFO compensation vs. SNR for CFOs of different size ω. Solid: ICI compensation. Dashed: no compensation. $\mu = 1$, $Q = 2$, $N/L_e = 16$

proper frequency pre-compensation of their transmit signals. We denote this as *frequency advance*, which has been the basic concept for our real-time system implementation that has been reported in [48]. It is worth noting that the analysis presented in this paper and in particular the derived bounds for the SIRs served as an important guideline in preparing the experiments that have been summarized in that reference, which have shown that a convenient system operation in a practical setup can be achieved.

Finally, note that if the CFOs are kept small, the signal degradation from ICI is limited, and thus common pilot-based channel estimation techniques can still be used to obtain channel estimates of sufficient quality. The more pilots available in one OFDM symbol can be used for that channel estimation, the better the ICI can be suppressed, as the ICI behaves similar to AWGN. Moreover, the CFOs ω_q of the single users $q \in \{1, \ldots, Q\}$ can be obtained from observing the phase drift of the estimated subcarrier channels λ_k over several successive OFDM symbols. With (2.51), the ICI coefficients $u(\kappa)$ can then be determined, which can finally be applied in (2.63) for proper ICI compensation of the single users' signals.

2.2.6 Conclusion chapter 2.2

We have investigated OFDM-SDMA uplink transmission in the presence of multiple users' CFOs. We modified the common signal model suitably to enable a subcarrier-wise SDMA equalization followed by a user-specific CFO compensation, yielding a simple equalization process ready to be applied in practice. However, as CFOs violate the periodic structure of the OFDM signals, some interference remains in the system after CFO compensation, which cannot be compensated as long as simple frequency domain processing is targeted. The SIR conditions in OFDM-SDMA systems have been analyzed if CFOs are compensated according to the proposed scheme as well as if they are not. We derived suitable upper bounds for the SIRs depending on the system parameters, which have been verified by numerical simulations. To enable a convenient operation of the proposed scheme, we conclude from the results that the users' CFOs should not exceed values that are much larger than a few percent of the OFDM subcarrier spacing, which classifies this scheme as a technique for fine frequency synchronization. Correspondingly, coarse frequency synchronization has to be ensured, which can easily be established if the CFO estimates from the downlink are used in the uplink for a proper pre-distortion of each user's transmit signal, as suggested also in [69] and practically realized in [48]. Together with this concept, the proposed scheme can be regarded as a convenient solution to synchronize the OFDM-SDMA uplink. Note that this concept based on coarse synchronization also enables to estimate user channels based on common pilot-based channel estimation techniques. Suitable estimates of the users' CFOs can then be obtained from the phase drift of the estimated channels observed over several consecutive OFDM symbols.

3 Practical link adaptation for multi-user MIMO-OFDM

Once the multi-user MIMO-OFDM system has been synchronized, data transmission of high spectral efficiency can be established by properly utilizing the capabilities of the MIMO channel. It is well-known that the capacity gains promised by the MIMO channel [29] can be enabled by adapting the transmission to the current channel conditions [76]. In particular, this requires some information on the channel conditions to be available at the transmitter's side. For downlink transmission, there are basically two different approaches for attaining this information at the BS: In time division duplex (TDD) systems, one can rely on the reciprocity of the channel and correspondingly use the channel information that could be attained when the BS was receiving signal from the UTs (i.e. during uplink). In frequency division duplex (FDD) systems, however, downlink and uplink channels are substantially different, and thus the UTs have to report some information on their current channel conditions to the BS via a feedback channel in that case. Evidently, adaptation in FDD systems is quite challenging, as the data rate of the feedback channel is limited in practice, which means that usually only partial information on the actual channel conditions can be conveyed to the BS. Based on the channel information available at the BS, the BS can adapt the transmission signals designated for a specific UT by applying so called beamforming vectors matching the MIMO channel, as well as by tuning the data rate according to current signal and interference conditions. As this adaptation procedure is intended to optimize the quality of single communication links, the whole process is summarized with the term *link adaptation*.

In practice, proper application of a link adaptation of this kind requires the radio channels to be quasi-static, i.e. the channels are required to vary slowly over time, so that they can be considered constant over several transmission frames. Over this duration, the link adaptation can be held constant once it has been determined. An update of the link adaptation is then required to be made as soon as the underlying channel has noticeably changed. However, if the requirement of quasi-stationarity of the channel is not met, the concept does not loose its relevance immediately, as for limited channel dynamics the channels can be predicted based on linear inter- and extrapolation techniques.

In this chapter, we will first provide the theoretical background for channel adaptive transmission in the multi-user MIMO-OFDM downlink of FDD systems. In section 3.2, we

present a practical link adaptation solution with limited demands on system complexity and feedback. Finally, in section 3.3 we propose an extension of that link adaptation concept for time-varying channels, which is based on channel prediction techniques.

3.1 Theoretical background

The spatial dimension of the MIMO radio channel can be accessed in spatial multiplexing (SMUX) or in spatial diversity transmission mode. While in SMUX mode multiple data streams are transmitted simultaneously via the radio channel, the diversity mode utilizes the independent propagation paths between different antenna pairs to improve the quality of the signal transmission. Early results from investigations on system-level [27] indicated that the mode achieving the highest spectral efficiency depends on the actual channel and signal conditions experienced by a user. Later, this relationship was substantiated by the fundamental tradeoff pointed out between diversity and SMUX mode in [126]. This crucial finding motivated the development of an adaptive transmission system which selects the transmission mode depending on the actual channel quality in order to improve the error rate performance for fixed data rate transmission [34, 63] or to increase the spectral efficiency [16, 19, 58, 86]. In those works, the channel conditions are evaluated at the receiver's side, and the decision on the mode together with a channel quality identifier (CQI) is fed back to the transmitter, resulting in little feedback demands. While the aforementioned concepts benefit from adapting the transmission to the instantaneous channel conditions, it was shown in [28] that the capacity can also be enhanced if the mode selection is based on the long-term channel statistics represented by the covariance matrix of the MIMO channel.

In recent years, the focus in MIMO communications has been shifted from point-to-point towards multi-user links [31]. The available multi-user diversity [54] in those systems enables further enhancements of the achievable spectral efficiency. The key idea is to assign the simultaneously transmitted streams of the SMUX mode to different users, thus enabling SDMA. The capacity of the MIMO broadcast channel (BC) exploiting SDMA transmission has been shown in [13, 112, 113] to be achievable with the dirty paper coding technique [21]. For individual user constraints like desired target SINRs, a framework for the optimum solution of the multi-user downlink beamforming problem has been presented in [91]. All those solutions are based on the assumption that full channel state information (CSI) is available at the BS. In recent work [8], information theory analysis revealed that for the low SNR regime, it is optimum to transmit a single stream to a single user only, while with increasing SNR, support for additional SDMA users should successively be added. This result already suggests that mode switching can be applied beneficially also in multi-user MIMO systems.

For proper application of SDMA, information on the state of each user's channel is

required at the BS. As availability of full CSI from all the users at the BS is hardly possible in FDD systems, solutions based on limited feedback have been introduced that provide partial CSI to the BS [61]. A promising concept with comparatively low demands on feedback is opportunistic beamforming [114], where the BS generates random precoding vectors (beams). These are evaluated at the UTs in terms of their reception SNR, which is then reported to the BS. In case of a high SNR value, it is likely that the selected precoding vector points close into the direction of the actual channel, thus yielding the desired partial CSI. While the original concept was designed for the transmission of a single stream to a single user, a solution for SDMA has been introduced in [96], where the BS provides sets of unitary beams that are served simultaneously with equal power. In this latter work, it was proposed that the UTs determine the signal to interference and noise ratio (SINR) for each received beam and convey the index of the best received beam together with the corresponding SINR value to the BS, which then assigns each beam to the user achieving highest rate. It was shown that for a large number of users, the achievable downlink capacity of this system scales equivalently to the capacity of the MIMO BC.

To ease system implementation, fixed instead of random beams can be used, as suggested in proposals for next generation radio systems [1, 42]. As the fixed beams are available at any time, the user does not have to wait until a beam is provided that matches his channel conditions, and thus potential latency problems can be avoided.

While [96, 114] exclusively support a single transmission mode, initial performance results on mode switching in multi-user links based on a fixed set of unitary beams have been presented in [86], where the throughput performance of a 2×2 MIMO configuration with two users was compared to a 4×2 point-to-point link. Further results for single-antenna UTs have been presented in [24, 117], where the switching problem was formulated in terms of a balance between multi-user diversity and multiplexing gain. Feedback is given in terms of CQI for all provided beams, which is still a comparatively small amount. [117] further reports significant performance gains compared to the single mode schemes [96, 114], revealing that the mode switching concept has a high potential especially in cases where the number of available users is not exceptionally large (sparse network [31]).

In a multi-user system we have to care for fairness in the resource assignment process. In particular, it has to be ensured that resources will also be assigned to users experiencing relatively poor channel conditions. This can be achieved by applying scheduling policies at the BS tailored to meet predefined fairness constraints. One of these policies is the proportional fair scheduler [114], which enables each user to realize a constant fraction of his total achievable rate. The score-based scheduler proposed in [11] represents an efficient heuristic approach that aims at assigning all users the same amount of resources. In case all users are experiencing identical fading conditions, the scheduler asymptotically achieves

proportional fairness. The set of resources to be scheduled can be defined arbitrarily over all dimensions (time/frequency/space) and can be flexibly adapted to any latency constraints. Due to these properties, the approach enables a simple and efficient resource allocation process, which makes it a favourable solution for the employment in practical systems.

3.2 Spatial adaptation concept for quasi-static channels

The motivation for the work presented in this paper was the development of a practical concept for downlink transmission in a real-time multi-user MIMO-OFDM system, aiming at a high throughput while meeting desired fairness constraints within a predefined time frame. Therefore, we extend the score-based scheduling approach for the support of spatial mode switching, including SDMA access. Precoding based on fixed beams is adopted to obtain partial CSI at the BS. Opposed to existing work in the field [117], we assume UTs with multiple antennas, which enable interference suppression to improve the SINRs of the received beams. Assuming linear receivers, the UTs determine the achievable per-beam rates for the different spatial transmission modes and convey information on their preferred beams and the corresponding rates per mode to the BS via a low-rate feedback channel. This serves as the input for the extended score-based scheduler, which implicitly selects the spatial transmission mode per user. By introducing a weighting of the user-specific scores generated by the scheduler, we can adapt the targeted degree of fairness, which is illustrated with the example of equal rates for all users. The capabilities of the scheduling concept are numerically analyzed for a 2×2 MIMO configuration, showing that mode switching as well as enabling SDMA access lead to substantial performance gains.

The downlink capacity achievable with the proposed system concept for the 2×2 MIMO configuration is finally compared with the capacity of the MIMO BC based on full CSI. This comparison reveals that the proposed system concept is capable of realizing a large proportion of that BC capacity.

3.2.1 System model

We consider the downlink of a broadband multi-user MIMO-OFDM system, where a BS with N_t antennas communicates with K UTs equipped with N_r antennas each. The BS provides $B \geq N_t$ fixed beams $\mathbf{b}_i$, which are used for spatial precoding of the transmission signals (grid of beams (GoB) concept, presented in [40]). We assume a uniform transmit power allocation over all subcarriers; hence the transmission equation for each subcarrier's signal is given by

$$\mathbf{r} = \mathbf{HCs} + \mathbf{n} \tag{3.1}$$

where $\mathbf{H}$ is the $N_r \times N_t$ dimensional MIMO channel and $\mathbf{C}$ is the precoding matrix comprising N_t of the B beams $\mathbf{b}_i$ with unitary property, which may be simultaneously active. The transmit vector $\mathbf{s}$ contains up to N_t non-zero transmit symbols with constant transmit power $E\{\mathbf{s}^H\mathbf{s}\} = P_s$, i.e. the power P_s is uniformly distributed over all non-zero transmit symbols in $\mathbf{s}$. Finally, $\mathbf{n}$ is the noise vector with N_r circularly symmetric complex Gaussian entries, and its covariance is given by $E\{\mathbf{n}\mathbf{n}^H\} = N_0 \cdot \mathbf{I}$.

Transmission is based on a slotted time structure, where each slot is constituted of several consecutive OFDM symbols. The total transmission resources of a slot are given by the subcarriers available for signal transmission. By subdividing the signal bandwidth into single sub-bands confined to a fixed number of consecutive subcarriers, we partition these transmission resources into blocks, which are denoted as *chunks* in the following. The chunks form the basic scheduling resources that can be individually assigned to distinct users. Each chunk is processed separately, and thus the spatial transmission mode may be selected individually per chunk. The supported spatial modes are termed as single-stream (ss) and multi-stream (ms), which relate to the diversity mode and SMUX mode, respectively. Thanks to the multiple antennas at the UTs, a single user can also receive multiple spatial streams in ms mode. To differentiate between the two cases in ms mode where the available spatial streams are assigned either to a single user or to multiple different users, the terms single-user MIMO (SU-MIMO) and multi-user MIMO (MU-MIMO) are used, respectively.

The channel is assumed to be perfectly known at the receiving UTs only. Based on the GoB, the UTs can evaluate the channel per chunk and determine the rates they are able to achieve in the different spatial modes with each beam. Beams achieving highest rate are selected for potential transmission. Each user conveys information on the beam selection per spatial mode and the achievable rate per beam to the BS, which then carries out the user scheduling process. To simplify the concept further, we assume linear equalization techniques are being applied at the multi-antenna receivers. Hence, to recover the i-th symbol s_i within vector $\mathbf{s}$, we multiply the received vector $\mathbf{r}$ with the equalization vector $\mathbf{w}_i$ according to

$$\hat{s}_i = \mathbf{w}_i^H \mathbf{r} \tag{3.2}$$

In this chapter, we consider MRC for ss mode and minimum mean square error (MMSE) equalization for ms mode. For these techniques, closed form expressions for the post-detection SINRs[1] of the spatial streams exist, facilitating the evaluation and proper comparison of the rates that can be achieved with the different spatial modes.

The applied scheduling process is based on the score-based scheduling strategy [11], which is a simple heuristic process aiming to assign each user his best resources from a set of resources defined over arbitrary dimensions: The resources of each user within the set

---

[1]The post-detection SINR is the SINR of the useful signal achieved after equalization.

are ranked by their quality, and corresponding scores are assigned. The BS then assigns a resource to the user providing the best score. On average, this scheduling strategy assigns an equal amount of resources to each user. For identical fading statistics, each user thus can realize a constant fraction of his total achievable rate, yielding (asymptotically) a degree of fairness similar to that of the proportional fair scheduler [114]. In our research, we confine the set of resources to those comprised in a transmission slot. Hence, all users will be scheduled within the same time-slot, and the score-based scheduling translates to an even distribution of the chunks over all users. In this work, we consider two kinds of fairness constraints: First, fairness in terms of an equal number of resources being assigned to the users. Hereby, we account for the users' capabilities to support transmission of multiple spatial streams in ms mode, i.e. users supporting ms mode are assigned correspondingly more spatial streams than users supporting ss mode. On the other hand, we show in section 3.2.3.5 that the fairness target of the score-based scheduler can be altered by introducing a weighting of the scores. As an example, we tune the scheduler to achieve fairness in terms of an equal rate for all users in the system.

3.2.2 Precoding: The Grid of Beams

In this subsection, we will give some details on the proper choice of the vectors constituting the GoB: The GoB concept itself can be understood as a quantization scheme for the precoding vectors to be used for signal transmission. It is well known that the optimum choice of precoding vectors in single-user MIMO links are the eigenvectors of the matrix product $\mathbf{H}^H\mathbf{H}$. The optimum quantization of these vectors in uncorrelated MIMO Rayleigh-fading channels has been elaborated in [62] for diversity transmission and in [60] for SMUX transmission. For the Rayleigh-fading assumption, it follows an isotropic distribution of the eigenvectors in the N_t-dimensional vector space of $\mathbf{H}^H\mathbf{H}$. Under this condition, the authors in [62] formulated the problem of finding the optimum quantization vectors as a subspace packing problem in the manifold of all linear subspaces of this vector space, which is called the Grassmannian manifold. By using a suitable distance metric, the optimum set of quantization vectors for diversity mode is found as the one where the minimum distance between any pair of these vectors is maximized. For SMUX mode, the optimum solution is a set of unitary $N_t \times N_r$ matrices, which are found in a similar fashion, but based on different distance metrics.

However, due to per-antenna power constraints encountered in practice, it is desirable to use beams for precoding that distribute the power uniformly over the transmit antennas. In the literature, this is termed equal gain transmission (EGT). Quantization of precoding vectors for EGT has been studied in [59], where it was shown for uncorrelated Rayleigh-fading that a set of N_t unitary vectors is sufficient to guarantee achieving the full diversity gain of the channel $\mathbf{H}$. To obtain $B = rN_t$ suitable precoding vectors for EGT, with r

being an integer specifying the number of unitary beam sets with N_t beams, the authors in [59] propose to take the first N_t rows of the rN_t-dimensional DFT matrix. These precoding vectors are commonly referred to as DFT beams.

In practice, MIMO channels are often spatially correlated to some extent, so that the uncorrelated Rayleigh fading assumption, which was the basis for the investigations mentioned above, does not hold in general. One of the major differences is that in correlated channels, the distribution of the channel's eigenmodes is biased. This has a direct impact on the achievable spectral efficiency, which has been studied in [105]. In that work, it was shown that in case of an isotropic input (equal power per active beam, N_t beams simultaneously active), the channel correlation diminishes the achievable spectral efficiency compared to Rayleigh fading. Opposed to that, it was also shown that for a non-isotropic input (less than N_t beams are simultaneously active), the spectral efficiency can be improved.

If the channels are spatially correlated, the dominant eigenmodes are concentrated around the dominant eigenvector of the channel's covariance matrix $\mathbf{R}_H = E\{\mathbf{H}^H \mathbf{H}\}$. If the channels between transmit/receive antenna pairs have the same statistical properties – which is a common assumption also for realistic MIMO channels – $\mathbf{R}_H$ is a Toeplitz matrix with hermitian property, i.e. $\mathbf{R}_H^H = \mathbf{R}_H$, with a real-valued diagonal and, in general, with all entries being non-zero. The dominant eigenvector of a matrix with these properties is close to the N_t-dimensional vector with equal-weighted entries. This vector fulfils the properties of an EGT vector, suggesting that precoding based on DFT beams as described above may be a suitable choice especially for the case of correlated MIMO channels.

In a multi-user scenario, a solution achieving near-optimal performance is to serve multiple users simultaneously on their dominant channel eigenmodes [7]. This result suggests that the same quantization techniques from above can also be deemed suitable in the multi-user context.

Remarks from above suggest that DFT beams are a convenient choice for GoB-based precoding in practical systems, and hence we have also adopted them for our research. For SMUX transmission, we allow only sets of unitary beams to be active simultaneously, as precoding matrices of this kind were shown to optimize various performance measures in single user links (see [63] and references therein). Hence, the beams provided by the BS are constituted from r independent sets of N_t unitary DFT beams, i.e. $B = rN_t$. For example, for $N_t = 2$, the $r = 2$ unitary DFT beam sets $\mathbf{C}_1$ and $\mathbf{C}_2$ that will be used as precoding matrices in (3.1) are given as:

$$\mathbf{C}_1 = \frac{1}{\sqrt{2}} \cdot \begin{bmatrix} 1 & 1 \\ i & -i \end{bmatrix}, \mathbf{C}_2 = \frac{1}{\sqrt{2}} \cdot \begin{bmatrix} 1 & 1 \\ 1 & -1 \end{bmatrix}, \tag{3.3}$$

where the $B = 4$ beams $\mathbf{b}_i$, $i \in \{1, \ldots, B\}$ are given as the columns of the two matrices.

3.2.3 Resource scheduling with spatial mode selection

We will now describe the adaptive transmission concept, which is based on a 2-step procedure illustrated in Fig. 3.1. It consists of a channel evaluation unit at the side of the UT (step 1) and the resource scheduling and transmission mode selection unit at the BS (step 2). In step 1, a user carries out a chunk-wise evaluation of the different transmission modes and determines the achievable rates per beam. The single per-beam rates from all modes over all chunks are then ranked by their quality, and corresponding scores are assigned. This also yields a ranking of the single chunks of that user. The scores are used by the BS in step 2 to assign the beams in a chunk individually to the users and to make a final decision on the transmission mode per chunk, which is taken under the premise of guaranteeing a high throughput for each user. Note that the chunk-wise selection of the transmission mode allows to serve users in different modes simultaneously, enabling an improved link adaptation and thus a higher user throughput.

3.2.3.1 Channel evaluation at UT, step 1

Based on the actual channel $\mathbf{H}$, a UT determines for each transmission mode the beams it can achieve the highest data rate with. Evaluation is carried out for each chunk separately, which is represented by the different layers in Fig. 3.1(a).

In ss GoB mode (upper branch of Fig. 3.1(a)), a single beam is assumed to be powered with full transmit power P_s. At the receiver MRC is used, where the equalization vector for beam $\mathbf{b}_i$ is defined as $\mathbf{w}_i = \mathbf{H}\mathbf{b}_i$. Based on MRC, the post-detection SINR for each beam $\mathbf{b}_i$ can be determined according to

$$\mathrm{SINR}_{ss}(i) = \frac{P_s}{N_0} \|\mathbf{H}\mathbf{b}_i\|^2 \, , \, i \in \{1, \ldots, B\} \tag{3.4}$$

where $\|\mathbf{x}\|^2 = \mathbf{x}^H \mathbf{x}$ is the square of the Euclidean norm of vector $\mathbf{x}$. The equation yields the SINR for a single subcarrier signal. The SINR for the entire chunk can be obtained by determining an effective SINR from the per-subcarrier SINRs of that chunk, which can be based on the methods introduced in [73]. However, if the channel conditions do not vary considerably over the frequency width of a chunk, it may be sufficient to determine the SINR for the center subcarrier within the chunk only. Once the SINR values for all B beams are obtained, the achievable rate $r_{ss}(i)$ per beam $\mathbf{b}_i$ can be determined by using a suitable mapping function $\mathcal{M}(\cdot)$:

$$r_{ss}(i) = \mathcal{M}\left(\mathrm{SINR}_{ss}(i)\right)$$

(a) Step 1: Channel evaluation and determination of the scores at the UT.

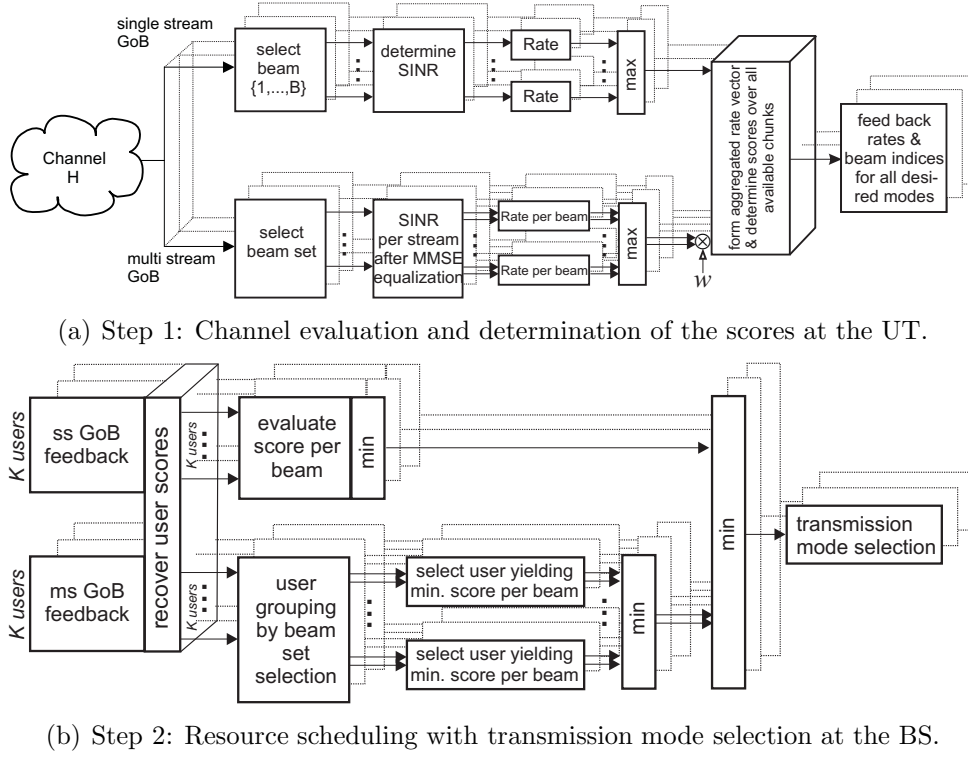(b) Step 2: Resource scheduling with transmission mode selection at the BS.

Fig. 3.1: Structure of the 2-step procedure constituting the adaptive transmission concept.

The beam favoured for ss mode is the one achieving maximum rate, i.e. $R_{ss} = \max_i r_{ss}(i)$.

In ms GoB mode (lower branch of Fig. 3.1(a)), $Q \leq N_t$ unitary beams are served in parallel with equal transmit power P_s/Q per beam. As r unitary beam sets of dimension N_t are provided, there exist a total of $M = r\binom{N_t}{Q}$ sets of unitary beams of dimension Q. The following evaluation is performed for each set of beams $m \in \{1, \ldots, M\}$ separately: To recover the data stream transmitted on the i-th beam of set m, denoted as $\mathbf{b}_{mi}$, $i \in \{1, \ldots Q\}$, we use the MMSE equalizer. The corresponding MMSE equalization vector is defined as

$$\mathbf{w}_{mi} = \mathbf{Z}^{-1}\mathbf{H}\mathbf{b}_{mi}, \quad \mathbf{Z} = \frac{QN_0}{P_s} \cdot \mathbf{I} + \sum_{k=1}^{Q} \mathbf{H}\mathbf{b}_{mk}\mathbf{b}_{mk}^H\mathbf{H}^H \tag{3.5}$$

The post-detection SINR for each beam $\mathbf{b}_{mi}$ is then given by

$$\mathrm{SINR}_{ms}(m,i) = \frac{\|\mathbf{w}_{mi}^H\mathbf{H}\mathbf{b}_{mi}\|^2}{\mathbf{w}_{mi}^H\mathbf{Z}\mathbf{w}_{mi} - \|\mathbf{w}_{mi}^H\mathbf{H}\mathbf{b}_{mi}\|^2} \tag{3.6}$$

From the SINR values obtained for the chunks from (3.6), one can determine the achievable rate per beam by applying the mapping function again: $r_{ms}(m,i) = \mathcal{M}\left(\mathrm{SINR}_{ms}(m,i)\right)$. The beam set $\bar{m}$ preferred for ms transmission is the one that comprises the beam achieving highest overall rate.[2]

$$\bar{m} = \arg\max_m \left(\max_i r_{ms}(m,i) \right)$$

---

[2]This criterion for beam set selection for MU-MIMO mode has also been suggested in [52].

Once the beam set is selected, the Q per-beam rates belonging to that set are stored, yielding $R_{ms,i} = r_{ms}(\bar{m}, i)$, while all others may be discarded.[3]

For $N_t > 2$, the number of active streams Q supported in ms mode may be in the range $\{2, \ldots, N_t\}$. In this case, the evaluation branch for ms mode in Fig. 3.1(a) may be processed for each single value of Q, yielding a set of rates $R_{ms,i}$ for each of these ms mode options.

3.2.3.2 Determination of the scores

In the following, the score concept is introduced. Therefore, let u be the chunk index and U be the total number of available chunks. The scores are used to rank the per-beam rates $R_{ss}(u)$ and $R_{ms,i}(u)$ of each user over all chunks U according to their quality. We use a single score set $\mathcal{S}$ for the ranking of the user rates from all transmission modes to enable an implicit selection of the transmission mode within the score-based scheduling process following in step 2. However, this approach requires a direct comparison of the single per-beam rates from the different spatial modes, whereby it must be taken into account that each mode supports a different number of simultaneously active beams. A practical solution to enable the desired comparison with simple means is the introduction of a weighting factor w, which is used to weight the rates of the ms mode to account for its spatial multiplexing capability. For proper choice of w, we will take into account some basic considerations:

As we aim for a high user throughput, spatial mode selection should follow the rationale to favour ss mode whenever the user rate can be expected to be larger than the rate expected in ms mode. Consider that if a user decides globally for ms mode with Q active beams, the available spatial streams compared to ss mode are increased by factor Q. As a general result from that, we can assume that the user will be assigned also Q times the streams he would get if he globally selected ss mode. Hence, we can conclude that decision in favour of ss mode should be taken if the rates for the different modes in a single chunk u fulfil

$$R_{ss}(u) > Q \cdot \max_i R_{ms,i}(u) \,, \tag{3.7}$$

suggesting $w = Q$ as a suitable choice for the weighting factor of per-beam rates in ms mode.

We now return to the generation of the user scores: The per-beam rates from ss mode $R_{ss}(u)$ as well as the weighted rates from ms mode $R_{ms,i}(u)$ from all chunks U are aggregated into one vector, which is sorted by magnitude in descending order.[4] The index within the sorted vector represents the score ς of each beam.

Optionally, the user may use the scores to make a pre-selection of his best chunks as

---

[3]It is clear that this approach is suboptimum, however, it keeps the required feedback demand low and thus forms a suitable solution for practical application.

[4]In the case of multiple resources yielding identical rates, these are ordered in a random fashion.

well as of his preferred mode per chunk u, which could be a suitable measure to further reduce the amount of required feedback.[5] For all selected chunks, the user finally feeds back the achievable rates for the beams supported by the desired transmission modes as well as the corresponding beam indices.

3.2.3.3 Resource scheduling at BS, step 2

The second step of the process comprises the resource scheduling with implicit transmission mode selection and is carried out at the BS, which collects the feedback information from the K users, see Fig. 3.1(b). As a first step, it recovers the scores ς^k for user k from the provided rates over all U chunks. Hereafter, the scores are partitioned according to the transmission mode they refer to, yielding $\varsigma_{ss}^k(u)$ and $\varsigma_{ms}^k(u, i)$, respectively. Resource allocation with transmission mode selection is then carried out for all chunks successively. Hereby, an individual set of users is selected per chunk, and the number of beams assigned to each user is continuously tracked.

For each chunk u, the user selection process is carried out for each transmission mode separately: For ss mode (upper branch of Fig. 3.1(b)), the favoured user is the one providing the minimum score for that mode.[6]

$$k(u) = \arg \min_{k \in \{1, \dots, K\}} \varsigma_{ss}^k(u) \quad \forall u \in \{1, \dots, U\}$$

The lower branch of Fig. 3.1(b) illustrates the user selection for ms mode. Here, users that chose the same beam set m are possible candidates for MU-MIMO access and are thus put into one group, forming the user set $\mathcal{K}$. In each group $m \in \{1, \dots, M\}$, each of the Q available beams is assigned to the user providing the minimum score for that beam.

$$k(u, m, i) = \arg \min_{k \in \mathcal{K}} \varsigma_{ms}^k(u, i), \quad \forall i \in \{1, \dots, Q\}$$

Obviously, this user selection implicitly includes the SU-MIMO access mode, as all spatial streams will be assigned to the same user if he provides the minimum scores for all Q available beams. After user selection has been carried out for all groups, we pick the group $\tilde{m}$ containing the user with minimum score

$$\tilde{m}(u) = \arg \min_m \left(\min_i \varsigma_{ms}^{k(u,m,i)}(u, i) \right)$$

Finally, we compare the scores of the users selected for the different transmission modes in chunk u and select the transmission mode embracing the user with minimum score. In essence, selection of the transmission mode and beam set for each chunk is thus dictated

---

[5]This kind of user-driven chunk selection has also been suggested in [108].

[6]In the case of multiple users providing identical scores, the stream is given to the user assigned the least beams so far.

by the user providing minimum overall score. The decision on the mode and the user allocation per chunk is then signalled forward to the UTs, who configure their receivers accordingly.

Remark: Although the concept of the scheduling process has been developed for an isolated cell scenario, where only intra-cell interference from simultaneously active beams is taken into account in (3.4) and (3.6), the scheme can readily be employed in a multi-cell environment. The only modification required is to substitute the noise figure $N_0\mathbf{I}$ in the MMSE equalizer by an interference plus noise correlation matrix that takes into account the inter-cell interference. Evaluation of the scheduling concept in a multi-cell environment has been carried out in [85, 101, 103].

3.2.3.4 Feedback

For the evaluations carried out in section 3.2.4, we assume the UTs to feed back the information on the achievable rates per evaluated transmission mode for all available chunks (full feedback). For practical applications, however, the concept offers a high potential for further feedback reduction, as the score-based ranking allows each user to preselect his best chunks as well as his preferred mode to be served with. A score-based pre-selection of the transmission mode may result in a severe performance loss, though, which is illustrated by the following two examples: If there are not sufficient users in the system (sparse network), it may occur that no MU-MIMO partner can be found for a user who provided the best score for the ms mode. In this case, this user could be served either via multiple beams in SU-MIMO mode or, alternatively, in diversity mode. To achieve highest possible throughput for that user, the final mode selection should be based on his achievable rate – which requires also the availability of the ss rate at the BS. On the other hand, if a user prefers ss mode, but a ms user is selected, the former could still be assigned resources if he provided appropriate rates for ms mode.

As the scheduling process aims at assigning each user his best resources only, it is certainly not economical to let the users report on all available resources, but on their best chunks only. These can easily be selected after the scores have been determined by the UTs, which is related to the suggestion in [108] denoted as *Top-M feedback*. Furthermore, a similar selection can also be done for the rates referring to the transmission modes in a chunk, including the options for different Q. For example, for $N_t = N_r = 2$, a practical solution could be to let the users report two rates: The best ms rate enabling MU-MIMO access, and additionally the ss rate (enabling diversity mode) or the next ms rate (enabling dual-stream SMUX for that user). The adequate choice of the second rate to report could be based on the higher rate achievable with diversity mode or dual-stream SMUX mode.

Moreover, the frequency-selective feedback information for the utilized transmission band will be highly correlated, so that proper compression techniques can conveniently be applied, yielding a further reduction of the required feedback per user. Elaborating on

the adequate amount of total required feedback is an interesting field for further studies, but lies out of the scope of this thesis.

3.2.3.5 Fairness steering

As for every user the same score set is used to rank the available resources, the score-based scheduler will on average distribute the available resources evenly over all users (see also [11]). For identical fading statistics, each user will be able to realize about the same fraction of his total achievable rate. However, one can think of applications where it might be desirable to distribute the resources with a different scheduling target. Forcing our proposed scheduler to assign the resources according to such an altered target can easily be achieved by applying a user-specific weighting of the scores determined at the BS (step 2 of the process). As this weighting will have a direct impact on the degree of fairness the scheduler is able to establish, we denote this process as *fairness steering*.

As an example, we will present an algorithm targeting at equal rates for all users in the time-slot. Assume that the achievable rates of all users are known. To go for equal user rates, the resources can be redistributed over all users by following the "Robin-Hood principle", where resources are taken from high rate users and are given to low rate users in order to improve their realizable rate. Specifically, this can be achieved by weighting the scores of the users by a factor proportional to the achievable rate of each user. This results in the fact that high rate users are considered less frequently in the resource scheduling process in favour of the low rate users, so that the latter will be assigned more resources than the high rate users. To develop a suitable algorithm for the fairness steering, we will firstly derive some basic relations based on the average behaviour of the score-based scheduler. These are then used as a guideline for the development of an algorithm tailored to approach the equal rate target in an iterative fashion.

Let R_k be the achievable rate of user $k \in \{1, \ldots, K\}$. If no weighting of the scores is applied, the scheduler assigns on average all users the same amount of resources u, so that the average rate per resource for user k can be given as R_k/u. Now let w_k and w_l be the weighting factor of k-th and l-th user, respectively, and $x = w_k/w_l$ be their ratio. Then we can conclude that user l will be considered within the resource scheduling process by factor x more frequently than user k. As a result, the average amount of resources u_l assigned to user l will be by factor x larger than the amount of resources u_k assigned to user k. It follows

$$\frac{u_l}{u_k} = x = \frac{w_k}{w_l} \tag{3.8}$$

With the weighted scores, the scheduling yields the new achievable rate $\bar{R}_k$ for user k, which can be approximated by

$$\bar{R}_k \approx u_k \cdot R_k/u \tag{3.9}$$

The target rate $\bar{R}_k$ should be identical for all users, so we have $\bar{R}_k = \bar{R}_l \quad \forall k \neq l$, With

equations (3.8) and (3.9), we obtain

$$w_k = \frac{R_k}{R_l} \cdot w_l \qquad (3.10)$$

If we define user l as the reference user, whose weighting factor we set to unity, $w_l = 1$, the weighting factors for all users k can be obtained simply from the ratio of their achievable rate R_k and the achievable rate of the reference user, R_l.

Evidently, the obtained result cannot be applied directly to our scheduler, as some relations have been simplified and hold for the average behaviour of the scheduler only. However, we can use it as a guideline for the construction of an iterative weighting and scheduling process, which enables us to approach the equal rate target in a stepwise manner. In each iteration, the closeness to the equal rate target is checked by determining the deviation of each user rate from the mean rate over all users. The stopping criterion is fulfilled if this deviation cannot be further decreased. The iterative algorithm is described as follows:

1. run scheduling process with unweighted scores, yielding an achievable rate R_k for each user

2. determine mean rate $\bar{R}$ over all users, $\bar{R} = \frac{1}{K} \sum_{k=1}^{K} R_k$

3. calculate sum of deviations between user rates and $\bar{R}$, i.e. $D = \sum_{k=1}^{K} |R_k - \bar{R}|$

4. determine $R_{min} = \min_k R_k$ as the reference rate

5. normalize all rates to the reference rate, i.e. $\bar{R}_k = R_k / R_{min}$

6. determine weighting factors $w_k = q \cdot \bar{R}_k + (1 - q)$, where $q \in [0, 1]$ is a tuning parameter used to control the strength of the weighting

7. multiply each user's score vector with corresponding w_k

8. rerun scheduling process

9. determine D for new obtained rates R_k

10. if D is smaller than previous value, goto step 4; else use resource assignment from previous iteration and end process

The tuning parameter q used for the weighting factors is intended to enable smooth transitions of the scheduling results from successive iterations, as this better accommodates the heuristic nature of the scheduling process. Certainly, the parameter q will also influence the convergence speed of the algorithm, as the stopping criterion will be achieved faster for large q. However, it can be expected that a smaller q in return will achieve

a better final result in terms of a smaller deviation D, which will be confirmed by the simulation results presented later in section 3.2.4. Eventually, there will be a tradeoff between convergence speed of the algorithm and quality of the result.

3.2.4 Investigations on link-level

The properties of the scheduler with transmission mode switching are investigated in a single-cell link-level simulation environment with multiple users. These kind of link-level investigations enable an isolated examination of the system behaviour depending on fixed SNR conditions, which are assumed to be common for all involved users. Thus, we are able to gain insights into the basic relationships that influence the performance of multi-user MIMO communication systems. As our main interest here is to illustrate the fundamental behaviour of the adaptive system concept, we focus on the simplest MIMO configuration with $N_t = N_r = 2$ antennas. For performance results for MIMO configurations of higher order in realistic environments, the interested reader is referred to [85, 101, 103].

3.2.4.1 Link-level assumptions

We assume K UTs being equipped with $N_r = 2$ antennas each and a BS with $N_t = 2$ antennas, which provides the two unitary DFT beam sets $\mathbf{C}_1$ and $\mathbf{C}_2$ introduced in (3.3). Possible multi-stream modes are thus 2-user MU-MIMO or dual-stream SU-MIMO. We use the channel model provided by the European WINNER project (WIM) in its configuration for a wide area urban macro scenario. This model assumes a uniform linear array of co-polarized antennas; antenna spacing is set to 4λ at the BS and to 0.5λ at the UTs, yielding a low degree of correlation between the paths emanating from the antennas. The mean channel power is normalized to unity; channels for different users are modeled independently. The mean reception SNR thus is P_s/N_0 for any user. An OFDM system with 1024 subcarriers spanning a bandwidth of 40 MHz is assumed, accommodating 128 chunks of 8 subcarriers width. To obtain the per-stream SINR γ for the different transmission modes per chunk, (3.4) and (3.6) are calculated for the subcarrier in the center of the chunk[7] based on ideal knowledge of the channel $\mathbf{H}$.

For a given SINR value γ, the corresponding achievable rate can be determined via the Shannon information rate $\log_2(1 + \gamma)$. To obtain rates that are closer to those achievable in practice, we instead use a quantized rate mapping function, which was introduced as a component of the WINNER link to system interface, presented in [41]. This rate mapping function is based on a puncturable low density parity check (LDPC) code with constant block length of 1152 bits and supports the fixed symmetric modulation formats up to 64QAM. The discrete steps of the mapping function are derived from the SINR values

---

[7]Note that with the chosen set of system parameters, the channel variations over the frequency width of a chunk can be considered negligible.
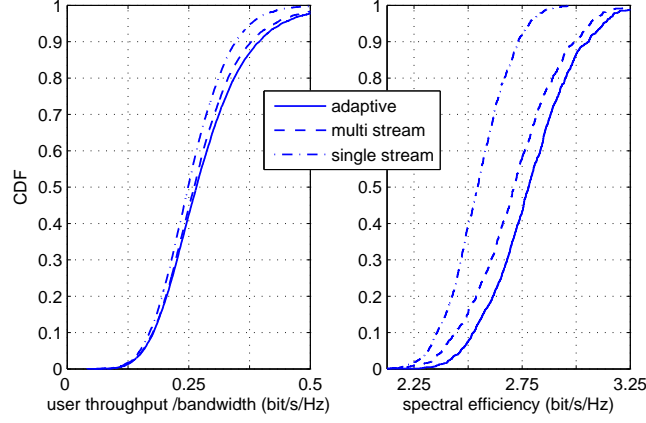
Fig. 3.2: CDFs of the achievable user throughput (left) and spectral efficiency in the cell (right) based on Shannon information rates. Beam set $\mathbf{C}_1$, $K = 10$ users, SNR = 0 dB.
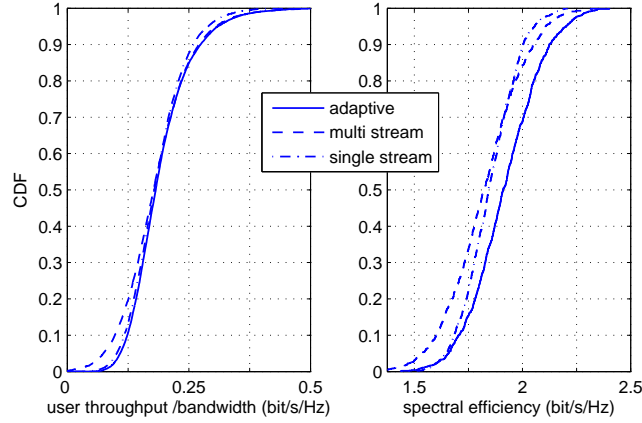

Fig. 3.3: System performance based on quantized rate mapping function. System setting as above.

required to meet a block error rate performance of 10^{-2} in an equivalent AWGN channel. As both the block length of the code as well as the modulation formats are limited, the rates supported by the mapping function are confined to a minimum rate of 0.5 and a maximum rate of 5.538 bit/s/Hz. This former value corresponds to BPSK modulation with code rate 0.5, while the latter is achieved with 64QAM modulation with code rate 24/26. All simulation results are obtained from a total of 10,000 independent channel realizations.

3.2.4.2 Performance of spatial mode switching

First we examine the system performance of the adaptive system when only the beam set $\mathbf{C}_1$ is available. We focus on the low SNR regime, $P_s/N_0 = 0$ dB, which is relevant for cell-edge users, where we expect the benefits from switching to single-stream mode to become prominent. First results are based on Shannon information rates. Fig. 3.2 presents

cumulative distribution functions (CDFs) of the achievable user throughput divided by the signal bandwidth (left) and the spectral efficiency in the cell (right) for $K = 10$ users. Focussing on the user throughput (left), we first point out that all users achieve non-zero rates, so indeed all users in the system are conveniently scheduled. We compare the adaptive system described above to a system supporting either single-stream or multi-stream mode exclusively. For the user throughput (left), we observe that the performance of the adaptive system benefits slightly from switching in the region where the CDF is above 0.5. Further, for the CDF region below 0.2, the single-stream curve is nearly identical to the multi-stream curve, and hence no gains from switching can be realized here. This observation can be explained as follows: Recall that a beam in single-stream mode is served with double the power used for a multi-stream beam. In the low SNR regime, where the noise dominates the interference from simultaneously active beams, we thus can expect that the SINR of the selected beam for single-stream mode is about twice as large as the SINR γ for the corresponding beam in multi-stream mode. Moreover, in multi-stream mode, the amount of beams assigned to each user is twice as large as in single-stream mode. As

$$\log_2(1 + 2\gamma) \approx 2\log_2(1 + \gamma) \quad \text{if } \gamma \ll 1$$

holds, the rates achievable with the two different modes are nearly identical. Considering the spectral efficiency within the cell (right subfigure in Fig. 3.2), we observe that the adaptive system benefits significantly from the mode switching over the entire CDF region.

Fig. 3.3 depicts performance curves for the same setting, but this time the quantized rate mapping function is used. For the user throughput (left), we observe here that the CDF of the adaptive system represents a hull curve of the two single-mode schemes. As the minimum supported rate to be assigned is bound here to 0.5 bit/s/Hz, the adaptive system now significantly gains from switching to single-stream mode if the SINR conditions are low (left region of the CDF curve). The CDF of the adaptive system is quite close to the one supporting single-stream mode only, suggesting that this mode is predominantly chosen at low SNR. Considering the spectral efficiency in the cell (right subfigure in Fig. 3.3), we observe that only the left tail of the adaptive system's CDF approaches the curve of the pure single-stream mode. In the remaining region, substantial gains from mode switching become visible.

In the next step, we will examine the system behaviour for varying SNR. Therefore, we focus on the median spectral efficiency in the cell based on quantized rate mapping, i.e. the value determined from the CDF for a probability of 0.5. Furthermore, we draw our attention to the probabilities of mode selection, which reveal the dominantly chosen mode depending on the SNR conditions. Fig. 3.4 depicts the median spectral efficiency in the cell versus the SNR for different configurations of the adaptive mode switching system.
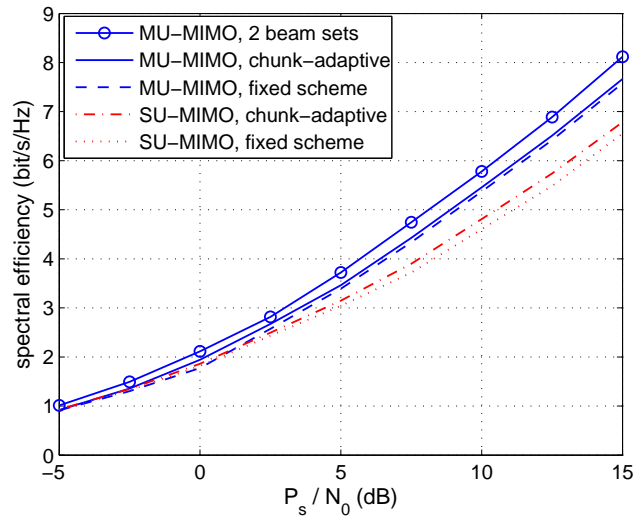
Fig. 3.4: Median spectral efficiency in the cell for different system configurations. Quantized rates, K=10 users, beam set $\mathbf{C}_1$.
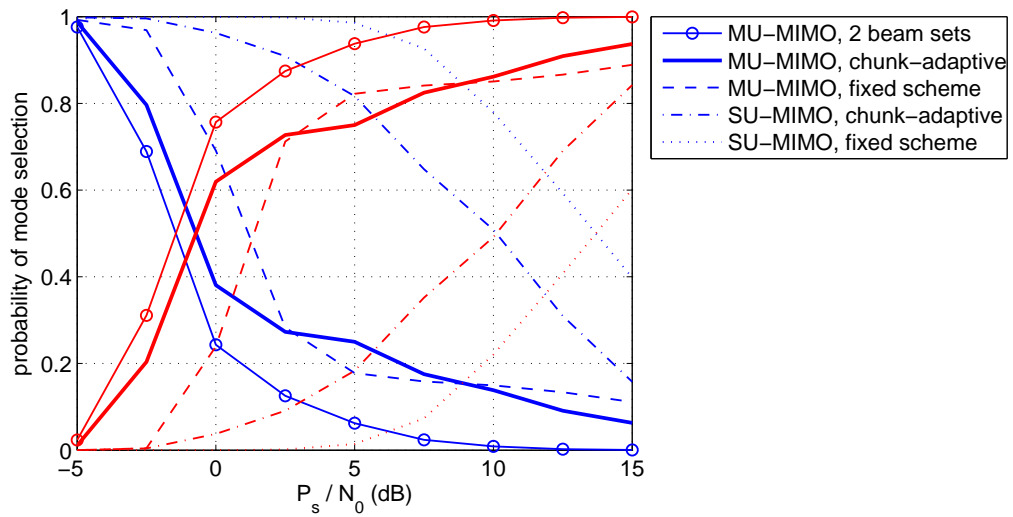

Fig. 3.5: Probability of mode selection vs. SNR. Blue: ss mode, red: ms mode. System setup as in Fig. 3.4.

The corresponding probabilities of mode selection are found in Fig. 3.5. The different configurations are as follows:

1. *MU-MIMO, 2 beam sets*: Similar as *MU-MIMO, chunk-adaptive* (see next entry), but here the two beam sets $\mathbf{C}_1$ and $\mathbf{C}_2$ from (3.3) are available.

2. *MU-MIMO, chunk-adaptive*: adaptive system as described in section 3.2.3 with chunk-wise selection of the spatial mode, i.e. a user may be served in different modes simultaneously.

3. *MU-MIMO, fixed scheme*: For each user, a fixed mode and, in case of ss mode, a fixed beam is selected. Therefore, each user sums up the rates of his best beams in ms mode and the rates of all beams in ss mode over all chunks of the frequency band. By considering the weighting factor w for ms mode, decision is taken in favour of the mode (and beam) achieving highest sum rate.

4. *SU-MIMO, chunk-adaptive*: MU-MIMO option is switched off, i.e. ms mode reduces to SMUX to a single user. Now only one user is served per chunk either in ss or SMUX mode.

5. *SU-MIMO, fixed scheme*: Fixed mode and, in case of ss mode, fixed beam per user. Selection is based on the mode (and the beam) achieving highest sum rate over the entire frequency band.

Reading this list from bottom to top, the different configurations can be understood to successively add additional degrees of freedom in the spatial domain to the user selection and resource allocation process. Fig. 3.4 and 3.5 clearly show that these additional degrees of freedom do not only increase the achievable system performance successively, but also promote the selection of the ms mode. The crossing point of the probability curves for ss and ms mode in Fig. 3.5 highlights the point in the SNR region where the ms mode becomes the dominantly selected one. Most interestingly, Fig. 3.5 reveals that by activating MU-MIMO (configuration 3), this crossing point is shifted by about 8 dB compared to configuration 4 to an SNR of about 1.5 dB. This result underlines that the MU-MIMO mode is the key to support the transmission of multiple data streams in the spatial domain already at low SNR. Together with the throughput gains shown in Fig. 3.4, the high potential of MU-MIMO to increase the overall system throughput is substantiated. Configuration 2 shifts the crossing point further to the left to an SNR below 0 dB. The throughput, however, is thereby increased only slightly. A significant additional gain in throughput can be achieved if an additional beam set is provided by the BS (configuration 1), which amounts to about 5% compared to configuration 2. The crossing point in Fig. 3.5 is also shifted further down to about -1.5 dB.
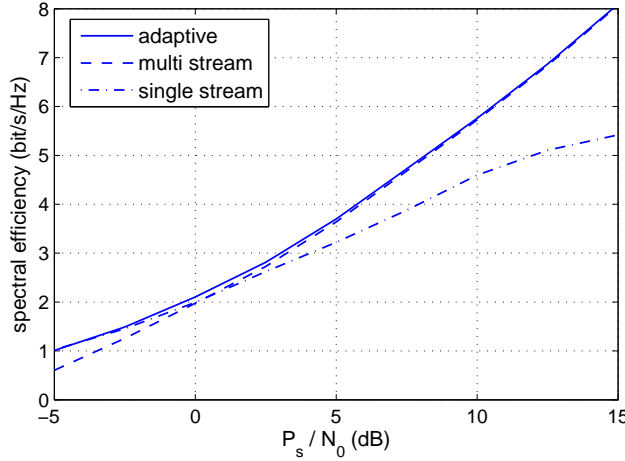
Fig. 3.6: Median spectral efficiency in the cell achievable with 2 beam sets and comparison to single mode systems. Quantized rates, K=10 users.

Close inspection of Fig. 3.5 further reveals that with increasing degrees of freedom, the probability curves exhibit a steeper slope and approach the upper and lower boundary areas more rapidly with increasing SNR. In particular, for the leftmost ss curve (MU-MIMO, 2 beam sets), we observe a rapid decline that falls below a probability of 0.1 above 5 dB SNR, suggesting that the adaptive system tends to behave similar to a system that uses a fixed mode in the low and high SNR regime, respectively, with a switching point set at a fixed SNR level. This conjecture is confirmed by Fig. 3.6, where we compare the median cell throughput for configuration 1 (adaptive MU-MIMO, 2 beam sets) with a similar system supporting either ss or ms mode exclusively, as done at the beginning of this section: The figure reveals that the adaptive system represents a hull curve of the performance of the two single mode systems, which turns out to be very tight.

We conclude this subsection with the important observation that proper application of the MU-MIMO mode enables to conveniently serve even users in the ms mode who experience relatively poor SNR conditions[8]. Thus, the MU-MIMO mode establishes a win/win situation for low- and high-rate users competing for a frequency or time resource, as low-rate user can now be served without blocking this resource for any high-rate user, who can support a rate on any of the available beams.

3.2.4.3 Steering the fairness to equal rates

In this subsection, we examine the behaviour of the scheduler if we apply the fairness steering option to achieve an equal rate scheduling target as described in section 3.2.3.5. We use different tuning factors q and compare the achievable distribution of the user rates as well as the required number of iterations. Investigations have been carried out for a mean SNR of 10 dB, which is equal for all $K = 10$ users in the time-slot. The CDFs

---

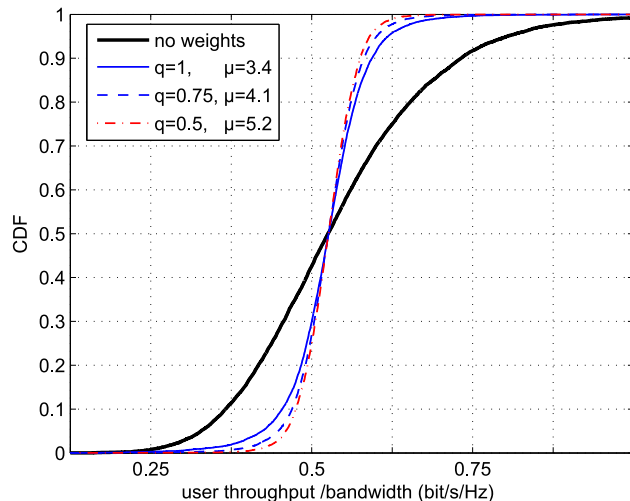[8]in a cellular system, these are the users at cell-edge

Fig. 3.7: Fairness steering towards an equal rate target based on iterative algorithm with tuning factor q. μ - mean required number of iterations. $K = 10$ users and SNR = 10 dB.

representing the rates of the successfully scheduled users are depicted in Fig. 3.7. We observe that for any choice of the tuning factor q, the fairness steering process seems to operate conveniently, as the CDF significantly gains in steepness and thus approaches the equal rate target, which would be represented by a vertical line. It is interesting to note that the median user throughput does not change due to the applied weighting, highlighting the convenient practicability of the proposed score weighting.

Taking a closer look at the curves for different q reveals that choosing a smaller value enables a better match of the equal rate target, as a steeper CDF of the user rates can be achieved. The price we pay for this is an increased number of iterations, whose expected value μ grows from 3.4 for $q = 1$ continuously to 5.2 for $q = 0.5$. For the application considered here, the choice of $q = 0.75$ would probably be well suited, as it achieves a CDF which is quite close to the desired target while requiring a moderate number of iterations.

The price we have to pay for the improved fairness is a loss of the achievable spectral efficiency in the cell. For the case considered here where all users have the same mean SNR, the loss is negligibly small, as it drops by 3% only. However, it should be noted that this loss will be substantially larger in real-world scenarios, where the mean SNRs of different users are likely to be significantly different.

3.2.4.4 Capacity scaling of the adaptive system

Finally we examine the downlink capacity achievable with the adaptive system and compare it to the upper bound, which is the capacity of the 2×2 BC when full CSI is available at the receivers as well as at the transmitter. As mentioned in the introduction,

the capacity of the BC was shown to be achievable with the dirty paper coding (DPC) technique. In [45] an algorithm was presented to compute it in an iterative manner for any given set of flat-fading user channels. While maintaining the equal power distribution over all chunks, we use this algorithm to compute the optimal user allocation and the corresponding precoding matrices per chunk to obtain the upper bound for the (flat-fading) capacity of the BC, which is depicted in Fig. 3.8 versus the SNR for $K = 10$ users. The achievable downlink capacity of our adaptive system is obtained by applying Shannon's information rates and carrying out maximum throughput scheduling (MT) based on the reported rates at the BS, which selects for each chunk the user (single-stream) or user constellation (multi-stream) that achieves the highest throughput. In Fig. 3.8 we observe that for an SNR above 0 dB, the capacity of our adaptive system utilizing partial CSI achieves a constant fraction of the capacity of the BC, which amounts to about 80% if one beam set is available. Utilization of two beam sets provides an extra gain in capacity of about 5%. Additionally, we included the capacity of the SISO channel achieved in an equivalent scenario. While we observe here that the capacity of the BC scales with factor 2 (corresponding to $\min(N_r, N_t)$) compared to the capacity of the SISO channel in the high SNR range, the capacity of our adaptive system (with one beam set) achieves a factor of 1.6. For comparison, we also added the spectral efficiency achievable with the fair score-based scheduling (SB) technique. It can be seen that the price we have to pay to obtain user fairness within one time-slot is only marginal, as the loss in spectral efficiency is only about 5%.[9]
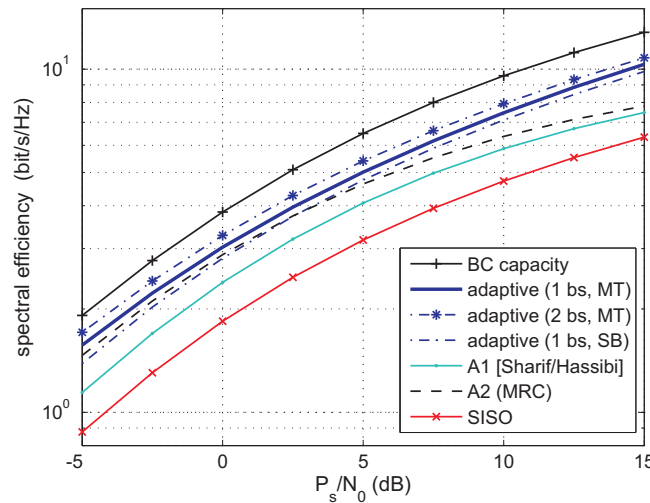

Fig. 3.8: Comparison of the capacity for various systems vs. SNR. $K = 10$ users, Shannon information rates. bs - beam sets; scheduling: MT - max. throughput, SB - score-based.

---

[9]Note that this loss may increase substantially if users with different mean SNRs are considered. This scenario has been in the focus of the investigations presented in [85, 101, 103].
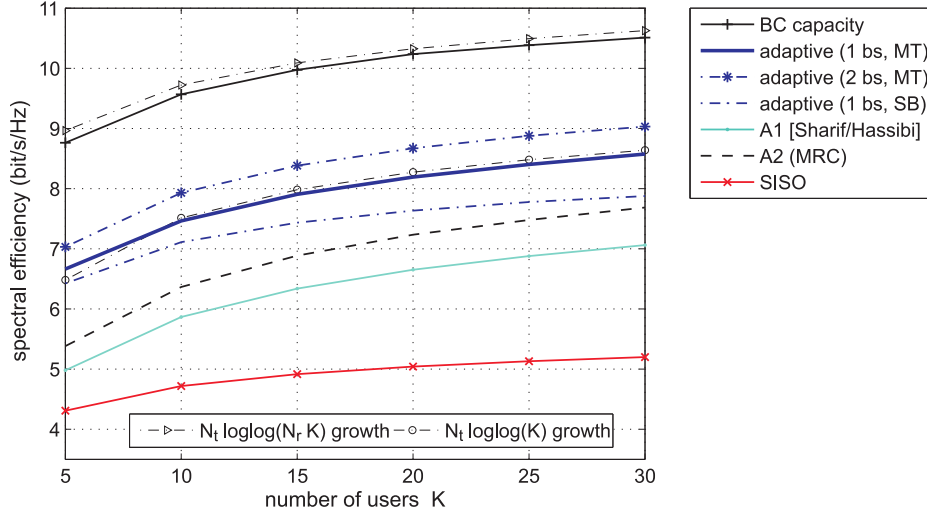
Fig. 3.9: Capacity scaling with number of users at SNR = 10 dB.

To see potential gains in the downlink capacity compared to other well-known limited feedback schemes, we further compare the adaptive system to two multi-stream approaches with $Q = 2$ simultaneously active beams, which we denote as A1 and A2. For both approaches, we assume beam set $\mathbf{C}_1$ to be available only. A1 is the approach presented in [96] and is sketched as follows: Each receive antenna at the UT is treated as an independent receiver. Hence, the per-antenna reception SINR is calculated for each beam, assuming that the other beam interferes. For each antenna, the UT feeds back the best beam together with the corresponding SINR, and the BS assigns each beam to the user having provided the highest SINR value for it.

In A2, we consider a multi-stream system where the UTs simply carry out MRC for each received beam, i.e. nothing is done to actively combat the interference. The corresponding post-detection SINR can be determined by equation (3.6), with the MRC equalization vector $\mathbf{w}_i = \mathbf{H}\mathbf{b}_i$. Feedback and beam assignment is then carried out as in A1.

Remark: For the 2×2 MIMO setup considered here, the feedback required for the adaptive system is by 50% larger than that for the two systems A1 and A2, as additionally to the two per-stream rates in ms mode the rate for the ss mode has to be reported. Within these investigations, however, the amount of feedback has not been taken into account, as the main focus here lies in the achievable downlink capacity relative to the capacity of the BC. A similar framework for this kind of performance evaluation has also been used in [44].

In Fig. 3.8, we observe that A1 achieves a significantly lower performance than the mode switching system – a result similar to the one found in [117] for single-antenna UTs. The relative difference in throughput increases with increasing SNR, as A1 suffers from the interference between active beams, which is actively suppressed in our adaptive system by the MMSE equalizer. The throughput of A2 is quite close to the performance

of the adaptive system in the low SNR region. Obviously, this is due to the fact that in the low SNR region the noise dominates the interference from the other spatial stream active in ms mode. In this case, the MMSE solution approaches the MRC solution, yielding similar post-detection SINRs for both equalizers, which finally translates into a similar throughput performance. For increasing SNR, however, the performance of A2 degrades significantly and approaches the throughput of A1. As in the former case, A2 suffers here from the interference between the simultaneously active beams.

In Fig. 3.9 we examine the downlink capacity for a constant high SNR = 10 dB for a variable number of users. First we compare the capacity of the adaptive system (MT) with the achievable spectral efficiency of the fair scheduling approach (SB). Although the loss in throughput to provide the desired fairness is again not exceptionally high, we observe that the gap between MT and SB scheduling increases with increasing number of users. This is not very surprising, as with a growing number of users, the probability of a user experiencing poor channel conditions increases, who imperatively has to be served by the system based on fairness. The support of these users by the fair scheduler thus costs a growing proportion of the maximum sum capacity.

Next we focus on the scaling of the downlink capacity versus the number of users and compare it to the other reference systems. In [96], it has been shown that the BC capacity for i.i.d. Rayleigh fading channels scales for a large number of users with $N_t \log \log(N_r K)$. This growth has also been plotted in Fig. 3.9, and we observe that the capacity of the BC for $K \geq 10$ users and the correlated channels considered is scaling similarly. For our adaptive system, it has been shown in the previous investigations that at SNR = 10 dB, the ms mode dominates the selection (compare with Fig. 3.5). In this case, the use of the MMSE equalizer reduces the spatial degrees of freedom at the receiver from $N_r = 2$ to 1 [119], resulting in a capacity scaling equivalent to $N_t \log \log(K)$ [96] for the setup given here. The plot of this growth in the figure shows a convenient agreement with the scaling of the corresponding efficiency curve of the adaptive system for $K \geq 10$ users.

We also plot the capacity of the SISO system, which grows roughly with a slope of $\log \log(K)$ [96] and thus less steep than the adaptive system. We observe that the capacity scaling factor relative to the SISO system of 1.6 is achieved by the adaptive system for $K = 10$ users, remaining about constant for further increasing K. Comparing finally the adaptive system to the reference systems A1 and A2, we observe that the adaptive system achieves a significantly higher downlink capacity, highlighting the gains that can be achieved by using the additional receive antennas to actively suppress the interference from other active beams. Note that A1 exhibits the same scaling over the number of users as the BC capacity, as has been shown in [96]. In the depicted range of users, the MRC-based system A2 exhibits the steepest slope over all curves, suggesting that for a large number of users its downlink capacity approaches the one of the adaptive system. This is reasonable, as we can expect that for a large number of users, we can find a user

in the active set whose MRC equalization vector is close to the corresponding MMSE equalization vector, which is the receiver architecture used in the adaptive system.

3.2.5 Remark to latest work in the field

Very recent work on the flat-fading MIMO broadcast channel has focussed on a relevant question [80]: If the amount of feedback is fixed, is it more beneficial to let all users report achievable SINRs for a fixed beam set, or to let a limited set of preselected users provide high-rate information on their quantized channel? To examine this question, the authors consider two different transmission concepts: GoB transmission with randomly changing beams, where all users report CQI for the fixed beams, and ZF precoding, where a selected set of users report their quantized channels with high resolution. Essentially, the problem turns out to be a question of the achievable gains from multi-user diversity versus the gains from beamforming. It has been shown that for single-antenna UTs (i.e. $N_r = 1$), the ZF precoding system significantly outperforms the GoB system in terms of the achievable system throughput. This work raises the question whether this fundamental statement found holds similarly for the system setting we have considered in our work.

Without carrying out additional investigations, some comments can be given to address this issue: First, note that our system concept is basically different, as we consider an OFDM system in frequency-selective channel environments, which allows to assign the users their best resources over frequency. As addressed in section 3.2.3.4, there is a high potential to beneficially reduce the user feedback down to very small amounts of bits. As the possibilities for feedback reduction for quantized user channels may be different, the amount of feedback bits needed for the two cases may not be compared similarly as in [80] in the OFDM context. Further, our system under investigation assumes the UTs to be equipped with $N_r = 2$ antennas, and thus the UTs are capable of actively combatting inter-beam interference. Our investigations have shown that we can already achieve a large proportion of the flat-fading BC capacity with only one beam set. With an additional beam set, allowing for improved beamforming gains due to a better quantization of the user channels, additional gains are clearly visible, but they are rather small. Hence, we can expect that the gains due to further improved beamforming will not be as significant as shown in [80]. However, addressing this fundamental question in more detail in the context of the adaptive system concept developed here is certainly of high interest and should therefore be an issue for future investigations.

3.2.6 Conclusion chapter 3.2

We have presented a concept for the downlink of a multi-user MIMO-OFDM system combining spatial transmission mode switching with a fair scheduling approach. Based on unitary fixed beamforming, the users report information on the rates they can achieve for distinct beams in the supported transmission modes via a low-rate feedback channel. According to the feedback given, the BS then selects the transmission mode per frequency resource and assigns each user the beams yielding highest rates. As an example, performance evaluation has been carried out for a 2×2 MIMO configuration, revealing significant gains in spectral efficiency as well as in user throughput due to mode switching. It turned out that MU-MIMO transmission, where the spatial beams are assigned to different users, is the key to enable simultaneous transmission of multiple spatial data streams even at low SNR conditions. If multiple beam sets are provided, the gains from instantaneous mode switching vanish in most parts of the SNR region, and the system turns into a pure spatial multiplexing system in the higher SNR range. We further introduced a fairness steering that can be configured to realize a desired fairness target the scheduler is supposed to provide; its potential has been shown with the example of an equal rate target. Finally, the achievable downlink capacity of the adaptive system has been compared to the capacity of the SISO and the MIMO broadcast channel as well as of two limited-feedback reference systems supporting MU-MIMO, but no interference suppression. This comparison illustrated that the system effectively achieves a high performance, excelling that of the two reference systems significantly. The scheduling concept introduced here can readily be employed in a multi-cell environment, where users with different mean SNR are present, as investigated in [101, 103]. Note that the elementary functionality of the proposed system concept has been tested already in real-time experiments, which have been conducted in a real-world broadband mobile communication environment; for details refer to [85, 120].

Final remark: The concept proposal presented here goes beyond the current standardization of 3G Long Term Evolution (LTE) [1]. In particular, we allow each user to select the spatial mode as well as the beam to be served on individually per chunk, while in LTE each user is supposed to make a selection for the entire band (similar to the *fixed scheme* configuration in the list given in section 3.2.4.2). Further, feedback in LTE is supposed to be given for sets of contiguous chunks instead of per chunk individually. Both measures significantly reduce the required feedback, but clearly come at the cost of a decreased system performance.

3.3 Spatial adaptation in time-variant channels

The channel-adaptive transmission concept proposed in the preceding section assigns each UT its best resources and adapts its transmission rate according to the instantaneous channel conditions that have been previously measured. However, feedback and resource allocation cause a delay between channel evaluation at the UTs and the final application of the resource assignment decision, where transmitter and receiver are configured according to the setup that has been selected during the channel evaluation phase. Thus, this resource assignment may be considered useful only if the channel behaves quasi-static. However, in case the UTs are moving at vehicular speed, the SINR conditions determined during the channel evaluation phase may drop down, which may cause severe performance degradations of the system. The expected drop of the SINR conditions due to movement of the UTs has been examined in [77]. In this work, a suitable expression to assess the expected SINR drop can be found, which is based on the maximum Doppler frequency affecting the CIR.

To overcome the problem of SINR drops, it would be desirable to modify the system concept accordingly to account for the temporal evolution of the channel and thus enable application of the channel-adaptive transmission concept also in a mobile scenario. In this section, we present an approach that relies on channel interpolation techniques [35] to predict the channels for a future time instant, where the resource assignment decision is expected to be applied. These predicted channels are used as a basis for the channel evaluation phase carried out at the UTs.

In section 3.3.1, we will first examine the possible degradations of the SINR conditions if the original concept from the preceding section is applied in time-varying channel environments. We then will derive the channel-prediction based approach in section 3.3.2 and compare its behaviour in time-varying environments to the original approach.

3.3.1 SINR loss due to channel's time variance

We use the system model that has been introduced in section 3.2.1, but extend it slightly to support the time-varying nature of the communication channel. Recall that we assume the radio transmission to be based on a slotted time structure, where each slot is constituted of several consecutive OFDM symbols. The transmission equation for a single subcarrier signal received by a UT in OFDM symbol i is given by

$$\mathbf{r}(i) = \mathbf{H}(i)\mathbf{C}\mathbf{x}(i) + \mathbf{n}(i) \tag{3.11}$$
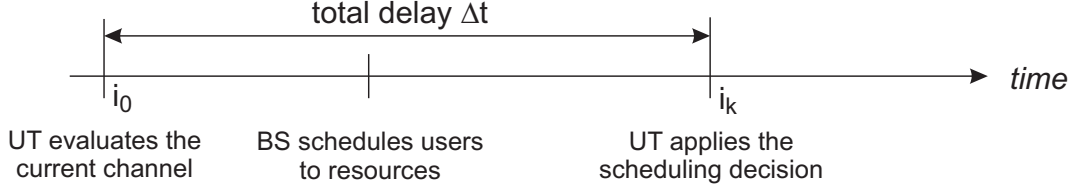
Fig. 3.10: Delay occurring in a practical system between channel evaluation and application of the resource allocation.

with vectors and matrices as defined in (3.1), but being dependent on the OFDM symbol index i now. The $N_r \times N_t$ channel matrix will be partitioned according to

$$\mathbf{H}(i) = [\mathbf{h}_1(i) \cdots \mathbf{h}_{N_t}(i)] \tag{3.12}$$

where each column vector $\mathbf{h}_n(i)$ represents the N_r-dimensional channel between the n-th transmit antenna and the receive antenna array.

According to the channel adaptive concept presented in section 3.2, each UT uses the relations (3.4) and (3.6) to evaluate the post-detection SINRs for the data streams transmitted in the different spatial modes based on the channel measured at time instant i_0, i.e. $\mathbf{H}(i_0)$. The scheduling decision will be applied at time instant $i_k > i_0$, resulting in a delay Δt, see Fig. 3.10. During this time, the channel may change, so that the SINR conditions measured at i_0 may no longer be valid. In case the SINR conditions in a resource drop down, the channel will be overloaded, which means a bit rate will be used in that resource that can no longer be supported. Hence, detection errors are very likely to occur, resulting in severe performance degradations.

In particular, variations of the SINR conditions will take effect if the delay Δt is in the order of the channel's coherence time T_c, which we define as $T_c = f_D^{-1}$, with f_D being the maximum Doppler frequency. For a fixed system configuration, Δt is in general a constant system parameter, and hence only the Doppler frequency f_D, which is invoked by the speed of the UT, impacts the SINR variations. We will therefore examine how the channel's time variance will degrade the SINR conditions. For that purpose, we set up a following framework:

The channel evaluation process is carried out at the UT to determine the achievable rates based on the actual channel at OFDM symbol index i_0. Once the SINRs have been determined for all available chunks and all supported transmission modes, we select per transmission mode half the chunks with best SINR values. This is done to account for the fact that chunks with poor quality will not be assigned by the scheduler, as it aims at assigning each UT its best chunks only (refer to section 3.2.3 for further details). After the delay Δt, we end up at OFDM symbol index $i_k = i_0 + \Delta i$, with Δi being the number of OFDM symbols spanning the duration of the delay Δt. Based on the evolved channel $\mathbf{H}(i_k)$ at this OFDM symbol index, we recalculate the SINR values for the selected chunks
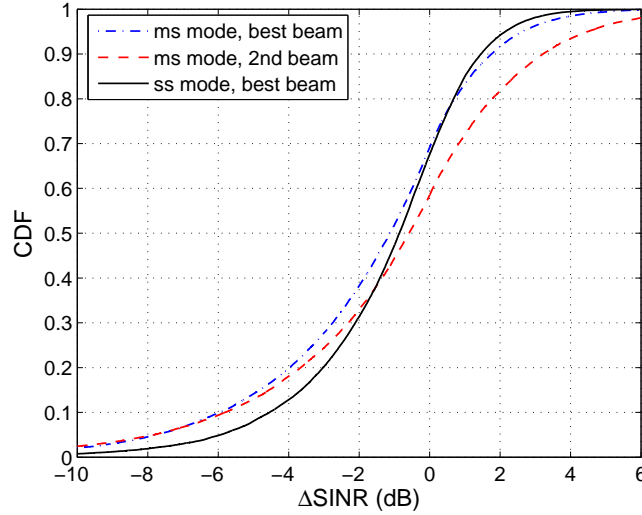
Fig. 3.11: CDF of the deviation of the per-stream SINR for the different transmission modes ms and ss. $\Delta t = 0.2 T_c$, $P_s/N_0 = \ 10$ dB.

per mode and determine the difference ΔSINR to the original SINR values based on $\mathbf{H}(i_0)$, which represents our evaluation measure.

Similar to section 3.2.4, we focus on a 2×2 MIMO configuration supporting ss and ms transmission mode for our investigations. The precoding matrix is always fixed to $\mathbf{C}_1$ from (3.3). Further, we use the WIM channel model again with the same parameter setting as specified in section 3.2.4. Recall that the transmit antenna spacing was set to 4λ and receive antennas spacing to 0.5λ. For the evaluation, we assume constant mean SNR conditions characterized by $P_s/N_0 = 10$ dB. Fig. 3.11 shows the CDF of ΔSINR (measured in dB) for the streams of the different transmission modes for channel dynamics characterized by $\Delta t = 0.2 T_c$. In each chunk, the two streams of ms mode have been ordered by the quality of their SINR. Note that only negative values of ΔSINR translate into a drop of the measured SINR value and thus may result in a performance degradation. From Fig. 3.11, we observe that the median value of ΔSINR is negative, which means that the SINR conditions in the selected chunks tend to drop down. Further, we observe that all CDFs exhibit a broad left tail. From these observations, we conclude that severe SINR degradations are likely to occur. Obviously, the two beams of the ms mode suffer the most from SINR degradations, while the beam in ss mode suffers least, as the left tail of its corresponding CDF lies significantly below the ones of the two beams in ms mode. An explanation for that can be found in the higher robustness of the MRC equalizer used for the ss mode to inaccurate channel information, as highlighted by the investigations in [102].

In Fig. 3.12, we depict the 10-percentile of the ΔSINR-CDF for variable channel dynamics $\Delta t/T_c$. For all spatial beams, we observe that the SINR loss first rises steeply with increasing channel dynamics up to $\Delta t = 0.3 T_c$, revealing a high sensitivity of the
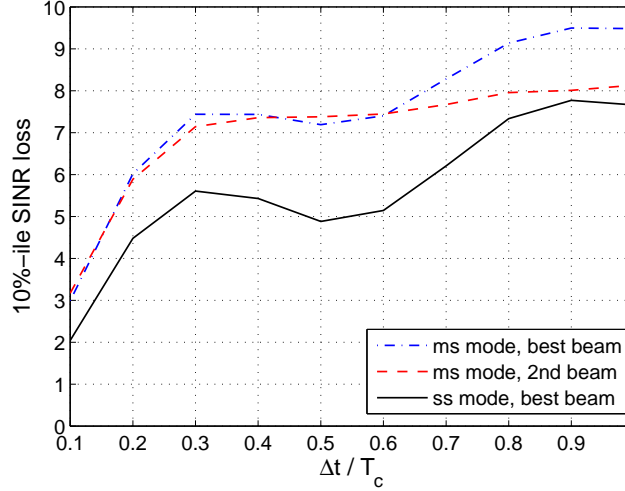
Fig. 3.12: Loss of the per-stream SINR (in dB) for the 10-percentile of the ΔSINR-CDF
vs. channel dynamics.

measured SINR conditions towards the time variances of the channel. Again, we observe
here that the beam in ss mode suffers the least from SINR losses over the considered
dynamic range.

3.3.2 Predicting SINR conditions by channel interpolation techniques

To alleviate the effect of SINR degradations, it would be desirable to predict the channel
state at time instant $i_k = i_0 + \Delta i$ at the UT and carry out the channel evaluation process
based on that channel, $\mathbf{H}(i_k)$. In this section, we develop such a channel prediction
approach based on linear channel interpolation techniques [35], which relies on a specific
arrangement of the receive antenna array.

As variations of the channel $\mathbf{H}(i)$ over the duration Δt become significant at vehicular
speeds, it is reasonable to assume that the receive antennas of the mobile terminal can
be mounted at a fixed position on the moving vehicle. We assume the antennas to be
arranged as a uniform linear array with fixed antenna spacing a, with its broadside oriented
perpendicular to the moving direction (see Fig. 3.13 for a dual-antenna array) – an idea
which has already been presented in [53]. With this configuration, the channel seen at
receive antenna $m + 1$ (Rx2 in Fig. 3.13) is a delayed version of the one seen at receive
antenna m (Rx1). The delay D, measured in integer numbers of OFDM symbols, depends
on the spacing a of the two antennas as well as on the vehicle's speed. The channel vector
for n-th transmit antenna can thus be given as

$$\mathbf{h}_n(i) = [h_n(i) \ h_n(i - D) \ \cdots \ h_n(i - (N_r - 1)D)]^T \tag{3.13}$$

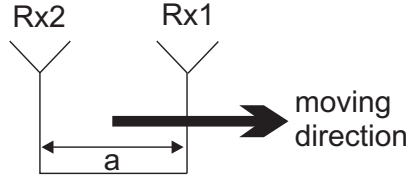According to this notation, the channel vector $\mathbf{h}_n(i)$ contains N_r equi-spaced sampling

Fig. 3.13: Configuration of the linear antenna array used for the prediction-based approach.

points of the time-variant channel function $h_n(i)$.

3.3.2.1 Statistical properties of the channel vectors

We will now characterize the statistical properties of the channel vectors $\mathbf{h}_n(i)$. We consider all channel functions $h_n(i)$, $n \in \{1, \ldots, N_t\}$, constituting those vectors to have identical statistics. Hence, we focus on a channel for a single transmit antenna and omit the index n for notational convenience.

The channel's autocorrelation function (ACF) is given as $\varphi_{hh}(k) = E_i\{h(i)h^*(i+k)\}$. Assuming Jakes' model for the temporal evolution of the channel function $h(i)$, the autocorrelation function yields [79]

$$\varphi_{hh}(k) = E_i\{h(i)h^*(i+k)\} = J_0(2\pi k f_D \cdot T_o) \tag{3.14}$$

$J_0(\cdot)$ is the the Bessel function of the first kind resulting from Jakes' Doppler power spectrum, and T_o is the OFDM symbol duration. The covariance matrix of the channel vector $\mathbf{h}(i)$ is defined as

$$\mathbf{R}_{hh} = E\{\mathbf{h}(i)\mathbf{h}^H(i)\}$$

Using (3.13), its elements can be related to the ACF φ_{hh} according to

$$[\mathbf{R}_{hh}]_{cd} = \varphi_{hh}((d-c)D) = J_0(2\pi(d-c)D f_D \cdot T_o) \tag{3.15}$$

where $[\mathbf{R}_{hh}]_{cd}$ represents the element of matrix $\mathbf{R}_{hh}$ found in c-th row and d-th column. The delay D can be related to the antenna spacing a and the speed v of the mobile vehicle according to $DT_o = a/v$. Further, v relates to the Doppler frequency f_D via $v = f_D\lambda$, with λ being the wavelength of the carrier frequency. Thus, we obtain

$$D = \frac{a}{\lambda f_D T_o} \tag{3.16}$$

Inserting this expression into (3.15), we obtain for the elements in the correlation matrix $\mathbf{R}_{hh}$

$$[\mathbf{R}_{hh}]_{cd} = J_0(2\pi(d-c)a/\lambda) \tag{3.17}$$

3.3.2.2 Channel prediction by linear interpolation techniques

The channel vector $\mathbf{h}(i_0)$ according to (3.13) supplies N_r equi-spaced sampling points of the channel function $h(i)$. Hence, we can use channel interpolation techniques to determine $h(j)$ for an arbitrary j and thus obtain an estimate for the channel vector $\mathbf{h}(i_k)$ for a future time instant $i_k > i_0$. However, for proper application of the interpolation techniques, it has to be ensured that the density of sampling points of $h(i)$ obtained from the vector $\mathbf{h}(i)$ complies to the requirement of the sampling theorem, which yields [35]

$$2f_D D T_o \leq 1 \quad \Leftrightarrow \quad a \leq \lambda/2$$

where we used equation (3.16). From this result, we can conclude that the channel prediction based on channel interpolation techniques requires an antenna spacing of at most $\lambda/2$.[10]

Next we turn our focus on the realization of the channel predictor. Note that the interpolation-based prediction gets the more reliable, the more information on the channel function $h(i)$ can be taken into account. Hence, we use the past measured channels $\mathbf{h}_n(i)$ gathered over an observation window of length N_o, i.e. $i \in \{-N_o + 1, \ldots, 0\}$, as input for the predictor. We assume here that $i_0 = 0$ is the index of the last OFDM symbol where measured channel information is available (see Fig. 3.14). Let

$$\mathbf{y}_m = [h(-(m-1)D - N_o + 1) \cdots h(-(m-1)D)]^T \qquad (3.18)$$

be a vector comprising the N_o successive observations of the channel coefficient at m-th receive antenna. A compound observation vector is formed by stacking the single vectors $\mathbf{y}_m$ into one according to their temporal order, i.e. $\mathbf{y} = [\mathbf{y}_{N_r}^T \cdots \mathbf{y}_1^T]^T$. The MMSE solution of the linear interpolator [35] yields for the estimate of the future channel vector $\hat{\mathbf{h}}(i_k)$

$$
\begin{aligned}
\hat{\mathbf{h}}(i_k) &= \theta^H(i_k)\Phi^{-1}\mathbf{y} \qquad (3.19)\\
\theta(i_k) &= E\{\mathbf{y}\mathbf{h}^H(i_k)\}\\
\Phi &= E\{\mathbf{h}\mathbf{h}^H\} + \gamma^{-1}\mathbf{I}_{N_r N_o}
\end{aligned}
$$

where γ is the SNR of the measured channels contained in $\mathbf{y}$, characterizing the quality of the single measurements. The matrix $E\{\mathbf{y}\mathbf{y}^H\}$ constituting Φ can be structured into submatrices $\mathbf{A}_{mj}$ of dimension $N_o \times N_o$, which result from the outer products of the subvectors $\mathbf{y}_m$ in $\mathbf{y}$, i.e. $\mathbf{A}_{mj} = E\{\mathbf{y}_m\mathbf{y}_j^H\}$. Their elements relate to the channel's ACF $\varphi_{hh}(k)$ according to

$$[\mathbf{A}_{mj}]_{cd} = \varphi_{hh}((j-m)D + (d-c))$$

---

[10]Note that an antenna spacing $a < 0.5\lambda$ may result in modified radiation patterns due to mutual antenna coupling. However, this effect has not been taken further into account here.
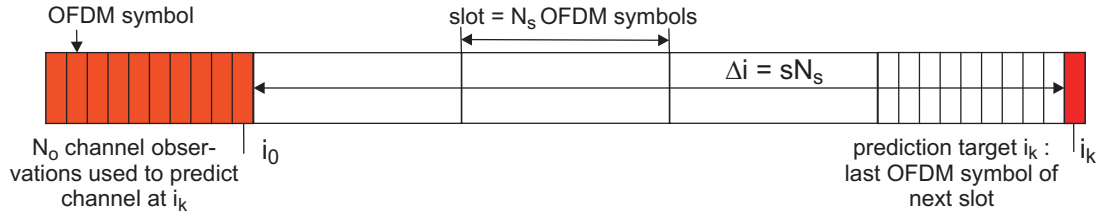
Fig. 3.14: Signal structure used for the prediction-based approach.

Correspondingly, the matrix $\theta(i_k)$ can be structured into submatrices $\mathbf{B}_m = E\{\mathbf{y}_m \mathbf{h}^H(i_k)\}$ of dimension $N_o \times N_r$, whose elements relate to the ACF as

$$[\mathbf{B}_m]_{cd} = \varphi_{hh}(-(m-d)D - k + c)$$

Once we have obtained the predicted channel vectors $\hat{\mathbf{h}}_n(i_k) \ \forall n \in \{1, \ldots, N_t\}$ from (3.19), we can construct the predicted channel matrix $\hat{\mathbf{H}}(i_k)$ according to (3.12). Based on this matrix, the UT can then determine the future SINRs for the different spatial modes according to (3.4) and (3.6), respectively.

3.3.2.3 Evaluation of the prediction-based approach

As shown in [35], the mean square error (MSE) μ_j of the j-th predicted coefficient in $\hat{\mathbf{h}}(i_k)$ can be determined from the j-th diagonal element of matrix $\mathbf{M}$, which is calculated according to

$$\mathbf{M} = \sigma_h^2 \cdot \mathbf{I} - \theta^H(i_k) \Phi^{-1} \theta(i_k)$$

where σ_h^2 is the mean power of the CIR $h(i)$. To illustrate the achievable quality of the predicted coefficients in $\hat{\mathbf{h}}(i_k)$, we firstly evaluate their individual MSEs μ_j, $j \in \{1, \ldots, N_r\}$. For the system setting, we assume $N_r = 2$ receive antennas with spacing $a = \lambda/2$. A transmission slot is assumed to consist of $N_s = 20$ successive OFDM symbols. The delay Δi and thus the channel prediction interval is set to $\Delta i = 4N_s$, i.e. the duration of $s = 4$ complete slots (see Fig. 3.14). This setting can be considered a suitable value to account for feedback and processing delays that may be encountered in practical systems.

The individual MSEs of the predicted channel coefficients in $\hat{\mathbf{h}}(i_k)$ versus the channel dynamics $\Delta t/T_c$ are depicted in Fig. 3.15, where we consider a varying number of past channel observations N_o of estimation quality $\gamma = 20$ dB. If the number of channel observations taken into account is sufficiently large ($N_o \geq 20$), we clearly observe that the coefficient of Rx2 can be conveniently predicted for $\Delta t < 0.5 T_c$. For an explanation, note that the second entry of the channel vector $\mathbf{h}_n(i_k)$ according to (3.13) reads $h_n(i_k - D)$. Thus, the channel predictor (3.19) generates this entry from an interpolation between the entries of $\mathbf{h}_n(i_0)$, i.e. $h_n(i_0 - D)$ and $h_n(i_0)$, as long as the prediction interval fulfils

$\Delta i = i_k - i_0 < D$. Substituting D with (3.16) in this relation, we yield

$$\Delta i T_o < \frac{a}{\lambda f_D} \quad \Leftrightarrow \quad \Delta t < \frac{a}{\lambda} T_c \qquad (3.20)$$

For $a = \lambda/2$ chosen here, we obtain $\Delta t < 0.5 T_c$, which therefore will be denoted as the interpolation range for Rx2. Beyond this limit, i.e. $\Delta t > 0.5 T_c$, the coefficient for Rx2 has to be extrapolated, and correspondingly the MSE depicted in Fig. 3.15 rises continuously. For Rx1, the coefficient is obtained from an extrapolation over the entire range of channel dynamics, and hence we observe a continuous increase of the MSE here. Note that the MSE for Rx2 for $\Delta t > 0.6 T_c$ increases similarly as the MSE for Rx1 for $\Delta t > 0.1 T_c$ does, which is intuitively clear, as the channel seen at Rx2 is that of Rx1 delayed by $D T_o = 0.5 T_c$.

Increasing the number of observations N_o decreases the MSE significantly and leads to a more and more smooth slope of its curve in the range where the channel of the corresponding receive antenna is extrapolated. For $N_o > 1000$, we achieve only slight further improvements of the MSE (not shown), so that we can assume that the depicted curve for $N_o = 1000$ is already quite close to the performance that is achievable if the channel's total past is taken into account (i.e. $N_o \to \infty$) for channel estimates with fixed quality $\gamma = 20$ dB.

Varying the SNR γ of the channel estimates has a similar effect on the quality of the predicted channels. This is shown in Fig. 3.16, where the MSE is depicted for varying quality γ of the channel observations and a fixed number of observations $N_o = N_s = 20$. Obviously, the improvement of the estimates is much larger when going from $\gamma = 10$ dB to $\gamma = 20$ dB than the additional improvement when going to $\gamma = 30$ dB. Consider that an initial estimation quality for the CIR coefficients $h(n)$ of $\gamma = 20$ dB is already a challenging target for practical systems. Thus, it might not be considered reasonable to long for values of γ that lie significantly above 20 dB if practical applications are targeted.

In what follows, we evaluate the potential of the channel prediction approach if it is applied for channel-adaptive transmission in a time-varying environment. Therefore, we carry out similar investigations as performed in section 3.3.1 based on the same system conditions. Resorting to the illustrations from above, we use $\gamma = 20$ dB for the quality of the past channel estimates and $N_o = 20$ for the number of observations used, corresponding to the number of OFDM symbols contained in a slot N_s.

The delay remains at $\Delta i = 4 N_s$, mean SNR conditions are again fixed at $P_s / N_0 = 10$ dB. Hence, γ lies 10 dB above the SNR, which means we implicitly assume an estimator gain of 10 dB. Such an estimator gain can be achieved if sophisticated channel estimation techniques are applied [5]. The ACF φ_{hh} of the channels for the single transmit/receive antenna links is assumed to be ideally known.

Results from numerical evaluations are given in Fig. 3.17-3.19. Fig. 3.17 shows the
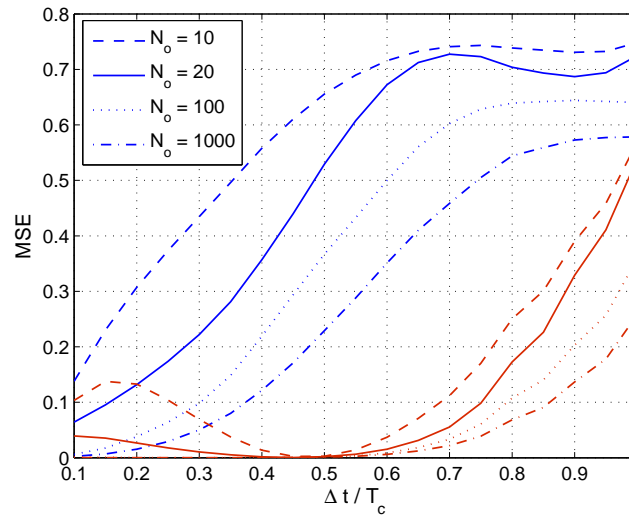
Fig. 3.15: MSE of the predicted channel coefficients in $\hat{\mathbf{h}}(i_k)$ vs. channel dynamics, channel observations N_o of quality $\gamma = 20$ dB. Blue: Rx1, red: Rx2.
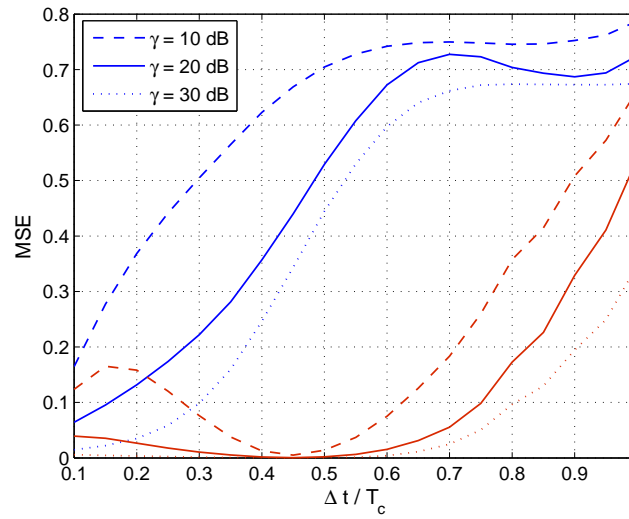

Fig. 3.16: MSE of the predicted channel coefficients in $\hat{\mathbf{h}}(i_k)$ vs. channel dynamics, $N_o = 20$ channel observations of quality γ. Blue: Rx1, red: Rx2.
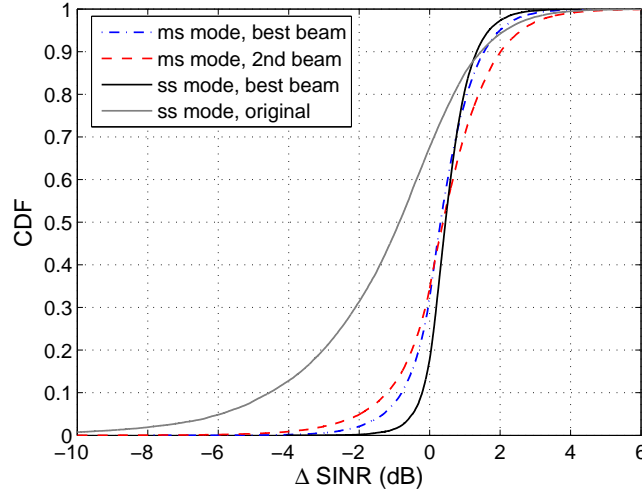
Fig. 3.17: CDF of the deviation of per-stream SINR for the different transmission modes ms and ss. $\Delta t = 0.2 T_c$, prediction-based approach.

CDFs of the difference in SINR, ΔSINR, per spatial stream and mode for the predicted channels $\hat{\mathbf{H}}(i_k)$ and the true channel $\mathbf{H}(i_k)$. For comparison, we also added the CDF for ss mode from Fig. 3.11 as solid grey line, which is based on $\mathbf{H}(i_0)$. We clearly observe that the prediction-based approach results in CDF curves with significantly steeper slopes than the curves based on $\mathbf{H}(i_0)$, which means that the variance of ΔSINR is significantly decreased. Further, we observe that the median value of ΔSINR is positive now, i.e. the SINR conditions do not tend to drop down any longer. Regarding the left tail of the CDFs reveals that the probability of high SINR losses to occur is significantly reduced. The curve of ss mode exhibits the steepest slope, indicating that this mode is still the one which suffers the least from SINR degradations.

Obviously, the improved stability of the SINR conditions for the different beams comes at a price, which is attributed to the imperfect predictability of channels based on extrapolation. This is revealed in Fig. 3.18, where we depict the median SINR values determined for $\hat{\mathbf{H}}(i_k)$ versus the channel dynamics: As the channel gain for the first receive antenna Rx1 is effectively obtained by an extrapolation through (3.19), the channel predictor tends to underestimate the channel, which translates into a drop of the median achievable SINR with increasing channel dynamics. However, for $\Delta t < 0.5 T_c$, this drop is rather small and amounts to not more than 2 dB for $\Delta t = 0.5 T_c$.

For $\Delta t > 0.5 T_c$, however, the slope of the curves representing the SINR drop increases significantly for the beams supported in ms mode, as then the channels for both antennas have to be extrapolated (see explanation above). As an extrapolation clearly yields less reliable estimates than an interpolation does, the degradations of the signal conditions becomes much more severe. In that sense, we can expect that for proper applicability of the prediction-based approach, the channel dynamics are limited by the expression given in (3.20).
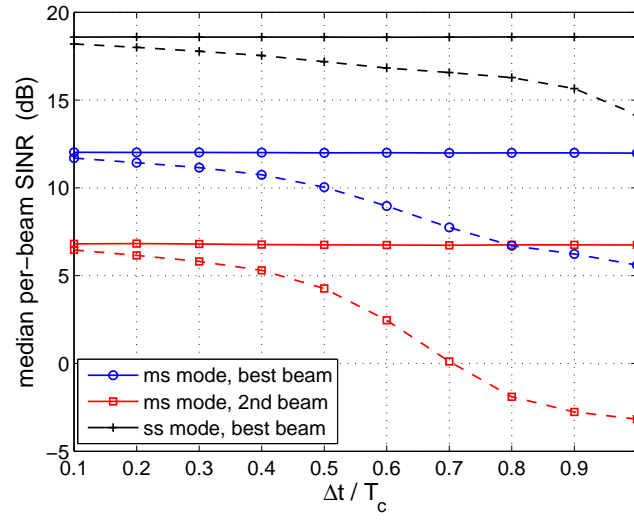
Fig. 3.18: Median SINR values from channel evaluation at UTs based on measured (solid curves) and predicted channels (dashed curves).
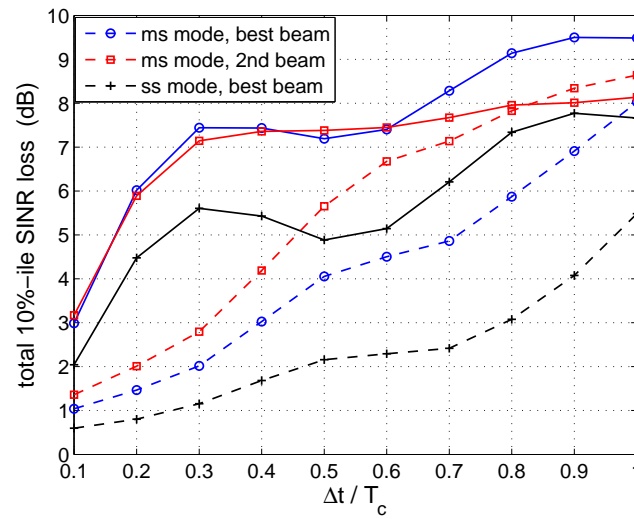

Fig. 3.19: Total loss of the per-stream SINR (in dB) for the 10-percentile of the ΔSINR-CDF measured (solid) and predicted channels (dashed).

To account for the median SINR loss inherent to the channel prediction approach, we add the corresponding losses obtained from Fig. 3.18 (in dB) to the ΔSINR values obtained for each value of $\Delta t/T_c$. Fig. 3.19 depicts the 10-percentile of the corresponding ΔSINR-CDFs in comparison to the original curves shown in Fig. 3.12. We clearly observe here that for $\Delta t < 0.5 T_c$, the SINR degradation increases much more smoothly than in the original case. The reduction in the total SINR loss is between 3 and 4 dB for this range of interest, indicating that the prediction-based approach is capable of diminishing SINR drops substantially. Thus, the proposed approach can be seen as a promising concept to support channel adaptive transmission also in mobile environments.

3.3.3 Conclusion chapter 3.3

We have focussed on the behaviour of the spatial adaptation concept presented in section 3.2 in time-variant channel environments, where the UTs move at vehicular speeds. It has been shown that if the original concept is applied without alterations, the delay occurring between channel evaluation and application of the scheduling decision may cause the evaluated SINR to drop down substantially. This may result in severe degradations of the system performance. Significant SINR drops can be observed already for a time lag of less than 1/10 of the channel's coherence time. For a suitable configuration of the receive antenna array at a mobile UT, we proposed a concept to predict the channels for a future time instant based on linear interpolation techniques. These predicted channels can be used for the determination of the SINR values to improve their reliability. The prediction-based approach has been evaluated for the 2×2 system configuration already used in section 3.2.4. It has been shown that the estimated SINR values become much more stable and SINR losses can be significantly reduced, as long as the prediction interval remains within the limits dictated by the receive antenna spacing. These results let the prediction-based approach pave the way towards a beneficial application of the channel-adaptive MIMO transmission concept also in mobile environments.

4 MIMO-OFDM in high mobility environments

If the UTs move at higher vehicular speeds (e.g. velocities above 100 km/h), the channel-adaptive transmission concept proposed in chapter 3, where the transmission rate is adapted to the instantaneous channel conditions, can no longer be beneficially applied. However, in that case, one can still benefit from the capabilities offered by the MIMO channel by adapting to the long-term channel statistics represented by the channel's co-variance matrix [28,81] or by using space-time coding techniques [100] that do not require any knowledge on the channel at the receiver. Both ideas can also be combined to utilize the advantages from both approaches simultaneously, as done in [116]. The major benefit from those approaches can be related to the the fact that the rate supported by the MIMO channel tends to become deterministic if the diversity offered by the spatial radio channel is properly exploited to stabilize the signal conditions, which has been pointed out in [64].

At very high speeds, however, a distortion effect occurs in OFDM systems that requires special treatment: High mobile speeds result in rapid changes of the communication channel due to the Doppler effects encountered in the communication medium. If the channel varies on a time scale close to the OFDM symbol duration, the orthogonality of the different subcarrier signals is violated, giving rise to ICI [46]. The performance limiting effect of Doppler-induced distortions in highly mobile environments has been thoroughly studied in [12]; suitable bounds for the power of ICI have been derived in [56]. During the past years, various approaches have been proposed to combat the Doppler-induced ICI by appropriate signal processing at the receiver (see [71,90,115] and references therein). However, the approaches that try to remove the ICI by considering their instantaneous distortions result in complex solutions, and hence their practical applicability may be limited to cases where sufficient signal processing power is available at the receiver.

For systems with receive antenna arrays, solutions to combat ICI with lower complexity demands exist. These rely either on receive beamforming patterns used to partition the Doppler spectrum and compensate for the mean frequency shifts separately [17,93], or they rely on statistical information of the ICI, which is utilized in the channel equalization process [92]. There are also solutions applying spatial interpolation techniques to generate virtual antennas that experience quasi-static channel conditions [53,124], but these demand a high complexity as well. For MIMO systems, there is a solution for combined

transmit beamforming and receive combining [23], which assumes instantaneous CSI to be available at transmitter and receiver. Although results are promising, the availability of instantaneous CSI at the transmitter in high mobility environments is an unsolved problem yet.

For a practical solution for MIMO-OFDM transmission in high mobility environments, we propose the following: Firstly, transmit beamforming based on the long-term channel statistics will still be an adequate choice. In FDD systems, this requires the UTs to feed back the channel's covariance matrix to the BS regularly, however, the update intervals now may be larger. For equalization at the receiver, the multiple antennas should be used to suppress the ICI. This section is devoted to the latter topic. We characterize the ICI by a single frequency-selective interference function, which can be estimated with simple means utilizing common pilot-based channel estimation techniques. With the estimated ICI, we can use the optimum combining approach [118], which individually maximizes the SINR of each subcarrier signal. Optimum combining enables a subcarrier-wise equalization, and hence the complexity demands are quite low. Compared to the low-complexity solutions for multiple antenna receivers summarized above, our proposal has the advantage that the instantaneous distortions from the ICI are taken into account.

For better illustration of our ICI suppression concept, we consider the case that a single stream is transmitted to the mobile UT, which then uses the available receive antennas for ICI suppression. This scenario is equivalent to a single-input multiple-output (SIMO) system, which will correspondingly be the base of our system model used here.

4.1 Simplified signal model for OFDM with Doppler-induced ICI

4.1.1 Time-variant channel in OFDM

We consider a time-variant radio channel $h(t, \tau)$, which can be modeled by a set of complex-valued coefficients a_{li} defined in the discrete Doppler/delay plane according to

$$h(t, \tau) = \sum_{l=0}^{L-1} \left(\sum_{i=-D}^{D} a_{li} \exp(j2\pi f_i t) \right) \delta(\tau - lT_s)$$

The Doppler spectrum is assumed double-sided consisting of $2D + 1$ discrete Doppler frequencies f_i, with $f_i < f_{i+1}$ and f_D being the maximum Doppler frequency. L is the number of available channel taps. δ denotes the Dirac-function and T_s is the time interval defining the resolution of the delay axis.

For an OFDM system with N subcarriers based on a sampling period of T_s, the frequency-domain channel distortion function $H(\Theta, \Omega)$ can be obtained from the time-

variant channel $h(t, \tau)$ as follows: First, time and delay dimension of $h(t, \tau)$ are sampled based on T_s, yielding discrete points in the time/delay plane. Second, the DFT with basis N is applied to the points of each dimension. Given with an analytical expression, this reads

$$H(\Theta, \Omega) = \frac{1}{N} \sum_{n=0}^{N-1} \sum_{m=0}^{N-1} h(nT_s, mT_s) \exp(-j\frac{2\pi}{N}(n\Theta + m\Omega)) \tag{4.1}$$

For the time variant channel given above, we thus obtain

$$H(\Theta, \Omega) = \frac{1}{N} \sum_{n=0}^{N-1} \sum_{l=0}^{L-1} \sum_{i=-D}^{D} a_{li} \exp\left(-j2\pi\Omega l/N\right) \times \exp\left(j2\pi n \left(-\Theta/N + f_i T_s\right)\right) \tag{4.2}$$

As definition ranges, we define

$$\begin{aligned}
\Omega &\in& \mathbb{K} &:= \{0, \ldots, N-1\} \\
\Theta &\in& \mathbb{M} &:= \{-N/2 + 1, \ldots, N/2\}
\end{aligned}$$

For $\Theta \neq 0$, $H(\Theta, \Omega)$ represents the interference that is imposed from the subcarrier signal at position Ω on the subcarrier that is spaced Θ subcarriers apart, whereby the sign of Θ specifies the direction. We thus call $H(\Theta \neq 0, \Omega)$ the interference function for subcarrier distance Θ. The channel coefficient of the subcarrier at position Ω is obtained for $\Theta = 0$; $H(0, \Omega) =: H(\Omega)$ thus is referred to as the channel transfer function (CTF).

The expressions in (4.2) can be simplified further by considering that the sum over the terms depending on parameter n represents a geometric series. Taking into account that Θ may take integer values only and that N usually is large, we obtain

$$H(\Theta, \Omega) = \sum_{l=0}^{L-1} \sum_{i=-D}^{D} a_{li} \underbrace{\exp(j\pi\omega_i) \frac{\sin(\pi\omega_i)}{\pi(\omega_i - \Theta)}}_{c_i(\Theta)} \exp\left(-j2\pi l \frac{\Omega}{N}\right) \tag{4.3}$$

where $\omega_i = N f_i T_s$ are the Doppler frequencies normalized to the subcarrier spacing.

4.1.2 Representation of the Doppler channel by two basic functions

The function $c_i(\Theta)$ in (4.3) can be regarded as a shaping function that reshapes the Doppler spectrum in the channel profile a_{li} depending on Θ. The product $a_{li} \cdot c_i(\Theta)$ can thus be considered to form a new channel profile $\tilde{a}_{li}(\Theta)$. For $\Theta = 0$ and $\Theta \neq 0$, the shaping functions are significantly different, which is illustrated in Fig. 4.1. From this fact it results that the channel profiles $\tilde{a}_{li}(\Theta)$ for the CTF $H(0, \Omega)$ and any interference function $H(\Theta \neq 0, \Omega)$ will differ substantially as well, so that we may conclude that CTF and interference functions can be considered to be statistically independent, although they are related to the same statistical process.
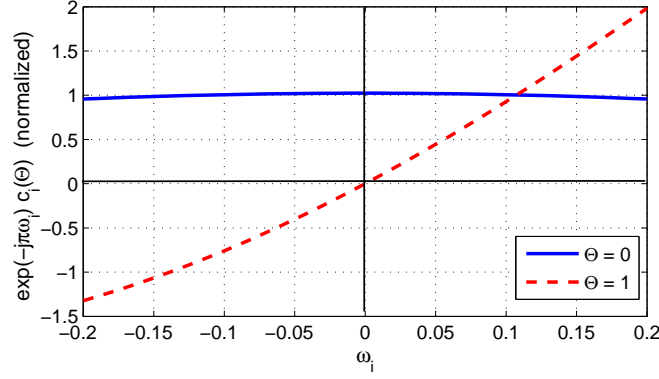
Fig. 4.1: Normalized Doppler shaping function $c_i(\Theta)$ (excluding complex factor $\exp(j\pi\omega_i)$) for $\Theta \in \{0, 1\}$.

Close inspection of $c_i(\Theta)$ reveals strong similarities between the coefficients $c_i(\Theta)$ for different $\Theta < 0$ and $\Theta > 0$, respectively. For small ω_D, it turns out that $c(\Theta)$ decreases according to $|\Theta|^{-1}$. We can thus identify the relationships $c_i(\Theta > 0) \approx |\Theta|^{-1}c_i(1)$ and $c_i(\Theta < 0) \approx |\Theta|^{-1}c_i(-1)$, respectively. With respect to $H(\Theta, \Omega)$, this translates to

$$H(\Theta \neq 0, \Omega) \approx \underbrace{\frac{1}{|\Theta|} \cdot \begin{cases} H(+1, \Omega) & \Theta > 0 \\ H(-1, \Omega) & \Theta < 0 \end{cases}}_{F(\Theta, \Omega)} \tag{4.4}$$

This relation enables us to characterize the entire ICI distorting the OFDM signals solely by the two interference functions $H(1, \Omega)$ and $H(-1, \Omega)$. The approximated function for $H(\Theta \neq 0, \Omega)$ will in the following be denoted as the interference function (IF) $F(\Theta, \Omega)$.

Based on the time-variant OFDM channel $H(\Theta, \Omega)$ from (4.3), the transmission equation for the received signal $r(k)$ at a fixed subcarrier k can be given as

$$r(k) = \sum_{u \in \mathbb{M}} H(u, k - u)x(k - u) + n(k) \tag{4.5}$$

where $x(k)$ and $n(k)$ are the transmit signal and the AWGN, respectively. By using the IF $F(u, k)$ instead of $H(u, k)$, we obtain

$$r(k) = H(k)x(k) + \sum_{u \in \mathbb{M}\backslash 0} F(u, k - u)x(k - u) + n(k)$$

with $H(k) = H(0, k)$ being the CTF. The first term in this structure represents the useful signal, while the sum term represents the distortions from ICI, which are now described in terms on the IF.

4.1.3 Mean power of channel and interference coefficients

To get insights into the signal and interference conditions, we focus next on the mean power of all channel and interference coefficients, which is calculated as

$$P_c = E\{H(u, k) \cdot H^*(u, k)\}.$$

According to the WSSUS[1] channel modeling assumption, the single channel weights a_{li} in (4.3) are modeled as independently Rayleigh fading, which means they are considered to be drawn independently from complex Gaussian normal distributions with zero mean and variance σ_{li}^2. By exploiting this fact, the mean power of the coefficients yields

$$P_c(u) = \sum_{l=0}^{L} \sum_{i=-D}^{D} \sigma_{li}^2 \, \mathrm{si}^2(\pi(\omega_i - u))$$

where $\mathrm{si}(x) = \sin(x)/x$ is the si-function. Complying with the WSSUS assumption, P_c is independent of the subcarrier position k and depends on u only.

For a fixed delay l, σ_{li}^2 with $i \in \{-D, \ldots, D\}$ represents the discrete Doppler power spectrum of the l-th delay tap. For rich scattering conditions, it is common to assume that all channel taps $l \in \{0, \ldots, L-1\}$ experience the same (normalized) Doppler power spectrum p_i. Accordingly, the power distribution σ_{li}^2 can be separated into multiplicative components, $\sigma_{li}^2 = \sigma_h^2 \cdot p_l \cdot p_i$, where p_l is the normalized power delay profile and σ_h^2 represents the mean power of the channel. With these assumptions, the power of the coefficients yields

$$P_c(u) = \sigma_h^2 \sum_{i=-D}^{D} p_i \, \mathrm{si}^2(\pi(\omega_i - u)) \tag{4.6}$$

A lower bound for the power of the coefficients of the CTF can be given as:

$$P_c(0) \geq \sigma_h^2 \cdot \mathrm{si}^2(\pi\omega_D) \tag{4.7}$$

The power of the interference coefficients can be bounded similarly by

$$P_c(u) \leq \sigma_h^2 \cdot \mathrm{si}^2(\pi(\omega_D - u)), \quad \forall \, u \neq 0 \tag{4.8}$$

Note that in contrast to (4.7), this is an upper bound.

4.1.3.1 Signal to ICI power ratio

With the power of the channel and interference coefficients obtained in (4.6), we can now derive an expression for the mean signal to interference ratio (SIR) affecting each

---

[1]wide sense stationary uncorrelated scattering

subcarrier signal. To this end, we assume i.i.d. transmit symbols $x(k)$ with power P_s that occupy the entire signal bandwidth, i.e. $x(k) \neq 0 \; \forall k \in \mathbb{K}$. According to (4.5), the mean power of the useful signal at subcarrier k is $\bar{P}_u = P_s \cdot P_c(0)$, while the mean power of the ICI $\bar{P}_{ICI}$ distorting this useful signal amounts to

$$\bar{P}_{ICI} = \sum_{u \in \mathbb{M} \backslash 0} P_c(u) \cdot P_s = P_s \left(\sigma_h^2 - P_c(0) \right) \tag{4.9}$$

Note that $\sum_{u \in \mathbb{M}} P_c(u) = \sigma_h^2$ holds, yielding the expression on the right hand side of the above equation. With the obtained results, we can determine the mean SIR according to

$$\text{SIR} = \frac{\bar{P}_u}{\bar{P}_{ICI}} = \frac{P_c(0)}{\sigma_h^2 - P_c(0)} \geq \frac{\text{si}^2(\pi \omega_D)}{1 - \text{si}^2(\pi \omega_D)} \tag{4.10}$$

where the exact $P_c(0)$ can be determined from (4.6), and the lower bound on the right hand side was obtained by using the power bound (4.7).[2]

4.1.4 MSE resulting from applying the IF

As the IF is based on an approximation for $H(u, k)$, the use of this function will introduce an error, whose magnitude is assessed in this subsection. The error resulting from the comparison of the IF with the original interference function can be determined as $F(u, k) - H(u, k)$. The mean power of this error, which corresponds to the MSE μ, can be determined according to

$$\mu = E\{|F(u, k) - H(u, k)|^2\} \tag{4.11}$$

As the two functions $H(\pm 1, k)$ constituting the IF $F(u, k)$ according to (4.4) have identical statistical properties, it suffices to examine one of the partial functions only, and hence we focus on $H(+1, k)$ and the positive values $u > 0$. Inserting the corresponding coefficients from (4.3) into the above equation and taking into account the assumptions made in the preceding section where we derived the power of channel and interference coefficients, we obtain for the MSE

$$\mu(u) = \sigma_h^2 \sum_{i=-D}^{D} p_i \left(\frac{\sin(\pi \omega_i)}{\pi(\omega_i - u)} \right)^2 \left(\frac{(u-1)\omega_i}{u(1 - \omega_i)} \right)^2$$

$$\leq \underbrace{\sigma_h^2 \sum_{i=-D}^{D} p_i \left(\frac{\sin(\pi \omega_i)}{\pi(\omega_i - u)} \right)^2}_{P_c(u)} \left(\frac{(u-1)\omega_D}{u(1 - \omega_D)} \right)^2 < P_c(u) \underbrace{\left(\frac{\omega_D}{1 - \omega_D} \right)^2}_{\eta} \tag{4.12}$$

---

[2]Note that this bound is similar to the bound for CFO distortions derived in (2.52).

According to the WSSUS assumption, the MSE depends on the subcarrier spacing u only and is independent of k, as it was the case for the mean power of channel and interference coefficients given in (4.6). Finally, we obtain the upper bound for the MSE $\mu(u)$ given on the right hand side of the equation, which is valid for arbitrary $u > 1$.

Similarly as in (4.9), we can now bound the total power of the MSE depending on the Doppler frequency ω_D: The power of the MSE from the single interference functions $H(u, k)$ affecting the signal at subcarrier k will sum up over the occupied frequency band according to

$$P_{MSE} = \sum_{u \in \mathbb{M} \setminus 0} \mu(u) \leq \sum_{u \in \mathbb{M} \setminus 0} P_c(u) \left(\frac{(u-1)\omega_D}{u(1-\omega_D)} \right)^2 < \left(\sigma_h^2 - \sum_{u=-1}^{1} P_c(u) \right) \eta \qquad (4.13)$$

To obtain the bound on the right hand side, we used the relation $\sum_{u \in \mathbb{M}} P_c(u) = \sigma_h^2$ again, as done in the preceding section to derive (4.9). The above result clearly suggests that as long as the Doppler frequency is sufficiently small ($\omega_D < 0.25$), the influence of the MSE introduced by applying the IF is negligible.

4.2 Optimum combining at multiple antenna receiver

Corresponding to (4.5), the k-th subcarrier signal received at a receiver with N_r antennas reads

$$\mathbf{r}(k) = \mathbf{h}(k)x(k) + \underbrace{\sum_{u \in \mathbb{M} \setminus 0} \bar{\mathbf{h}}(u, k-u)x(k-u) + \mathbf{n}(k)}_{\mathbf{z}(k)} \qquad (4.14)$$

All signals printed in bold letters represent N_r-dimensional vectors, where $\mathbf{h}(k)$ and $\bar{\mathbf{h}}(u, k)$ comprise the coefficients from CTF $H(k)$ and interference function $H(u, k)$ for the channels seen from the N_r single receive antennas. $\mathbf{n}(k)$ is the noise vector containing N_r samples of i.i.d. AWGN noise with mean power N_0. The equation represents the N_r-dimensional useful signal, which is distorted by additive interference and noise, aggregated in $\mathbf{z}(k)$. As this transmission equation exhibits the same principal structure as the transmission model in [118], the optimum combining (OC) approach can be used to derive an equalization vector $\mathbf{w}(k)$ that maximizes the SINR after signal combining. The OC approach requires the interference-plus-noise correlation matrix $\mathbf{Z}(k) = E\{\mathbf{z}(k) \cdot \mathbf{z}^H(k)\}$. With the i.i.d. assumption for the transmit signals $x(k)$, the correlation matrix yields

$$\mathbf{Z}(k) = P_s \sum_{u \in \mathbb{M} \setminus 0} \bar{\mathbf{h}}(u, k-u)\bar{\mathbf{h}}^H(u, k-u) + N_0\mathbf{I} \qquad (4.15)$$

The OC approach then yields for the equalization vector

$$\mathbf{w}(k) = \varepsilon \mathbf{Z}^{-1}(k)\mathbf{h}(k) \tag{4.16}$$

where ε is a constant of arbitrary value, which is usually chosen to normalize $\mathbf{w}(k)$ to a power of unity. Equalization of the received signal $\mathbf{r}(k)$ is carried out by calculating $\mathbf{w}^H(k) \cdot \mathbf{r}(k)$.

In what follows, we simplify the calculation of the equalization vector $\mathbf{w}(k)$ further to pave the way for a practical employment. First note that although the signal at subcarrier k will be affected from ICI of all subcarriers carrying data symbols, the subcarrier signals in close vicinity around k will generate the major proportion of this ICI. Hence, it may be sufficient to confine the set of subcarriers to be considered for the calculation of $\mathbf{Z}(k)$ in (4.16) to the nearest neighbours of subcarrier k. In particular, relation (4.4) clearly suggests that the ICI power decays inversely proportional to the square of the subcarrier distance Θ, and hence the ICI power from a subcarrier at distance $\Theta = 3$ drops by nearly 10 dB compared the one at distance $\Theta = 1$. Thus, a practical choice is to limit u to the set $\mathbb{L} = \{-2, \ldots, 2\} \backslash 0$ within the calculation of $\mathbf{Z}(k)$ according to (4.15). To ease calculation further, we can use the IF instead of the true interference functions in $\bar{\mathbf{h}}(u, k)$: Let $\mathbf{f}(u, k)$ be the vector comprising the N_r coefficients of the IF $F(u, k)$ for the channels seen from the N_r single receive antennas. Herewith, we can substitute $\bar{\mathbf{h}}(u, k)$ with $\mathbf{f}(u, k)$ in (4.15). These simplifications yield a practical solution for the equalization vector as

$$\mathbf{w}(k) = \bar{\varepsilon} \left[\sum_{u \in \mathbb{L}} \mathbf{f}(u, k - u)\mathbf{f}^H(u, k - u) + \frac{N_0}{P_s}\mathbf{I} \right]^{-1} \mathbf{h}(k) \tag{4.17}$$

Note that we use a modified factor $\bar{\varepsilon}$ here, as $\mathbf{Z}(k)$ has been normalized by P_s compared to (4.16). As CTF and IF are considered to be statistically independent (see section 4.1.2), we expect the equalizer (4.17) to conveniently suppress the ICI.

4.2.1 Performance evaluation with ideal channel knowledge

4.2.1.1 Evaluation framework

We evaluate the performance of the OC equalizer defined in (4.17) by simulating signal transmission in a Rayleigh-fading environment and comparing its performance to the one of a simple MRC receiver, which is characterized by the equalization vector $\mathbf{w}(k) = \varepsilon \mathbf{h}(k)$. In fact, MRC can be considered as a special case of the OC receiver (4.16) that totally ignores the interference in $\mathbf{Z}(k)$. We assume transmission based on a slotted time structure with transmission resources denoted as chunks, as introduced in section 3.2.1. For a brief recap: Each slot is constituted of several consecutive OFDM symbols. For the duration of a slot, the data dedicated for a single terminal is contained in a frequency subband

confined to a fixed number of consecutive subcarriers. This partition of time and frequency resources is denoted as a *chunk*.

As a performance measure, we use the SINR of the useful signal achieved after equalization, termed *post-detection SINR*. It is defined as the ratio of useful signal power, P_u, and the power of interference and noise, P_{in}, which is averaged over the set of simulated samples:

$$\text{SINR} = E\left\{\frac{P_u}{P_{in}}\right\} \geq \frac{E\{P_u\}}{E\{P_{in}\}} \tag{4.18}$$

The lower bound on the right hand side stems from Jensen's inequality and is referred to as the (empirical) SINR lower bound. We use it within the investigations to enable comparisons with the analytical SIR from (4.10).

After equalization of $\mathbf{r}(k)$ from (4.14) with the equalization vector $\mathbf{w}$, the post-detection power P_u of the useful subcarrier signal $x(k)$ amounts to

$$P_u = \|\mathbf{w}^H(k)\mathbf{h}(k)\|^2 \cdot P_s$$

As all other subcarrier signals are assumed i.i.d. with equal power P_s, we yield for the power of interference and noise distorting the useful signal at subcarrier k

$$P_{in} = \sum_{u \in \mathbb{M}\backslash 0} \|\mathbf{w}^H(k)\bar{\mathbf{h}}(u, k - u)\|^2 \cdot P_s + N_0 = \mathbf{w}^H \mathbf{Z}(k)\mathbf{w}$$

Note that there is no scaling of the noise power N_0, as we assume $\mathbf{w}(k)$ to be normalized to unit power.

The equalization vector $\mathbf{w}(k)$ is calculated according to (4.17). We simulate transmission of 500 independent time slots and evaluate the powers P_u and P_{in} at the subcarriers of a chunk located at a fixed position in the frequency band, which are then averaged according to (4.18).

4.2.1.2 System setup

The channels seen at the $N_r = 2$ receiving antennas are modeled as i.i.d. Rayleigh fading with a common Doppler spectrum and PDP. The Doppler power spectrum is modeled according to Jakes [79] with $D = 12$ equidistantly spaced discrete Doppler frequencies. The PDP is exponentially decaying with decaying factor $2L/5$, its length is set to $L = 20$. Parameters of the transmission system are similar to the system specification of 3G-LTE: The $N = 1024$ subcarriers of the OFDM system span a bandwidth of 15 MHz, yielding a subcarrier spacing of 15 KHz. A guard interval of length $G = 64$ samples is employed. A time slot consists of 7 consecutive OFDM symbols, and the frequency width of a chunk spans 25 subcarriers. For the transmit symbols on all subcarriers, 16QAM modulation is used.
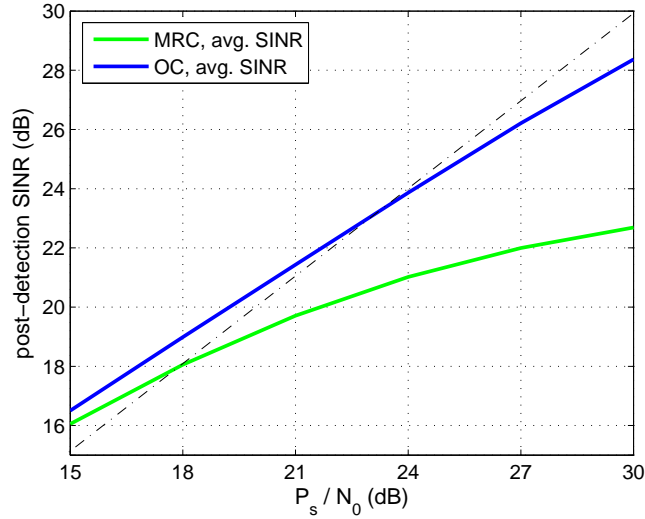
Fig. 4.2: Achievable SINR performance with maximum ratio combining (MRC) and optimum combining (OC) based on true interference functions as well as IF. $\omega_D = 0.1$

4.2.1.3 Results

Fig. 4.2 shows the average post-detection SINR versus the SNR $= P_s/N_0$ for a normalized Doppler frequency $\omega_D = 0.1$. Blue line represents MRC performance, red line the performance of the proposed OC. As MRC does not combat the ICI, its performance curve approaches a saturation level for high SNR which is dictated by the ICI power level. The OC solution combatting the ICI exhibits clear performance gains which increase with increasing SNR. The dash-dotted black line represents the SNR-identity curve. At low SNR, where signal conditions are dominated by the noise, the OC solution is able to achieve an additional combining gain which is similar to MRC, and thus the OC curve lies above the SNR-identity curve. For increasing SNR, the ICI gains prominence. The OC uses then the spatial degrees of freedom at the receiver for ICI suppression, and consequently the additional SNR gain from MRC-like signal combining vanishes. For SNR $>$ 23 dB, the OC curve falls below the identity curve and thereafter tends towards saturation, which is due to the fact that the equalizer cannot suppress the entire ICI. This deficiency results on the one hand from the limited set of subcarriers being considered in $\mathbb{L}$ in (4.17). On the other hand, the receiver has only one spatial degree of freedom available to combat ICI from several neighbouring subcarrier signals. These signals leave slightly different spatial signatures, and thus they can be considered as sources of distortions which are partially independent. With independent sources of distortions at high SNR conditions, the OC equalizer still maximizes the post-detection SINR, but it is not capable of forcing these distortions completely to zero.

Fig. 4.3 illustrates the post-detection SINR versus ω_D for an SNR approaching infinity. Comparing MRC performance with OC performance reveals that the OC combiner may deliver gains of more than 10 dB; however, for increasing Doppler frequency ω_D, the
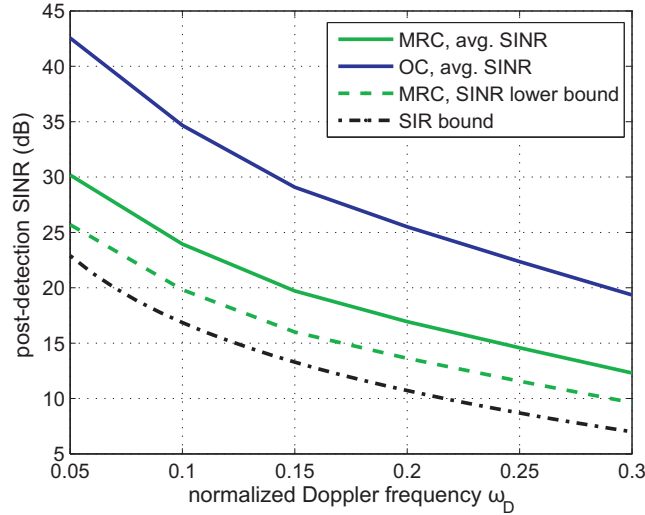
Fig. 4.3: Achievable SINR performance with MRC and OC versus ω_D and performance bounds (4.18) and (4.10) for $P_s/N_0 \to \infty$.

relative gains decrease. The two lowermost curves represent the (empirical) SINR lower bound achieved with MRC according to (4.18) and the (analytical) SIR (4.10) based on $P_c(0)$ according to (4.6), respectively. We observe that the former curve lies exactly 3 dB above the latter. Obviously, MRC is capable of providing a gain here which is similar to the SNR gain achieved in AWGN. This observation confirms the AWGN-like behaviour of the ICI distortion, which has been pointed out already in [94]. Furthermore, it also confirms the independency of interference functions and CTF, as conjectured in section 4.1. Note that this behaviour is contrary to CFO distortions, where the full MRC gain cannot be provided due to the correlation of interference and CTF, as analyzed in the second chapter in section 2.2.4.

4.3 Estimation of channel and ICI in the downlink

In this section we focus on the estimation of the CTF and the IF for a single antenna link. We will consider downlink transmission, where a base station transmits a broadband OFDM signal to several mobile terminals. For channel estimation, pilot signals are spread over the entire time and frequency resources of the time slot based on a regular grid. From the channel estimates at the pilot positions, the channel of the chunk assigned to the mobile user can be obtained by applying frequency- and time-domain channel interpolation techniques [35, 88].

Let k be the subcarrier index and i the index of the OFDM symbol within the chunk assigned to a mobile user. We denote the time-variant CTF and IF for this chunk as $H_i(k)$ and $H_i(\pm 1, k)$, respectively. Their estimation is addressed in the next subsections.

4.3.1 CTF estimation

As we assume the transmit signals $x(k)$ to be i.i.d., the distortion evoked by the ICI in (4.5) can be considered as additional noise with Gaussian-like properties[3]. Thus, estimation of the CTF can be carried out with the common techniques under SNR conditions that are equivalent to the one from AWGN with power equal to the sum of noise and ICI power. With N_0 being the power of the AWGN process, the ICI power from (4.9) and the bound for the power of the useful channel (4.7), the SNR conditions valid for estimating the CTF can be characterized by the bound

$$\text{SNR} \geq \frac{\text{si}^2(\pi\omega_D)}{(1 - \text{si}^2(\pi\omega_D)) + N_0/(P_s\sigma_h^2)} \tag{4.19}$$

To estimate the CTF, the pilot-based $2 \times 1\text{D}$ MMSE estimator proposed in [35] can be used: First, the frequency-domain channel $\mathbf{H}_i(k)$ is estimated for the OFDM symbols i within the time slot where pilot symbols are available. In the second step, for each subcarrier of the chunk, the channel is interpolated over time to yield the channel for the remaining OFDM symbols of the slot. MMSE estimation in frequency requires knowledge of the frequency correlation function as well as the SNR given by (4.19), which both need to be estimated additionally in practice. Time interpolation requires the time correlation function and the SNR of the estimates used as input. While the former needs to be estimated as well, the SNR of a channel estimate can be obtained from its normalized MSE μ via the relation $\text{SNR} = (1 - \mu)/\mu$. The subcarrier-specific MSE μ itself can be derived analytically from the applied MMSE estimator [35], whereby the SNR of the initial channel estimate at the pilot symbol serves as input. For further details on the estimation process, refer to [35, 88].

Note that for proper estimation of the CTF, the pilot grid needs to meet certain requirements derived from the sampling theorem. In particular, the pilot spacing d_f in frequency domain has to fulfil $d_f \leq N/(2L)$ [35]. With T_o being the total duration of the OFDM symbol (i.e. including the cyclic prefix), we yield for the spacing d_t in time-domain $2f_D T_o d_t \leq 1$. As T_o usually is not significantly larger than NT_s, we may use $T_o \approx NT_s$, so that we obtain

$$2\omega_D \cdot d_t \leq 1 \tag{4.20}$$

This expression establishes a direct relation between the required time-domain pilot spacing d_t and the maximum normalized Doppler frequency ω_D.

---

[3]Refer to the preceding section, where this consideration was confirmed by simulation results

4.3.2 IF estimation

In [71], a linear model has been introduced to describe the temporal evolution of the time-domain multi-tap channel between two successive OFDM symbols, which has been used as a suitable approximation for cases where $\omega_D \leq 0.2$ holds. Here, we adopt this linear model to characterize the time evolution of the channel $H_i(k)$ at subcarrier k. The subcarrier channel itself is considered frequency-flat, and hence its corresponding time-domain channel $h_{ik}(n)$ can be given as a one-tap channel evolving with a linear slope $\Delta_i(k)$ over sampling index n:

$$h_{ik}(n) = H_i(k) + \Delta_i(k) \cdot n \tag{4.21}$$

The linear slope can be determined from the difference of the channels measured at successive OFDM symbols: $\Delta_i(k) = (H_{i+1}(k) - H_i(k))/N_s$, with $N_s = T_o/T_s$ being the total length of an OFDM symbol in samples of duration T_s. From the equivalent time-domain channel (4.21), we can determine the two functions $H_i(\pm 1, k)$ constituting the IF by applying the DFT according to (4.1) with $\Theta = \pm 1$ for the sample indices $n \in \{-N/2 + 1, \ldots, N/2\}$ that span the i-th OFDM symbol:

$$
\begin{aligned}
H_i(\pm 1, k) &= \frac{1}{N} \sum_{n=-N/2+1}^{N/2} h_{ik}(n) \exp(\mp j2\pi n/N) \\
&= \underbrace{- \left(1 - \exp(\mp j2\pi/N)\right)^{-1}}_{\alpha^{\pm}} \cdot \Delta_i(k)
\end{aligned}
\tag{4.22}
$$

As $H_i(k)$ in (4.21) is constant, it does not influence $H_i(\pm 1, k)$. The constant scaling factor $\alpha^{\pm}$ in (4.22) thus results from the DFT of the linear parameter n in (4.21) only (compare with [71], where $\alpha^{\pm}$ has also been calculated).

4.3.2.1 Improved piece-wise linear model

The accuracy of the linear model in (4.21) can be improved further if we take into account not only information on the channel state from the succeeding OFDM symbol $H_{i+1}(k)$ via $\Delta_i(k)$, but also from the preceding symbol $H_{i-1}(k)$ via $\Delta_{i-1}(k)$. This extended linear approximation approach has also been used in [71]. By adopting it in our system setting, we obtain for the time-domain subcarrier channel $h_{ik}(n)$ a piece-wise linear slope, yielding

$$
h_{ik}(n) = \begin{cases} H_i(k) + \Delta_i(k) \cdot n & n \geq 0 \\ H_i(k) + \Delta_{i-1}(k) \cdot n & n < 0 \end{cases}
\tag{4.23}
$$

Applying the DFT as done in (4.22), we obtain

$$
\begin{aligned}
H_i(\pm 1, k) = {} & 0.5\alpha^{\pm}(\Delta_{i-1}(k) + \Delta_i(k)) \\
& + 2(\alpha^{\pm})^2/N(\Delta_{i-1}(k) - \Delta_i(k))
\end{aligned}
\tag{4.24}
$$

Again, the constant term $H_i(k)$ in (4.23) does not influence $H_i(\pm 1, k)$. Thus, $H_i(\pm 1, k)$ is constituted from constant terms resulting from the DFT of the linear parameter n, multiplied with the linear slopes $\Delta_i(k)$ and $\Delta_{i-1}(k)$, respectively. Corresponding calculation of $H_i(\pm 1, k)$ can be done similarly as in [71], yielding the expression given in (4.24).

4.3.3 Applying the estimates for the equalization vector

According to (4.17), calculation of the equalization vector for the signal at subcarrier k requires knowledge of the IF from adjacent subcarriers. Hence, we can no longer confine ourselves solely to the chunk assigned to the user, but have to consider the ICI from subcarrier signals flanking the edges of the assigned chunk, which requires estimation of the IF at these subcarrier positions. A proper solution for that can easily be found if we assume that the user terminal may access also the frequency-domain chunks being located next to the one assigned.[4] Then a super-block can be formed by concatenating the three chunks. Estimation of CTF and IF can be carried out based on the pilots available within the super-block according to the process detailed in the preceding subsections. By applying this approach, we do not only yield a reliable estimate of the IF at the subcarriers close to the edges outside the assigned chunk. As the channel interpolation process takes advantage of the channel information from all pilots contained in the super-block, the estimate of the CTF for the assigned chunk does not suffer from edge effects that commonly occur in classical chunk-based estimation [88]. Thus, the quality of the estimates of CTF as well as IF becomes similar for the subcarriers of the assigned chunk.

Note that the proposed ICI suppression technique has comparably low demands on computational complexity: The IF is obtained from the CTF according to (4.22) or (4.24) by a few simple operations. For the calculation of the equalization vector per subcarrier k according to (4.17), we have to construct and invert a matrix of dimension $N_r \times N_r$. The complexity required therefore is similar to the one required by a standard linear MMSE equalizer. In the context of spatial multiplexing transmission, this equalizer has already been shown to run in practice [47]. Hence, we can expect that the proposed technique can readily be implemented in a practical system.

---

[4]Note that this assumption is valid for the downlink only, as in the uplink, signals from adjacent chunks can stem from different users and thus may have experienced totally different channels.
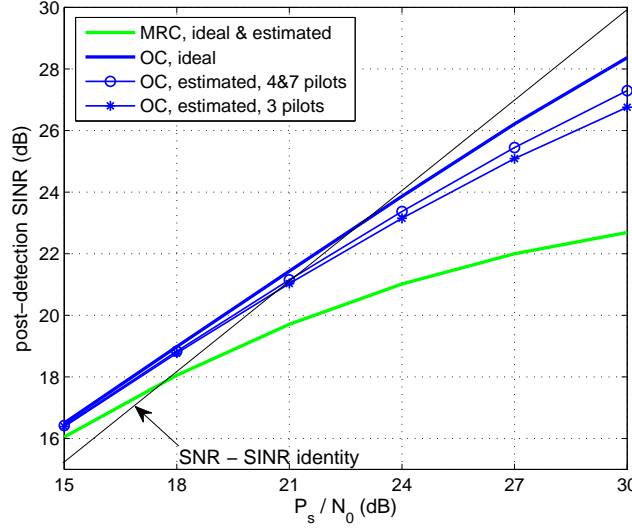
Fig. 4.4: Achievable SINR performance with maximum ratio combining (MRC) and optimum combining (OC) based on ideal and estimated channels. $\omega_D = 0.1$

4.3.4 Performance Evaluation

For performance evaluation, we use the same evaluation framework and system setup as described in section 4.2.1. Additionally, we integrate a regular grid of pilot signals into the resources of the time slot, whereby we consider three different pilot densities in the time domain with $d_t \in \{1, 2, 3\}$. Correspondingly, a chunk contains 7, 4 or 3 OFDM symbols carrying pilots. In frequency domain, the spacing between pilots is fixed to $d_f = 6$ subcarriers. To estimate the IF for the outer OFDM symbols of the chunk, the basic linear model (4.22) is applied, whereas the improved piece-wise linear model (4.24) is used for the inner OFDM symbols. For estimation of CTF and IF, time and frequency correlation functions of the channel as well as the SINR given in (4.19) are assumed to be ideally known.

Fig. 4.4 shows the achievable average post-detection SINR versus the SNR= P_s/N_0 for a normalized Doppler frequency $\omega_D = 0.1$. The figure contains the performance curves based on ideal channel knowledge from Fig. 4.2 and additionally the curves based on estimated CTF and IF for the different pilots densities considered. While we observe that the MRC performance based on ideal and estimated channels is nearly identical in the depicted SNR range, the performance of OC suffers only marginally if CTF and IF are estimated according to the proposed scheme. In particular, at high SNR, the loss is only slightly above 1 dB in case 4 or 7 time-domain pilots are available and stays below 2 dB for 3 pilots. These observations already suggest that the proposed approach is able to approach the theoretically predicted performance conveniently also in practical systems, where the time-variant channel shall be estimated with simple means.

Fig. 4.5 illustrates the achievable SINR conditions for varying ω_D at a fixed SNR
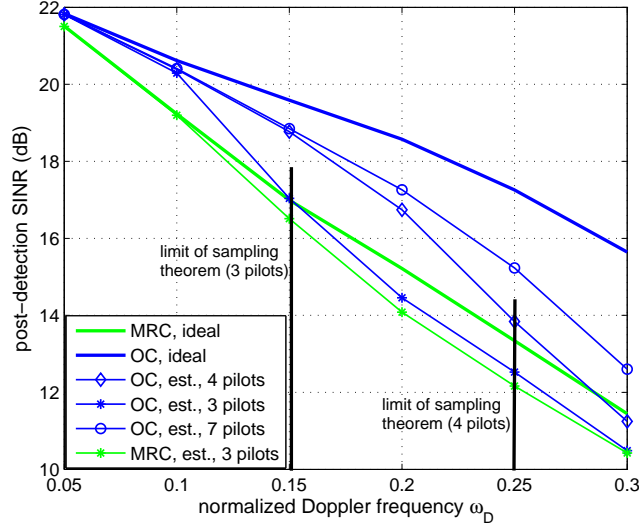
Fig. 4.5: Achievable SINR performance with MRC and OC versus ω_D for fixed $P_s/N_0 = 20$ dB.

$P_s/N_0 = 20$ dB. We observe that the OC approach is capable of delivering additional SINR gains of up to 4 dB compared to MRC at the given SNR level if CTF and IF are ideally known. In case both functions are estimated, the OC performance drops down, but still delivers a significant gain compared to MRC, which, however, decreases for increasing ω_D. In case 3 time-domain pilots are available, we reach the limit of the sampling theorem according to (4.20) at $\omega_D = 0.16$, and correspondingly the OC as well as the MRC performance drop significantly at this frequency level. For the case of 4 time-domain pilots, the limit of the sampling theorem is reached at $\omega_D = 0.25$, where we also observe a steep performance drop of the corresponding OC performance. Above these two Doppler frequency levels, the performance gain of the OC equalizer compared to MRC is only marginal.

In case each OFDM symbol carries pilots (7 pilots available), the OC solution exhibits a performance that lies significantly above the MRC performance for the whole range of depicted Doppler frequencies. However, its distance to the OC curve based on ideal knowledge of CTF and IF increases with the Doppler frequency. Clearly, this results from the limited validity range of the linear model used to describe the temporal evolution of the Doppler channel in (4.23), which forms the basis for the IF estimation (4.24). In [71], this range was limited to $\omega_D \leq 0.2$, and correspondingly the distance to the ideal OC curve increases significantly above this value.

Fig. 4.6 depicts the normalized MSE of the CTF as well as the IF estimates versus the ω_D for the different number of time-domain pilots available. We clearly observe here that the MSE of both functions rises steeply when the limits of the sampling theorem are reached, which is at $\omega_D = 0.16$ for 3 pilots and $\omega_D = 0.25$ for 4 pilots. Evidently, this will result in a severe performance loss of the corresponding OC equalizer, which was
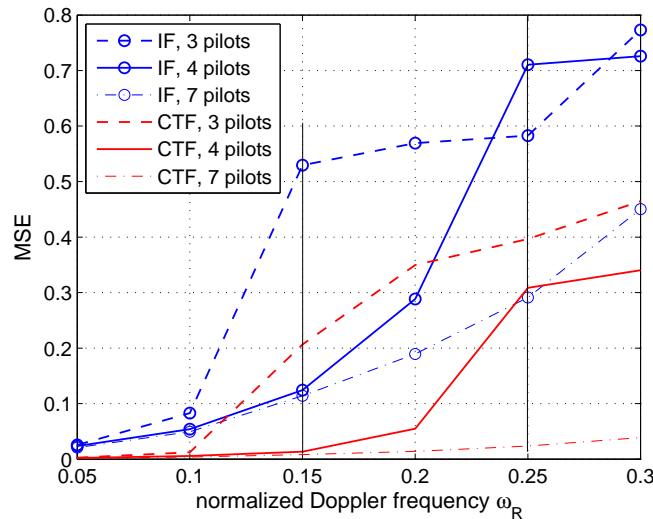
Fig. 4.6: MSE of CTF and IF estimates versus ω_D for fixed $P_s/N_0 = 20$ dB.

already pointed out above. We observe further that in case of 7 pilots, the MSE of the IF estimation rises significantly for $\omega_D > 0.2$, which also complies with the observations made earlier. The estimation of the CTF takes the full advantage of the enhanced pilot grid based on 7 time-domain pilots and consequently yields a low MSE over the entire range of Doppler frequencies.

We conclude that the proposed OC approach operates conveniently in practical systems and is capable of delivering substantial performance gains compared to common MRC while having slightly increased demands on the computational complexity only. Thanks to these properties, the OC approach can be seen a promising solution to combat ICI in practical high-mobility OFDM systems.

4.4 Conclusion chapter 4

For MIMO-OFDM systems operated in high mobility environments, we derived a solution based on the optimum combining approach [118] to suppress the Doppler-induced ICI at the multiple antenna receiver. Starting from an analytical description of the OFDM channel under high mobility conditions, we modeled the frequency-domain OFDM channel by the channel transfer function CTF and an interference function IF, which was shown to be independent of the former for general Doppler channels characterized by a Doppler spectrum. Based on this model, we could describe the received signal vector for a single subcarrier signal by a sum of the useful signal vector containing elements from the CTF and interfering signal vectors containing elements from the IF. This model enables us to apply the optimum combining solution, which coherently combines the useful signal portions from all receive antennas while suppressing the ICI distortions.

Further, we have proposed a simple method to estimate both functions CTF and IF per receive antenna based on common pilot signals, which is based on the linear channel evolution model presented in [71]. This method enables reliable estimate of both measures if the channel dynamics do not exceed the limits of the linear model, and if sufficient pilot symbols are available in time direction. The viability of the approach has been verified by simulations for a 1×2 SIMO link based on ideal knowledge of the channel function as well as based on their estimates. The performance of the ICI suppression technique has been compared to standard MRC combining that totally ignores the ICI. Herein, substantial performance gains could be shown. As our solution maintains an independent subcarrier-wise signal processing, its complexity demands are moderate, making it a promising solution for terminal receivers in practice.

5 Overall conclusion and future work

In this thesis, we have studied practical solutions for signal transmission in multi-user MIMO-OFDM systems over time-varying communication channels. For scenarios with different degrees of time variance, its influence on the behaviour of the system has been examined and adequate transmission concepts have been developed, which take advantage of the spatial dimension of the MIMO channel to improve the overall system performance. Within the thesis, three major topics have been addressed:

Synchronization: The simplest form of time variance is caused by CFOs, which result from impairments in the transmission chain. As CFOs distort the OFDM signal properties, synchronization of all communication units is a crucial requirement to enable a reliable signal transmission in MIMO-OFDM. We have developed a self-contained synchronization concept for downlink and uplink of a MIMO-OFDM based multi-user system: Synchronization starts with the downlink phase, where all UTs synchronize to a single BS based on a preamble signal transmitted by the latter. By analytical and simulative means, the achievable synchronization performance has been evaluated based on the length of the preamble. The obtained results allow to establish a framework for the proper design of the preamble to meet desired synchronization performance targets.

By postulating that the CFO estimates from the downlink phase are applied for a *frequency advance* of transmission signals in the uplink phase, the residual CFOs occurring in the links between UTs and BS can be assumed to be small. The system distortions resulting from these residual CFOs in the OFDM-SDMA uplink have been analyzed, and a simplified compensation concept has been derived, which operates in frequency domain and requires a low amount of computational complexity compared to other existing approaches.

Channel-adaptive transmission: Based on quasi-static channel conditions, which can be achieved in a static propagation environment if the communication units have been properly synchronized, we have developed a channel-adaptive transmission concept for the downlink of multi-user MIMO-OFDM systems, which allows to switch between different spatial transmission modes. This concept aims at a high throughput for the users as well as for the entire system while guaranteeing a certain degree of fairness for the single users. We have seen that enabling a simplified SDMA access based on fixed precoding beams yields substantial throughput gains and promotes the simultaneous transmission of multiple streams in the spatial domain already at low SNR conditions. This crucial

relation, which is well-known from theory, could thus be shown to be realizable also in a practical context.

For time-varying channels, the quasi-static channel condition no longer holds, and thus the concept has to be adapted to be applicable further on. Based on a specific antenna configuration suitable to be applied in environments where UTs move at moderate vehicular speeds, we developed an approach that enables to predict the channel conditions for a future time instant. By adapting the transmission to the predicted channels, application of the transmission concept can be maintained. The prediction-based approach yields reliable performance results for a limited range of the prediction interval, which depends on the actual antenna spacing of the antenna configuration.

Doppler-distorted OFDM: At very high velocities of UTs, the time variance of the channels increases to an extent that it distorts the orthogonality of the OFDM subcarrier signals. This gives rise to ICI, which may degrade the signal conditions severely. For general Doppler channels, a transmission concept has been proposed for the downlink, where the multiple receive antennas at the UTs are used to suppress the instantaneous ICI. The instantaneous ICI can be measured based on the common pilots used for channel estimation. The method was shown to be capable of suppressing ICI distortions in a convenient fashion and yields a reasonable system performance. Demands on complexity are rather low compared to other approaches targeting suppression of instantaneous ICI, as Doppler suppression is carried out individually per subcarrier based on an equalizer that is related to the linear MMSE equalizer.

5.1 Future work

We have seen that support for SDMA transmission in the downlink enables substantial gains in throughput for single users as well as for the entire system. One of the main reasons for that result is that SDMA promotes the transmission of multiple streams in the spatial domain even at low SNR conditions. However, SDMA requires some knowledge on the instantaneous channel conditions at the transmitter to deliver these gains. If it cannot be provided, the promising gains of channel-adaptive transmission break away immediately, and the system throughput will drop down to the one achievable with classical diversity-oriented coding techniques. For that reason, it is important that the channel-adaptive transmission concept can be applied for a wide range of mobility scenarios. Although we have developed an extension that enables to maintain the concept if the UTs move at low vehicular speeds, the game is over as soon as the UTs move faster. For that case, there remains only the possibility to adapt to long-term channel conditions and to exploit the available diversity for a reliable signal transmission. However, this results in a substantial decrease of the achievable throughput for user and system. Hence, a large gap between the two mobility scenarios opens up here. Therefore, it can be seen

as a challenge to close this gap in future research by extending the application range of the channel-adaptive transmission concept and to establish a smooth transition from one transmission concept to the other with increasing mobility of the UTs – similar to the smooth transition from spatial diversity and multiplexing transmission considered in the present thesis. For the channel-adaptive concept, we have assumed ideal knowledge of the communication channels at the receivers. Clearly, these have to be estimated in practice, which will introduce channel estimation errors that will certainly affect the system performance. The achievable performance under these errors will thus be another interesting field for future studies.

Further attention needs also the uplink, which has been considered within this work only within the synchronization concept. Although the basic ideas from the other concepts may mostly be adopted, the uplink has different specific properties, which need to be taken into account properly and might entail further challenges.

Finally, the concepts proposed here have been developed and evaluated for an isolated cell only. An interesting field of study is their evaluation and their further improvement for the application in multi-cell environments. The channel-adaptive concept for quasi-static channels is the only concept of the ones presented here where this system-level evaluation has already begun and it is still in progress [101]. It is evident that synchronization will play an important role also on the system-level, however, this issue has neither been extensively investigated nor evaluated yet. For future cellular systems that aim at a frequency reuse factor of one (i.e. all cells reuse the same frequency band), the synchronization issue has to be properly solved for the entire network to enable the high throughput gains promised from theoretical investigations.

List of abbreviations

ACF	autocorrelation function
AWGN	additive white Gaussian noise
BC	broadcast channel
BPSK	binary phase-shift keying
BS	base station
CDF	cumulative distribution function
CFO	carrier frequency offset
CIR	channel impulse response
CP	cyclic prefix
CPE	common phase error
CQI	channel quality identifier
CSI	channel state information
CTF	channel transfer function
DFT	discrete Fourier transform
DPC	dirty paper coding
EGT	equal gain transmission
FDD	frequency division duplex
GoB	grid of beams
GSM	Global System for Mobile Communications
i.i.d.	independent and identically distributed
ICI	inter-carrier interference
IF	interference function
LDPC	low density parity check
3G-LTE	3G Long Term Evolution
LTE	3G Long Term Evolution
MIMO	multiple-input multiple-output
ML	maximum likelihood
MRC	maximum ratio combining

MMSE	minimum mean square error
MSE	mean square error
ms	multi-stream
MT	maximum throughput scheduling
MU-**MIMO**	multi-user MIMO
NLOS	non line of sight
OC	optimum combining
OFDM	orthogonal frequency division multiplexing
PAPR	peak to average power ratio
pdf	probability density function
PDP	power delay profile
PN	pseudo noise
QAM	quadrature amplitude modulation
Rx	receiver
SB	score-based scheduling
SDMA	space-division multiple access
SFO	sampling frequency offset
SINR	signal to interference and noise ratio
SIMO	single-input multiple-output
SISO	single-input single-output
SMUX	spatial multiplexing
SU-**MIMO**	single-user MIMO
SNR	signal to noise ratio
ss	single-stream
TDD	time division duplex
TO	timing offset
Tx	transmitter
UMB	Ultra Mobile Broadband
UT	user terminal
WiMAX	Worldwide Interoperability for Microwave Access
WINNER	Wireless World Initiative New Radio
WSSUS	wide sense stationary uncorrelated scattering
ZF	zero forcing

Nomenclature

B	number of available beams
$\mathbf{C}$	precoding matrix
d_f	discrete pilot spacing in frequency (in subcarriers)
d_t	discrete pilot spacing in time (in OFDM symbols)
f_D	Doppler frequency
$F(u,k)$	interference function (IF)
h	channel
$H(k)$	channel transfer function (CTF)
J_0	Bessel function of the first kind
k	discrete frequency index (subcarrier position)
K	number of users in the system
L	number of channel taps
L_e	number of channel echoes, $L_e = L - 1$
M	number of antennas at BS (uplink scenario)
N	number of OFDM subcarriers
N_c	number of subcarriers within coherence interval
N_g	number of samples contained in guard interval
N_t	number of transmit antennas
N_r	number of receive antennas
N_0	AWGN noise power
n	discrete time index
$\mathbf{n}$	vector of AWGN samples
p	threshold used for preamble detection
P	period of the preamble
P_i	power of interference
P_{in}	power of interference and noise
P_{ICI}	power of inter-carrier interference
P_s	power of the useful signal
Q	number of simultaneously transmitted spatial streams
$\mathbf{R}_H$	covariance matrix of the channel $\mathbf{H}$
r	received signal
s	transmitted signal
$\mathrm{si}(x)$	si-function, $\mathrm{si}(x) = \sin(x)/x$

T_s	sampling period
T_c	coherence time, $T_c = f_D^{-1}$
T_o	duration of an OFDM symbol (including CP)
$\mathbf{w}$	equalization vector
W	width of the correlation window
x	transmit symbol
y	received symbol
z	noise signal
$\mathbf{Z}$	covariance matrix of interference and noise
γ	signal to interference and noise ratio (SINR)
$\delta(n)$	(discrete) Dirac delta function
φ	phase resulting from frequency distortion
φ_{hh}	autocorrelation function of the channel h
λ	wavelength of the carrier frequency
μ	spatial diversity gain [chapter 2.2]
μ	mean square error (MSE) [chapter 4]
ρ	correlation coefficient
σ_h^2	mean power of CIR, $\sigma_h^2 = \sum_{l=0}^{L_e} \sigma_l^2$
σ_l^2	mean power of l-th channel tap
σ_n^2	noise power
ω	frequency normalized to subcarrier spacing

Publication list

Journal papers

1. M. Schellmann and V. Jungnickel, "Multiple CFOs in OFDM-SDMA uplink: Interference analysis and compensation," *EURASIP Journal on Wireless Communications and Networking*, vol. 2009, article ID 909075, 2009.

2. M. Schellmann, L. Thiele, T. Haustein, and V. Jungnickel, "Spatial transmission mode switching in multi-user MIMO-OFDM systems with user fairness," to appear in *IEEE Transactions on Vehicular Technology*, 2009.

3. V. Jungnickel, M. Schellmann, L. Thiele, T. Wirth, T.Haustein, O. Koch, W. Zirwas, E. Schulz "Interference-Aware Scheduling in the Multiuser MIMO-OFDM Downlink", *IEEE Communications Magazine*, vol. 47. no. 6, pp. 56-66, Jun. 2009.

Book chapters

- M. Schellmann, L. Thiele, T. Wirth, V. Jungnickel and T. Haustein, "Resource management in MIMO-OFDM systems", in *"Orthogonal Frequency Division Multiple Access – Fundamentals and applications"*, to be published by Auerbach Publications, CRC Press, Taylor&Francis Group, 2009.

Conference papers

1. M. Schellmann, "Synchronization in OFDM Systems Based on a Multi-Periodic Preamble", *IEEE International Symposium on Wireless Communication Systems 2009 (ISWCS'09)*, Sep. 2009.

2. L. Thiele, T. Wirth, M. Schellmann, V. Jungnickel, "MU-MIMO with Localized Downlink Base Station Cooperation and Downtilted Antennas", *IEEE International Workshop on LTE Evolution in conjunction with ICC'09*, Jun. 2009.

3. L. Thiele, M. Schellmann, T. Wirth, V. Jungnickel, F. Boccardi, and H. Huang, "DFT-based vs. Cooperative MET-based MU-MIMO in the Downlink of Cellular

OFDM Systems," *International ITG Workshop on Smart Antennas (WSA 2009)*, Feb. 2009.

4. L. Thiele, M. Schellmann, T. Wirth, and V. Jungnickel, "Interference-Aware Scheduling in the Synchronous Cellular Multi-Antenna Downlink", *IEEE 69th Vehicular Technology Conference, VTC2009-Spring*, Apr. 2009, invited.

5. M. Schellmann, L. Thiele, and V. Jungnickel, "Low-complexity Doppler compensation in mobile SIMO-OFDM systems," *42nd Asilomar Conference on Signals, Systems and Computers*, Oct. 2008.

6. ——, "Predicting SINR conditions in mobile MIMO-OFDM systems by interpolation techniques," *42nd Asilomar Conference on Signals, Systems and Computers*, Oct. 2008.

7. L. Thiele, M. Schellmann, T. Wirth, and V. Jungnickel "Cooperative Multi-User MIMO based on Reduced Feedback in Downlink OFDM Systems," *42nd Asilomar Conference on Signals, Systems and Computers*, Oct. 2008.

8. V. Jungnickel, L. Thiele, M. Schellmann, T. Wirth, T. Haustein *et al.*, "Implementation Concepts for Distributed Cooperative Transmission," *42nd Asilomar Conference on Signals, Systems and Computers*, Oct. 2008.

9. L. Thiele, M. Schellmann, T. Wirth, and V. Jungnickel, "On the Value of Synchronous Downlink MIMO-OFDMA Systems with Linear Equalizers," *IEEE International Symposium on Wireless Communication Systems 2008 (ISWCS'08)* , Oct. 2008.

10. V. Jungnickel, T. Wirth, M. Schellmann, T. Haustein, and W. Zirwas, "Synchronization of Cooperative Base Stations," *IEEE International Symposium on Wireless Communication Systems 2008 (ISWCS'08)* , Oct. 2008.

11. M. Schellmann, "Suppressing Doppler-induced Intercarrier Interference with Multiple Receiving Antennas," *13th International OFDM-Workshop*, Aug. 2008.

12. V. Jungnickel, L. Thiele, T. Wirth, M. Schellmann, V. Venkatkumar, and T. Haustein, "Feedback Design for Multiuser MIMO Systems," *13th International OFDM-Workshop*, Aug. 2008.

13. L. Thiele, M. Schellmann, S. Schiffermüller, V. Jungnickel, and W. Zirwas, "Multi-Cell Channel Estimation using Virtual Pilots," *IEEE 67th Vehicular Technology Conference VTC2008-Spring*, May 2008.

14. M. Schellmann and T. Haustein, "Doppler compensation for chunk-based OFDMA systems," *7th International ITG Conference on Source and Channel Coding (SCC'08)*, Jan. 2008.

15. M. Schellmann, L. Thiele, V. Jungnickel, and T. Haustein, "A fair score-based scheduler for spatial transmission mode selection," *41st Asilomar Conference on Signals, Systems and Computers*, Nov. 2007.

16. L. Thiele, M. Schellmann, W. Zirwas, and V. Jungnickel, "Capacity Scaling of Multiuser MIMO with Limited Feedback in a Multicell Environment," *41st Asilomar Conference on Signals, Systems and Computers*, Nov. 2007, invited.

17. V. Jungnickel, M. Schellmann, A. Forck, H. Gäbler, S. Wahls *et al.*, "Demonstration of Virtual MIMO in the Uplink," *IET Smart Antennas and Cooperative Communications Seminar*, Nov. 2007, invited.

18. M. Schellmann, K. Manolakis, A. Ibing, and M. Kuszak, "Impact of the Preamble Bandwidth on the Synchronization Performance," *12th International OFDM-Workshop*, pp. 113–117, Aug. 2007.

19. M. Schellmann, V. Jungnickel, A. Sezgin, and E. Costa, "Rate-maximized switching between spatial transmission modes," *40th Asilomar Conference on Signals, Systems and Computers*, Oct. 2006.

20. A. Sezgin, M. Schellmann, V. Jungnickel, and E. Costa, "Throughput Analysis of Diversity and Multiplexing Schemes for MIMO-SIC OFDM systems," *40th Asilomar Conference on Signals, Systems and Computers*, Oct. 2006.

21. M. Schellmann, A. Sezgin, G. Wunder, H. Halbauer, and R. Münzner, "Performance of the wimax ranging process in high mobility environments," *The 9th International Symposium on Wireless Personal Multimedia Communications (WPMC)*, Sep. 2006.

22. A. Sezgin, P. Jung, M. Schellmann, H. Halbauer, and R. Muenzner, "On the impact of mobility on the channel estimation in WIMAX OFDMA-uplink," *Personal, Indoor and Mobile Radio Comm. (PIMRC), IEEE 17th Int. Symp. on*, Sep. 2006.

23. M. Schellmann, "Improvements for time and frequency synchronization in OFDM systems," *11th International OFDM-Workshop*, Aug. 2006.

24. M. Schellmann and V. Jungnickel, "Effects of multiple users' CFOs in OFDM-SDMA up-link – an interference model," *International Conference on Communications (ICC), IEEE*, Jun. 2006.

25. M. Schellmann and S. Stanczak, "Multi-user MIMO channel estimation in the presence of carrier frequency offsets," *39th Asilomar Conference on Signals, Systems and Computers*, pp. 462–466, Oct. 2005.

26. M. Schellmann, V. Jungnickel, and C. Helmolt, "On the value of spatial diversity for the synchronisation in MIMO-OFDM systems," *Personal, Indoor and Mobile Radio Comm. (PIMRC), IEEE 16th Int. Symp. on*, Sep. 2005.

27. M. Schellmann and V. Jungnickel, "Instantaneous synchronisation for the uplink of multi-user MIMO-OFDM systems," *10th International OFDM-Workshop*, pp. 104–108, Aug. 2005.

Patents

1. "Method to estimate a propagation delay between a first user terminal and a base station", M. Schellmann, V. Jungnickel, W. Zirwas, E. Schulz

2. "Method to estimate an impulse response of a radio channel and radio station", M. Schellmann, S. Stanczak, W. Zirwas and E. Schulz

3. "Method and device for data communication and communication system comprising such device", M. Schellmann, T. Haustein, V. Jungnickel, A. Forck and E. Schulz

6 further patents pending

Bibliography

[1] 3GPP TS 36.211V8.5.0, "E-UTRA – Physical channels and modulation (Release 8)," Dec. 2008.

[2] 3GPP2 C.S0084-001-0 v3.0, "Physical layer for ultra mobile broadband (UMB) air interface specification," Aug. 2008.

[3] S. Ahmed, S. Lambotharan, A. Jakobsson, and J. Chambers, "MIMO frequency-selective channels with multiple-frequency offsets: estimation and detection techniques," *Communications, IEE Proceedings*, vol. 152, no. 4, pp. 489–494, Aug. 2005.

[4] B. Ai, Z. Yang, C. Pan, J. Ge, Y. Wang, and Z. Lu, "On the synchronization techniques for wireless OFDM systems," *IEEE Transactions on Broadcasting*, vol. 52, no. 2, pp. 236–244, Jun. 2006.

[5] G. Auer, "Channel estimation for OFDM systems with multiple transmit antennas by filtering in time and frequency," in *Vehicular Technology Conference. VTC 2003-Fall. IEEE 58th*, vol. 2, 2003, pp. 1204–1208.

[6] S. Barbarossa, M. Pompili, and G. Giannakis, "Channel-independent synchronization of orthogonal frequency division multiple access systems," *IEEE Journal on Selected Areas in Communications*, vol. 20, no. 2, pp. 474–486, Feb. 2002.

[7] F. Boccardi and H. Huang, "A near-optimum technique using linear precoding for the MIMO broadcast channel," *Acoustics, Speech and Signal Processing. ICASSP 2007. IEEE International Conference on*, vol. 3, pp. III–17–III–20, Apr. 2007.

[8] H. Boche and E. Jorswieck, "On the performance optimization in multiuser MIMO systems," *European Transactions on Telecommunications*, vol. 18, no. 3, pp. 287–304, Sep. 2007.

[9] H. Bölcskei, "Blind high-resolution uplink synchronization of OFDM-based multiple access schemes," *Signal Processing Advances in Wireless Communications. SPAWC '99.*, pp. 166–169, May 1999.

[10] ——, "Blind estimation of symbol timing and carrier frequency offset in wireless OFDM systems," *IEEE Transactions on Communications*, vol. 49, no. 6, pp. 988–999, Jun. 2001.

[11] T. Bonald, "A score-based opportunistic scheduler for fading radio channels," *Proc. of European Wireless*, 2004.

[12] X. Cai and G. Giannakis, "Bounding performance and suppressing intercarrier interference in wireless mobile OFDM," *IEEE Transactions on Communications*, vol. 51, no. 12, pp. 2047–2056, Dec. 2003.

[13] G. Caire and S. Shamai, "On the achievable throughput of a multiantenna Gaussian broadcast channel," *IEEE Transactions on Information Theory*, vol. 49, no. 7, pp. 1691–1706, Jul. 2003.

[14] Z. Cao, U. Tureli, and Y.-D. Yao, "User separation and frequency-time synchronization for the uplink of interleaved OFDMA," *36th Asilomar Conference on Signals, Systems and Computers*, pp. 1842–1846, Nov. 2002.

[15] Z. Cao, U. Tureli, Y.-D. Yao, and P. Honan, "Frequency synchronization for generalized OFDMA uplink," *Global Telecommunications Conference. GLOBECOM '04. IEEE*, pp. 1071–1075, 2004.

[16] S. Catreux, V. Erceg, D. Gesbert, and J. Heath, R.W., "Adaptive modulation and MIMO coding for broadband wireless data networks," *Communications Magazine, IEEE*, vol. 40, no. 6, pp. 108–115, Jun. 2002.

[17] D. Chizhik, "Slowing the time-fluctuating MIMO channel by beam forming," *IEEE Transactions on Wireless Communications*, vol. 3, no. 5, pp. 1554–1565, Sept. 2004.

[18] J. Choi, C. Lee, H. Jung, and Y. Lee, "Carrier frequency offset compensation for uplink of OFDM-FDMA systems," *IEEE Communications Letters*, vol. 4, no. 12, pp. 414–416, Dec. 2000.

[19] S. Chung, A. Lozano, H. Huang, A. Sutivong, and J. Cioffi, "Approaching the MIMO capacity with a low-rate feedback channel in V-BLAST," *EURASIP JASP*, no. 5, pp. 762–771, 2004.

[20] F. Classen and H. Meyr, "Frequency synchronization algorithms for OFDM systems suitable for communication over frequency selective fading channels," *Vehicular Technology Conference, 1994 IEEE 44th*, pp. 1655–1659 vol.3, Jun 1994.

[21] M. Costa, "Writing on dirty paper," *IEEE Transactions on Information Theory*, vol. 29, no. 3, pp. 439–441, 1983.

[22] A. Czylwik, "Synchronization for systems with antenna diversity," *Vehicular Technology Conference. VTC 1999-Fall. IEEE*, vol. 2, pp. 728–732, Sep. 1999.

[23] S. Das and P. Schniter, "Beamforming and combining strategies for MIMO-OFDM over doubly selective channels," *40th Asilomar Conference on Signals, Systems and Computers*, pp. 804–808, Nov. 2006.

[24] R. de Francisco, D. Slock, and Y.-C. Liang, "Balance of multiuser diversity and multiplexing gain in near-orthogonal MIMO systems with limited feedback," *Wireless Communications and Networking Conference, WCNC 2007. IEEE*, pp. 1269–1274, 2007.

[25] M. El-Tanany, Y. Wu, and L. Hazy, "OFDM uplink for interactive broadband wireless: analysis and simulation in the presence of carrier, clock and timing errors," *IEEE Transactions on Broadcasting*, vol. 47, no. 1, pp. 3–19, Mar. 2001.

[26] R. Fantacci, D. Marabissi, and S. Papini, "Multiuser interference cancellation receivers for OFDMA uplink communications with carrier frequency offset," *Global Telecommunications Conference. GLOBECOM '04. IEEE*, vol. 5, pp. 2808–2812, Dec. 2004.

[27] F. Farrokhi, A. Lozano, G. Foschini, and R. Valenzuela, "Spectral efficiency of FDMA/TDMA wireless systems with transmit and receive antenna arrays," *IEEE Transactions on Wireless Communications*, vol. 1, no. 4, pp. 591–599, Oct. 2002.

[28] A. Forenza, M. McKay, A. Pandharipande, R. Heath, and I. Collings, "Adaptive MIMO transmission for exploiting the capacity of spatially correlated channels," *IEEE Transactions on Vehicular Technology*, vol. 56, no. 2, pp. 619–630, Mar. 2007.

[29] G. Foschini and M. Gans, "On limits of wireless communications in a fading environment when using multiple antennas," *Wireless Personal Communications*, vol. 3, pp. 311–335, 1998.

[30] X. Fu and H. Minn, "Initial uplink synchronization and power control (ranging process) for OFDMA systems," *Global Telecommunications Conference. GLOBECOM '04. IEEE*, pp. 3999–4003, Nov. 2004.

[31] D. Gesbert, M. Kountouris, R. Heath, C.-B. Chae, and T. Salzer, "Shifting the MIMO paradigm," *Signal Processing Magazine, IEEE*, vol. 24, no. 5, pp. 36–46, Sep. 2007.

[32] L. Häring, S. Bieder, and A. Czylwik, "Closed-form estimators of carrier frequency offsets and channels in the uplink of multiuser OFDM systems," *Acoustics, Speech and Signal Processing, IEEE International Conference on, ICASSP 2006*, vol. 4, pp. IV 661–664, May 2006.

[33] L. Häring and A. Czylwik, "Synchronization in MIMO-OFDM systems," *Advances in Radio Sciences*, vol. 2, pp. 147–153, 2004.

[34] R. Heath and A. J. Paulraj, "Switching between diversity and multiplexing in MIMO systems," *IEEE Transactions on Communications*, vol. 53, no. 6, Jun. 2005.

[35] P. Hoeher, S. Kaiser, and P. Robertson, "Pilot-symbol-aided channel estimation in time and frequency," *Proc. IEEE Global Telecommunnications Conference (GLOBECOM'97)*, pp. 90–96, Nov 1997.

[36] C.-Y. Hsu and W.-R. Wu, "Low-complexity CFO compensation for uplink OFDMA systems," *Personal, Indoor and Mobile Radio Communications, 2006 IEEE 17th International Symposium on*, pp. 1–5, 2006.

[37] D. Huang and K. Letaief, "An interference-cancellation scheme for carrier frequency offsets correction in OFDMA systems," *IEEE Transactions on Communications*, vol. 53, no. 7, pp. 1155–1165, Jul. 2005.

[38] C. Ibars and Y. Bar-Ness, "Inter-carrier interference cancellation for OFDM systems with macrodiverstiy and multiple frequency offsets," *Wireless Personal Communications*, vol. 26, no. 4, pp. 285–304, Sep. 2003.

[39] IEEE Std. 802.16e-2005, "Air interface for fixed and mobile broadband wireless access systems," Feb. 2006.

[40] IST-2003-507581 WINNER – D2.7, "Assessment of advanced beam forming and MIMO technologies," Feb. 2005.

[41] IST-4-027756 WINNER II – D2.2.3, "Modulation and coding schemes for the WINNER II system," Nov. 2007.

[42] IST-4-027756 WINNER II – D6.13.10 , "Final CG 'wide area' description for integration into overall system concept and assessment of key technologies," Nov. 2007.

[43] W. G. Jeon, K. H. Chang, and Y. S. Cho, "An equalization technique for orthogonal frequency-division multiplexing systems in time-variant multipath channels," *IEEE Transactions on Communications*, vol. 47, no. 1, pp. 27–32, Jan 1999.

[44] N. Jindal, "MIMO broadcast channels with finite-rate feedback," *IEEE Transactions on Information Theory*, vol. 52, no. 11, pp. 5045–5060, 2006.

[45] N. Jindal, W. Rhee, S. Vishwanath, S. Jafar, and A. Goldsmith, "Sum power iterative water-filling for multi-antenna Gaussian broadcast channels," *IEEE Transactions on Information Theory*, vol. 51, no. 4, pp. 1570–1580, Apr. 2005.

[46] P. Jung and G. Wunder, "On time-variant distortions in multicarrier transmission with application to frequency offsets and phase noise," *IEEE Transactions on Communications*, vol. 53, no. 9, pp. 1561–1570, Sep. 2005.

[47] V. Jungnickel, A. Forck, T. Haustein, S. Schiffermüller, C. von Helmolt *et al.*, "1 Gbit/s MIMO-OFDM Transmission Experiments," *Vehicular Technology Conference, VTC Fall 2005, IEEE*, Sep. 2005.

[48] V. Jungnickel, M. Schellmann, A. Forck, H. Gäbler, S. Wahls *et al.*, "Demonstration of Virtual MIMO in the Uplink," *IET Smart Antennas and Cooperative Communications Seminar*, Oct. 2007, invited.

[49] S. M. Kay, *Fundamentals of Statistical Signal Processing - Estimation Theory*, ser. Signal Processing Series. New Jersey: Prentice Hall PTR, 1993, vol. 1.

[50] T. Keller, L. Piazzo, P. Mandarini, and L. Hanzo, "Orthogonal frequency division multiplex synchronization techniques for frequency-selective fading channels," *IEEE Journal on Selected Areas in Communications*, vol. 19, no. 6, pp. 999–1008, Jun. 2001.

[51] R. Kennedy, *Fading Dispersive Communication Channels*. New York: Wiley Interscience, 1969.

[52] H. Kim, J. Kim, J. Li, and M. Kountouris, "On the performance of limited feedback multiuser MIMO transmission in 3GPP HSDPA," *Vehicular Technology Conference, VTC-2005-Fall. IEEE*, vol. 1, pp. 473–476, Sep. 2005.

[53] P. Klenner and K.-D. Kammeyer, "Spatially interpolated OFDM with channel estimation for fast fading channels," *Vehicular Technology Conference, 2007. VTC2007-Spring. IEEE 65th*, pp. 2455–2459, April 2007.

[54] R. Knopp and P. Humblet, "Information capacity and power control in single-cell multiuser communications," *Communications, IEEE International Conference on*, pp. 331–335, 1995.

[55] L. Kuang, J. Lu, Z. Ni, and J. Zheng, "Nonpilot-aided carrier frequency tracking for uplink OFDMA systems," *International Conference on Communications 2004, IEEE*, vol. 6, pp. 3193–3196, Jun. 2004.

[56] Y. Li and L. Cimini, "Bounds on the interchannel interference of OFDM in time-varying impairments," *IEEE Transactions on Communications*, vol. 49, no. 3, pp. 401–404, Mar 2001.

[57] H. Liu and U. Tureli, "A high-efficiency carrier estimator for OFDM communications," *IEEE Communications Letters*, vol. 2, no. 4, pp. 104–106, Apr 1998.

[58] J. Lopez-Vicario and C. Anton-Haro, "Adaptive switching between spatial diversity and multiplexing: A cross-layer approach," *IST Mobile Communications Summit*, Jun. 2005.

[59] D. Love and J. Heath, R.W., "Equal gain transmission in multiple-input multiple-output wireless systems," *IEEE Transactions on Communications*, vol. 51, no. 7, pp. 1102–1110, Jul. 2003.

[60] ——, "Limited feedback unitary precoding for spatial multiplexing systems," *IEEE Transactions on Information Theory*, vol. 51, no. 8, pp. 2967–2976, Aug. 2005.

[61] D. Love, J. Heath, R.W., W. Santipach, and M. Honig, "What is the value of limited feedback for MIMO channels?" *Communications Magazine, IEEE*, vol. 42, no. 10, pp. 54–59, Oct. 2004.

[62] D. Love, J. Heath, R.W., and T. Strohmer, "Grassmannian beamforming for multiple-input multiple-output wireless systems," *IEEE Transactions on Information Theory*, vol. 49, no. 10, pp. 2735–2747, Oct. 2003.

[63] D. Love and R. Heath, "Multi-mode precoding using linear receivers for limited feedback MIMO systems," *Communications, 2004 IEEE International Conference on*, pp. 448–452, 2004.

[64] A. Lozano, "Capacity-approaching rate function for layered multiantenna architectures," *IEEE Transactions on Wireless Communications*, vol. 2, no. 4, pp. 616–620, Jul. 2003.

[65] H. Minn, V. Bhargava, and K. Letaief, "A robust timing and frequency synchronization for OFDM systems," *IEEE Transactions on Wireless Communications*, vol. 2, no. 4, pp. 822–839, Jul. 2003.

[66] A. Mody and G. Stüber, "Synchronization for MIMO-OFDM systems," *Global Telecommunications Conference. GLOBECOM '01. IEEE*, vol. 1, pp. 509–513, Nov. 2001.

[67] P. Moose, "A technique for orthogonal frequency division multiplexing frequency offset correction," *IEEE Transactions on Communications*, vol. 42, no. 10, pp. 2908–2914, Oct. 1994.

[68] M. Morelli, "Timing and frequency synchronization for the uplink of an OFDMA system," *IEEE Transactions on Communications*, vol. 52, no. 2, pp. 296–306, Feb. 2004.

[69] M. Morelli, C.-C. Kuo, and M.-O. Pun, "Synchronization techniques for orthogonal frequency division multiple access (OFDMA): A tutorial review," *Proceedings of the IEEE*, vol. 95, no. 7, pp. 1394–1427, Jul. 2007.

[70] M. Morelli and U. Mengali, "An improved frequency offset estimator for OFDM applications," *IEEE Communications Letters*, vol. 3, no. 3, pp. 75–77, Mar 1999.

[71] Y. Mostofi and D. Cox, "ICI mitigation for pilot-aided OFDM mobile systems," *IEEE Transactions on Wireless Communications*, vol. 4, no. 2, pp. 765–774, 2005.

[72] ——, "A robust timing synchronization design in OFDM systems – part I: low-mobility cases," *IEEE Transactions on Wireless Communications*, vol. 6, no. 12, pp. 4329–4339, Dec 2007.

[73] S. Nanda and K. Rege, "Frame error rates for convolutional codes on fading channels and the concept of effective E_b/N_0," *IEEE Transactions on Vehicular Technology*, vol. 47, no. 4, pp. 1245–1250, Nov 1998.

[74] C. Oberli, "ML-based tracking algorithms for MIMO-OFDM," *IEEE Transactions on Wireless Communications*, vol. 6, no. 7, pp. 2630–2639, Jul. 2007.

[75] A. Papoulis and S. Pillai, *Probability, Random Variables and Stochastic Processes*. McGraw-Hill, 2002.

[76] A. Paulraj, D. Gore, R. Nabar, and H. Bölcskei, "An overview of MIMO communications - a key to gigabit wireless," *Proceedings of the IEEE*, vol. 92, no. 2, pp. 198–218, Feb. 2004.

[77] V. Pohl, P. H. Nguyen, V. Jungnickel, and C. von Helmolt, "Continuous flat-fading MIMO channels: achievable rate and optimal length of the training and data phases," *IEEE Transactions on Wireless Communications*, vol. 4, no. 4, pp. 1889–1900, Jul. 2005.

[78] M.-O. Pun, M. Morelli, and C.-C. Kuo, "Maximum-likelihood synchronization and channel estimation for OFDMA uplink transmissions," *Communications, IEEE Transactions on*, vol. 54, no. 4, pp. 726–736, Apr. 2006.

[79] T. S. Rappaport, *Wireless Communication - Principles and Practice*. Prentice Hall, 2002.

[80] N. Ravindran and N. Jindal, "Multi-user diversity vs. accurate channel feedback for MIMO broadcast channels," *Communications, 2008. ICC '08. IEEE International Conference on*, pp. 3684–3688, May 2008.

[81] H. Sampath and A. Paulraj, "Linear precoding for space-time coded systems with known fading correlations," *IEEE Communications Letters*, vol. 6, no. 6, pp. 239–241, 2002.

[82] M. Schellmann, K. Manolakis, A. Ibing, and M. Kuszak, "Impact of the Preamble Bandwidth on the Synchronization Performance," *12th International OFDM Workshop, Hamburg*, pp. 113–117, Aug. 2007.

[83] M. Schellmann, A. Sezgin, G. Wunder, H. Halbauer, and R. Münzner, "Performance of the WiMAX ranging process in high mobility environments," *The 9th International Symposium on Wireless Personal Multimedia Communications (WPMC)*, Sep. 2006.

[84] M. Schellmann and S. Stanczak, "Multi-user MIMO channel estimation in the presence of carrier frequency offsets," *39th Asilomar Conference on Signals, Systems and Computers*, pp. 462–466, Oct. 2005.

[85] M. Schellmann, L. Thiele, T. Wirth, T. Haustein, and V. Jungnickel, "Resource Management in MIMO-OFDM systems," in *OFDMA: Fundamentals and Applications*, T. Jiang, L. Song, and Y. Zhang, Eds. CRC Press, Taylor&Francis Group, 2009.

[86] M. Schellmann, V. Jungnickel, A. Sezgin, and E. Costa, "Rate-maximized switching between spatial transmission modes," *40th Asilomar Conference on Signals, Systems and Computers*, pp. 1635–1639, 2006.

[87] T. Schenk and A. van Zelst, "Frequency synchronization for MIMO-OFDM wireless LAN systems," *Vehicular Technology Conference, VTC 2003-Fall. IEEE*, vol. 2, pp. 781–785, 2003.

[88] S. Schiffermüller and V. Jungnickel, "Practical channel interpolation for OFDMA," *Global Telecommunications Conference. GLOBECOM '06. IEEE*, Dec. 2006.

[89] T. Schmidl and D. Cox, "Robust frequency and timing synchronization for OFDM," *IEEE Transactions on Communications*, no. 12, pp. 1613–1621, Dec. 1997.

[90] P. Schniter, "Low-complexity equalization of OFDM in doubly selective channels," *IEEE Transactions on Signal Processing*, vol. 52, no. 4, pp. 1002–1011, April 2004.

[91] M. Schubert and H. Boche, "Solution of the multiuser downlink beamforming problem with individual SINR constraints," *IEEE Transactions on Vehicular Technology*, vol. 53, no. 1, pp. 18–28, Jan. 2004.

[92] B.-S. Seo, S.-G. Choi, and J.-S. Cha, "Maximum ratio combining for OFDM systems with cochannel interference," *IEEE Transactions on Consumer Electronics*, vol. 52, no. 1, pp. 87–91, Feb. 2006.

[93] S. Serbetli and S. Baggen, "Doppler compensation by using dual antenna for mobile OFDM systems," *Vehicular Technology Conference,. VTC Spring 2008. IEEE*, pp. 1499–1503, May 2008.

[94] A. Sezgin, P. Jung, M. Schellmann, H. Halbauer, and R. Münzner, "On the impact of mobility on the channel estimation in WiMAX OFDMA-uplink," *Personal, Indoor and Mobile Radio Comm., IEEE 17th Int. Symp. on*, Sept. 2006.

[95] S. Sezginer and P. Bianchi, "Asymptotically efficient reduced complexity frequency offset and channel estimators for uplink MIMO-OFDMA systems," *Signal Processing, IEEE Transactions on*, vol. 56, no. 3, pp. 964–979, Mar. 2008.

[96] M. Sharif and B. Hassibi, "On the capacity of MIMO broadcast channels with partial side information," *IEEE Transactions on Information Theory*, vol. 51, no. 2, pp. 506–522, Feb. 2005.

[97] M. Speth, S. Fechtel, G. Fock, and H. Meyr, "Optimum receiver design for OFDM-based broadband transmission – Part II: A case study," *IEEE Transactions on Communications*, vol. 49, no. 4, pp. 571–578, Apr. 2001.

[98] ——, "Optimum receiver design for wireless broad-band systems using OFDM – Part I," *IEEE Transactions on Communications*, vol. 47, no. 11, pp. 1668–1677, 1999.

[99] G. L. Stüber, J. Barry, S. W. McLaughlin, Y. Li, M. A. Ingram, and T. G. Pratt, "Broadband MIMO-OFDM wireless communications," *Proceedings of the IEEE*, vol. 92, no. 2, pp. 271–294, Feb. 2004.

[100] V. Tarokh, A. Naguib, N. Seshadri, and A. Calderbank, "Space-time codes for high data rate wireless communication: performance criteria in the presence of channel estimation errors, mobility, and multiple paths," *IEEE Transactions on Communications*, vol. 47, no. 2, pp. 199–207, Feb 1999.

[101] L. Thiele, M. Schellmann, V. Jungnickel, and W. Zirwas, "Capacity scaling of multi-user MIMO with limited feedback in a multi-cell environment," *41st Asilomar Conference on Signals, Systems and Computers*, Nov. 2007.

[102] L. Thiele, M. Schellmann, T. Wirth, and V. Jungnickel, "On the Value of Synchronous Downlink MIMO-OFDMA Systems with Linear Equalizers," *IEEE International Symposium on Wireless Communication Systems (ISWCS)* , Oct. 2008.

[103] ——, "Interference-Aware Scheduling in the Synchronous Cellular Multi-Antenna Downlink," *IEEE 69th Vehicular Technology Conference, VTC2009-Spring*, Apr. 2009, invited.

[104] A. Tonello, N. Laurenti, and S. Pupolin, "Analysis of the uplink of an asynchronous multi-user DMT OFDMA system impaired by time offsets, frequency offsets, and multi-path fading," *Vehicular Technology Conference. VTC 2000-Fall. IEEE. 52nd*, vol. 3, pp. 1094–1099, 2000.

[105] A. Tulino, A. Lozano, and S. Verdu, "Impact of antenna correlation on the capacity of multiantenna channels," *IEEE Transactions on Information Theory*, vol. 51, no. 7, pp. 2491–2509, July 2005.

[106] U. Tureli, H. Liu, and M. Zoltowski, "OFDM blind carrier offset estimation: ES-PRIT," *IEEE Transactions on Communications*, vol. 48, no. 9, pp. 1459–1461, Sep. 2000.

[107] J.-J. van de Beek, P. Borjesson, M.-L. Boucheret, D. Landstrom, J. Arenas *et al.*, "A time and frequency synchronization scheme for multiuser OFDM," *IEEE Journal on Selected Areas in Communications*, vol. 17, no. 11, pp. 1900–1914, Nov 1999.

[108] J. van de Beek, "Channel quality feedback schemes for 3GPP's Evolved-UTRA downlink," *Global Telecommunications Conference, GLOBECOM '06, IEEE*, pp. 1–5, Nov. 2006.

[109] J. van de Beek, M. Sandell, and P. Borjesson, "ML estimation of time and frequency offset in OFDM systems," *IEEE Transactions on Signal Processing*, vol. 45, no. 7, pp. 1800–1805, Jul. 1997.

[110] A. van Zelst and T. Schenk, "Implementation of a MIMO-OFDM-based wireless LAN system," *IEEE Transactions on Signal Processing*, vol. 52, no. 2, pp. 483–494, Feb. 2004.

[111] P. Vandenameele, L. Van Der Perre, M. Engels, B. Gyselinckx, and H. De Man, "A combined OFDM/SDMA approach," *IEEE Journal on Selected Areas in Communications*, vol. 18, no. 11, pp. 2312–2321, Nov. 2000.

[112] S. Vishwanath, N. Jindal, and A. Goldsmith, "Duality, achievable rates, and sum-rate capacity of Gaussian MIMO broadcast channels," *IEEE Transactions on Information Theory*, vol. 49, no. 10, pp. 2658–2668, Oct. 2003.

[113] P. Viswanath and D. Tse, "Sum capacity of the vector Gaussian broadcast channel and uplink-downlink duality," *IEEE Transactions on Information Theory*, vol. 49, no. 8, pp. 1912–1921, Aug. 2003.

[114] P. Viswanath, D. Tse, and R. Laroia, "Opportunistic beamforming using dumb antennas," *IEEE Transactions on Information Theory*, vol. 48, no. 6, pp. 1277–1294, Jun. 2002.

[115] S. Vogeler, "Verfahren zur Kompensation von Doppler-Einflüssen in Mehrträger-Übertragungssystemen," Ph.D. dissertation, University of Bremen, Germany, Shaker Verlag, Aug 2006.

[116] M. Vu and A. Paulraj, "Optimal linear precoders for MIMO wireless correlated channels with nonzero mean in space-time coded systems," *IEEE Transactions on Signal Processing*, vol. 54, no. 6, pp. 2318–2332, Jun. 2006.

[117] J. Wagner, Y.-C. Liang, and R. Zhang, "Random beamforming with systematic beam selection," *Personal, Indoor and Mobile Radio Comm., IEEE 17th Int. Symp. on*, Sep. 2006.

[118] J. Winters, "Optimum combining in digital mobile radio with cochannel interference," *IEEE Transactions on Vehicular Technology*, vol. 33, no. 3, pp. 144–155, Aug. 1984.

[119] J. Winters, J. Salz, and R. Gitlin, "The impact of antenna diversity on the capacity of wireless communication systems," *IEEE Transactions on Communications*, vol. 42, no. 234, pp. 1740–1751, Apr. 1994.

[120] T. Wirth, V. Jungnickel, A. Forck, S. Wahls, T. Haustein *et al.*, "Realtime multi-user multi-antenna downlink measurements," *Wireless Communications and Networking Conference, WCNC 2008. IEEE*, pp. 1328–1333, Apr. 2008.

[121] K.-H. Wu, W.-H. Fang, and J.-T. Chen, "Joint DOA-frequency offset estimation and data detection in uplink MIMO-OFDM networks with SDMA techniques," *Vehicular Technology Conference. VTC 2006-Spring. IEEE 63rd*, vol. 6, pp. 2977–2981, 2006.

[122] B. Yang, K. Letaief, R. Cheng, and Z. Cao, "Timing recovery for OFDM transmission," *IEEE Journal on Selected Areas in Communications*, vol. 18, no. 11, pp. 2278–2291, 2000.

[123] Y. Yao and G. Giannakis, "Blind carrier frequency offset estimation in SISO, MIMO, and multiuser OFDM systems," *IEEE Transactions on Communications*, vol. 53, no. 1, pp. 173–183, Jan. 2005.

[124] Y. C. Yu, M. Okada, and H. Yamamoto, "Study for various array antenna assisted Doppler spread compensator with MRC diversity of ISDB-T receiver," *Vehicular*

Technology Conference. VTC 2006-Spring. IEEE 63rd, vol. 6, pp. 2947–2951, May 2006.

[125] Z. Zhang, K. Long, M. Zhao, and Y. Liu, "Joint frame synchronization and frequency offset estimation in OFDM systems," *IEEE Transactions on Broadcasting*, vol. 51, no. 3, pp. 389–394, Sept. 2005.

[126] L. Zheng and D. Tse, "Diversity and multiplexing: a fundamental tradeoff in multiple-antenna channels," *IEEE Transactions on Information Theory*, vol. 49, no. 5, pp. 1073–1096, May 2003.

[127] H. Zhou and Y.-F. Huang, "Fine timing synchronization using power delay profile for OFDM systems," *Circuits and Systems, 2005. ISCAS 2005. IEEE International Symposium on*, vol. 3, pp. 2623–2626, May 2005.

[128] X. Zhuang, K. Baum, V. Nangia, and M. Kudak, "Ranging improvement for 802.16e OFDMA PHY," Document IEEE C802.16e-04/143r1, Jul. 2004. [Online]. Available: http://ieee802.org/16